Design and Implementation of a Special Protection Scheme to Prevent Voltage Collapse

A Thesis
Submitted to the College of Graduate Studies and Research
in Partial Fulfillment of the Requirements
For the Degree of
Doctor of Philosophy
in the
Department of Electrical Engineering
University of Saskatchewan
Saskatoon, Saskatchewan
Canada
By

TARA ALZAHAWI

PERMISSION TO USE

In presenting this thesis in partial fulfillment of the requirements for a Doctor of Philosophy degree from the University of Saskatchewan, the author agrees that the Libraries of this University may make it freely available for inspection. The author further agrees that permission for copying of this thesis in any manner, in whole or in part, for scholarly purposes may be granted by the professors who supervised the thesis work or, in their absence, by the Head of the Department of Electrical Engineering or the Dean of the College of Engineering. It is understood that any copying or publication or use of this thesis or part thereof for financial gain shall not be allowed without the author's written permission. It is also understood that due recognition shall be given to the author and the University of Saskatchewan in any scholarly use which may be made of any material in this thesis.

Request for permission to copy or to make other use of material in this thesis in whole or in part should be addressed to:

Head of the Department of Electrical Engineering,
University of Saskatchewan,
Saskatoon, Saskatchewan, Canada S7N 5A9

ABSTRACT

The trend of making more profits for the owners, deregulation of the utility market and need for obtaining permission from regulatory agencies have forced electric power utilities to operate their systems close to the security limits of their generation, transmission and distribution systems. The result is that power systems are now exposed to substantial risks of experiencing voltage collapse. This phenomenon is complex and is localized in nature but has widespread adverse consequences. The worst scenario of voltage collapse is partial or total outage of the power system resulting in loss of industrial productivity of the country and major financial loss to the utility. On-line monitoring of voltage stability is, therefore becoming a vital practice that is being increasingly adopted by electric power utilities.

The phenomenon of voltage collapse has been studied for quite some time, and techniques for identifying voltage collapse situations have been suggested. Most suggested techniques examine steady-state and dynamic behaviors of the power system in off-line modes. Very few on-line protection and control schemes have been proposed and implemented. In this thesis, a new technique for preventing voltage collapse is presented.

The developed technique uses subset of measurements from local bus as well as neighbouring buses and considers not only the present state of the system but also future load and topology changes in the system. The technique improves the robustness of the local-based methods and can be implemented in on-line as well as off-line modes.

The technique monitors voltages and currents and calculates from those measurements time to voltage collapse. As the system approaches voltage collapse, control actions are implemented to relieve the system to prevent major disturbances.

The developed technique was tested by simulating a variety of operating states and generating voltage collapse situations on the IEEE 30-Bus test system. Some results from the simulation

studies are reported in this thesis. The results obtained from the simulations indicates that the proposed technique is able to estimate the time to voltage collapse and can implement control actions as well as alert operators.

ACKNOWLEDGEMENTS

I wish to express my gratitude and appreciation to Dr. M. S. Sachdev and Dr. R. Gokaraju for their supervision of this work. Their advice and assistance in the preparation of this thesis are thankfully acknowledged.

I also wish to thank the advisory committee members for their suggestions and advice. Assistance provided by the computing staff of the College of Engineering and also by the laboratory and secretarial staff of the Department of Electrical Engineering is gratefully recognized.

Finally, I am greatly indebted to my husband and to my children, Diar, Dalia, and Tania Alazawi, for their continued love, support, and patience. I also recognize my parents, for their constant encouragement and loving support throughout this work. Special acknowledgements are extended to my aunt, Pakhshan Najeeb, whose support is dearly recognized.

Financial support provided by the Natural Sciences and Engineering Research Council (NSERC) of Canada and University of Saskatchewan is thankfully acknowledged.

DEDICATION

Lovingly dedicated to
my supportive husband Mohamad, and
to dear children
Diar, Dalia and Tania Alazawi

(You are the light of my life)

In memory of my father
Mohamad Alzahawi

TABLE OF CONTENTS

Page

LIST OF FIGURES

Page

LIST OF TABLES

Page

LIST OF SYMBOLS AND ACRONYMS

AC	Alternating Current
ADC	Analog-to-Digital Converter
AVR	Automatic Voltage Regulator
CPU	Central Processing Unit
DC	Direct Current
DFT	Discrete Fourier Transform
DSP	Digital Signal Processors
EMS	Energy Management Systems
EPRI	Electric Power Research Institute
FTS	Full Time Scale
GPS	Global Positioning System
HVDC	High Voltage Direct Current
LOE	Loss of Excitation
LPC	Local Protection Centers
LS	Least Square
MSC	Mechanically Switched Shunt Capacitors
OLTC	On Load Tap Changer
OSC	Out of Step Characteristics
pu	Per Unit
PLC	Power Line Carrier
PMU	Phasor Measurement Units
PQ Bus	Active-Reactive Power Bus
PSA	Power System Automation
PT	Potential Transformer
QoS	Quality of Service
QSS	Quasi Steady-State
RAS	Remedial Action Schemes
SCADA/EMS	Supervisory Control and Data Acquisition/ Energy Management Systems

SPC	System Protection Center
SPS	System protection schemes
STATCON	Static Condensers
SVC	Static Var Compensation
SVR	Secondary Voltage Regulator
TEPCO	Tokyo Electric Power Company
VAR	Volt-Ampere Reactive
VCPI	Voltage Collapse Prediction Index
VHF/UHF	Very High Frequency / Ultra High Frequency
VIP	Voltage Instability Predictor
WAMS	Wide Area Measurement System

1. INTRODUCTION

1.1 Background

Angular stability and thermal overload capability of transmission lines have been major concerns in power system planning and operation for many decades. Power systems, however, have been operated closer to the limits of stability in the last three decades due to economical and environmental constrains. As a consequence, many systems around the world have experienced loss of voltage stability leading to partial or complete system collapse. A loss of voltage stability event is characterized by a slow change in the steady state operation of the system due to either load increase, due to contingences that cause gradual decrease in voltage magnitude or both until a sharp and accelerated decrease in voltage occurs [1, 2].

Bus voltage angle and frequency usually remain fairly constant prior to the sharp decrease in voltage magnitudes. The voltage control devices do not activate tap-changers because the voltage magnitudes prior to the sharp decrease lie within a permissible range. After the voltage decreases sharply, under-voltage relays trip and disrupt the network before operators at the control center observe any warning signals.

Voltage collapse phenomenon has received increased attention during the past many years and many papers have been published on this subject [3,4,5]. Several approaches have been proposed to detect voltage collapse so that the power system assets are better utilized. Both dynamic and steady state behaviour of voltage collapse have been studied, but very few protection and control schemes have been implemented.

The development of wide area protection systems has made it possible to monitor network stability and take remedial action to prevent critical situations such as voltage collapse. A new special protection scheme was designed and tested during the course of research reported in this thesis. This protection scheme is able to detect if a voltage collapse is likely to occur. The developed technique uses voltage and current measurements from the local bus as well as voltage and current

measurements from nearby buses. It examines not only the present state of the system but also takes into account future load changes.

1.2 Voltage collapse incidents

There have been numerous incidents of voltage collapse over the previous thirty years. Investigations of recent blackouts have indicated that loss of voltage stability is one of the major causes of loss of transmission lines that interconnect adjoining power systems [6,7]. Analysis of voltage collapse incidents is difficult because information about disturbances, human interaction, frequency deviation, etc. is not available in adequate detail and with sufficient accuracy. However, the following factors are common in several voltage collapse incidents.

- Transmission system limitations: Transmission system is unable to transmit reactive power to some areas when small generators in those areas either trip or are taken out of service. Inadequate reactive power support leads to voltage decline that becomes worst as the load in that area increases. Two out of many such examples are briefly described to illustrate the nature of the voltage collapse incidents [8].

  A major power system outage occurred on November 9, 1965 in New York, USA. The main cause for the outage was inadequate capacities of the transmission lines between northeast and southwest regions of the system.

  The Niagara Falls hydroelectric station of Ontario Hydro was supplying energy to the USA over five 230 kV transmission lines. The backup relay provided on one of the lines operated and tripped the line. This resulted in increased power flow on the remaining four lines. The voltage in the power system of the New York state decreased that increased the reactive power demand of the loads.

  The overloading of the remaining four lines from Niagara Falls generating station to the New York state resulted in the loading of lines. An overcurrent relay on another line disconnected it from the system. This continued until all lines connecting the Niagara Falls

generating station with the power system of the New York state were out of service. This resulted in overloading of the power system in the New York state tripping several lines in that system and causing an outage that affected 30 Million people and lasted 13 hours.

The second example of system collapse that was initiated because of inadequate capacity of transmission lines capacity was in the USA and Canada on August 14, 2003. Sixty three GW of load was interrupted resulting in a blackout that affected 50 million people. In this event 400 transmission lines and 531 generating units at 261 power plants were tripped. The major reason for the system collapse was insufficient capacity for generating reactive power that led to voltage collapse [9].

This power failure started in Ohio with the tripping of voltage regulator of Generator No. 5 of the East-Lake station due to over excitation. The generators at East-Lake were supplying power to loads located in northern Ohio. The reactive power demand on the East-Lake station continued to increase as the day progressed.

The 345 kV Chamberlin-Harding transmission line in Ohio was loaded with 44% of summer normal/emergency rating and tripped 90 minutes after the tripping at the East-Lake generating station due to a tree coming in contact with the line. Thirty eight minutes later, Hanna-Juniper 345 kV line that was loaded with 88% of summer emergency rating tripped due to another tree coming in contact with the line. This cascading loss of lines continued while load was shed or was disconnected due to the protective relays operating and tripping circuit breakers.

Finally, the zone 3 of the distance relays protecting the 345 kV Sammis-Star tie line operated due to line overload and depressed bus voltage and tripped the line circuit breaker. This led to further decrease of voltage in the system. Due to the cascading loss of major tie lines in Ohio and Michigan, the pattern of power transfer between the U.S. and Canada on the Michigan boarder changed. Power started flowing from Pennsylvania, to New York and then to Ontario and finally into Michigan and Ohio. The 3700 MW power flow was for loads in Michigan and Ohio, which was at this stage supplied from all other generation systems except Ontario. At this point, voltage collapsed due to heavily loaded transmission

lines resulting in cascaded outages of several hundred lines and generators that eventually led to major outage in large parts of Canada and USA.

- Load behaviour including on-load tap changers: On-load tap changer and load dynamics are major factors in several system collapse incidents [10]. Load recovery and/or operation of on-load tap changers aggravate a situation when system voltage starts to decline.

  The power system of the Tokyo Electric Power Corporation (TEPCO) experienced voltage collapse on July 23, 1987. The local temperature at that time was 39^0 C. On July 22, (TEPCO) forecasted that the next day's maximum power demand would be 38.5 GW if the temperature is 34^0 C and would be 40 GW if the temperature is 36^0 C. The disturbance was initiated on July 23 when the demand at 01:00 PM was 39.1 GW and was increasing at a rate of 400MW per minute. This exceeded the forecasted load demand. The voltage gradually dropped. The reactive power supply from generators increased and additional shunt capacitors connected to the 500 kV transmission network were switched on. The voltage of the 500 kV lines reduced to 460 kV at 01:15 PM when the load reached 39.3 GW. The voltage reduced further to 370 kV in the western part of Tokyo and to 390 kV in the central part of Tokyo at around 01:19 PM. Circuit breakers controlling transmission lines tripped due to the operation of protective relays. This resulted in the interruption of 8.16 GW of load and affected 2.8 million customers. The system was brought back to service at around 04:40 PM. The reason for the decline of voltage was that the power factor of the air conditioner motors became more lagging resulting in very high reactive power demand for operation at the low voltage levels. This characteristic is believed to have accelerated the voltage collapse [11].

- The influence of protection and control systems: Several system collapse incidents were caused by proper operation of protection devices and controllers.

  Nelson River HVDC system collapsed in April, 1986. An inverter transformer at the Dorsey station (southern end of the two ± 450 kV dc lines) was energized that resulted in large magnetizing inrush current flow into the transformer. This reduced the bus voltage at the converter station. The synchronous generators provided at the Dorsey station could not

generate enough reactive power to keep the voltage at the desired level. Consequently, the dc voltage at the Dorsey end of the dc line decreased substantially. The dc power flow controllers tried to maintain the power flow on the dc line at the set value but could not because the current flow on the line could be increased beyond the capacity of the converters. Voltage collapse occurred because the controllers could not regulate the voltage and keep it at an acceptable level. The undervoltage protection blocked the inverters and interrupted power flow on the line. This effectively resulted in the AC system in southern Manitoba having inadequate availability of power [12].

1.3 Literature review on voltage collapse

Traditional methods of voltage stability investigations have relied on static analysis using the conventional power flow models. These methods were considered viable because of the view that the voltage collapse is a relatively slow process and is, therefore, primarily a small signal phenomenon. The various analytical tools classified under steady state analysis were considered sufficient to address the phenomenon of voltage collapse. A variety of techniques, such as, the P-V curve, Q-V curve, eigenvalue approach and singular value approach, and sensitivity and energy based methods have been proposed [13, 14]. Ajjarapu studied the voltage collapse problem as a static bifurcation characterized by the disappearance of an equilibrium point and showed that bifurcation could describe instability in the magnitude and phase angle of the voltage [14, 15]. Thomas proposed the use of the minimum singular value of the Jacobian of the descriptor load flow equations, called a security index, and derived static control strategies based on the index. Glavistch developed a voltage stability index based on a feasible solution of power-flow equations [16]. Schleuter proposed definitions of voltage stability and voltage controllability that are based on the static analysis at major PQ buses in the power system under normal conditions and derived control criteria based on a linearized set of equations and their definitions [17].

Very few real-time methods that predict proximity to voltage collapse and take corrective actions have been proposed [18,19,20,21]. Gubina and Strmenil proposed voltage collapse index using only the voltage phasors at system buses and the technique is able to identify the critical transmission path for real and reactive power flow by computing a transmission path stability index [18,22].

Gubina proposed second technique to determine the maximum load that could be supplied at a particular bus in a power system by assuming that the load at the other buses remains constant [19]. This is not a realistic assumption. A simple and straightforward technique, which measures voltages and currents, and determines the maximum active and reactive power load that could be supplied at a bus is proposed by Haque [20, 21]. This technique monitors the load and continuously updates the values of the maximum load that can be supplied and calculates the voltage stability margin of the system.

The code-named SMART [Stability Monitoring and Reference Tuning] technique uses only local voltage and current measurements and calculates the maximum load that the transmission system can supply to a load bus [7]. This technique assumes that the voltage collapse occurs when the local load approaches the calculated maximum load. Although this approach is simple enough to be implemented in numerical relays, it is not capable of tracking load changes caused by voltage drop at nearby buses. Thévenin equivalents seen from other load buses are not observable in this technique.

1.4 Objectives of the research

As is evident from the voltage collapse incidents presented in Section 1.2, there is a real need to study, analyze and design a new technique that is suitable for use in a protection system for identifying an impending voltage collapse and taking remedial measures. The following main objectives of this research were, therefore, selected:

- Study the dynamic aspects of voltage collapse and investigate the existing literature relating to system collapse analysis;
- Estimate system parameters using Delta and Least Square (LS) techniques associated with Cumulative Sum Filter (CSF) to smoothen the estimation results;
- Design and implement an approach to prevent voltage collapse and initiate control actions to maintain system voltage stability when the system is approaching point of collapse;

- Create a new component in PSCAD/EMTDC to support continuous load flow studies and voltage stability analysis.

1.5 Outline of the thesis

This thesis is organized into six chapters and five Appendices. The first chapter introduces the subject of the thesis and describes its organization. It also presents a brief introduction on power system instability and provides background information of a few voltage collapse incidents. Important conclusions and objectives of the previously conducted research on this topic are drawn from the previously published literature.

The concepts of system collapse phenomenon are discussed in Chapter 2. An introduction to static voltage collapse and a simple example that illustrates this phenomenon are briefly presented as well. Factors affecting voltage collapse including reactive power capability and automatic voltage control of synchronous generators, loads, on-line tap changers and compensation devices are introduced. A number of countermeasures adopted by electric power utilities are discussed. The most commonly used methods for analyzing voltage collapse are introduced in section 2.6. An introduction to load flow analysis and a method of analyzing non linear equations are provided in this chapter because most of the analytical off-line techniques for voltage collapse studies are based on load flow equations. In addition to off-line methods, voltage collapse predictor and voltage collapse prediction index methods that are based on local measurements are presented in this chapter as well.

Literature review on previously used methods for system parameter estimation is provided in Chapter 3. The Delta and Least Square (LS) techniques were extended by using Cumulative Sum Filters (CSF) with them are presented. The main advantages and disadvantages of the developed techniques and the data window requirements for implementing the techniques are presented in this chapter as well. Results obtained from the implementing the techniques on an IEEE 30-Bus test system are presented.

An overview of the previously used techniques for analyzing the voltage collapse phenomenon and details of the developed time to voltage collapse technique are presented in Chapter 4. A brief description of local-based and subset-based techniques used for detecting voltage collapse is provided. The objective and motivation of the technique developed during the course of this research are reported in Section 4.3. The voltage collapse technique is explained by applying it to a two-bus system. A general form of the developed technique that takes into consideration measurements from N buses is then presented in Section 4.6.

Performance of the time to voltage collapse technique is studied in Chapter 5 by applying the developed technique to the IEEE 30-Bus test system. It is assumed in the first study reported in this chapter that voltage and current measurements are available from two load buses of the system and the load on one of the buses is increasing gradually. Then an outage of a transmission line is considered as part of the disturbance. Impact of load shedding is examined. The studies are then repeated with the assumption that data from three, four and then five load buses is available. The time to voltage collapse is calculated to demonstrate the suitability of the developed technique for implementation in an on-line mode as part of a system protection scheme. A comparison of the off-line results of the developed technique and its application on the PSCAD/EMTDC software is presented in this chapter as well.

Summary of work and main conclusions that can be drawn from this research are presented in Chapter 6. This final chapter is followed by a list of references. In appendix A the connectivity and electrical parameters of the IEEE 30-Bus test system used for studies reported in Chapters 3 and 5 are presented. In order to compute time to voltage collapse at any point in the power system, a set of parameters must be calculated for each measurement. Finding the general expression for these parameters can be difficult if not impossible for large power systems without the use of a symbolic calculation program such as MAPLE. In Appendix B, the MAPLE functions for calculating the parameters for time to voltage collapse technique are presented. The theoretical background of Phasor measurement units and synchronized phasor measurement units are introduced in Appendix C. In addition to the estimation techniques (Least Square and Delta) for system parameter identification presented in Chapter 3, there is another method not further developed in this thesis because the results obtained are similar to those generated by the Delta method. The method called Polar Coordinate technique and is presented in Appendix D. The proposed methodology for

creating a new PSCAD/EMTDC component called Variable Load Component is presented in Appendix E.

1.6 Contributions

The contributions made by the research project reported in this thesis are as follows:

- Delta and LS techniques have been modified and have been associated with CSF to monitor current and voltage measurements while estimating the parameters of system's Thévenin equivalent.

- A new technique to predict voltage collapse using a subset of measurements has been developed. The developed technique is able to track a dynamic system trajectory in an on-line mode.

- A relay that uses the developed technique can process local voltage and current measurements as well as measurements from surrounding buses.

- When the system is approaching voltage collapse, the developed technique is able to initiate control actions for preventing major disturbance.

- The developed technique is able to track the system trajectory taking into consideration load changes likely to be experienced in the near future.

1.7 Summary

An overview of voltage collapse phenomenon is presented in Chapter 1. Investigations on major disturbances that lead to voltage collapse and investigations of blackouts caused by loss of voltage stability are summarized in Section 1.2. Literature review on voltage collapse studies is presented in Section 1.3. Research objectives, thesis organization and major contributions of this thesis are included in this chapter as well.

2. VOLTAGE COLLAPSE IN POWER SYSTEMS

2.1 Introduction

The concepts of voltage collapse and some voltage collapse incidents have been introduced in chapter 1. A literature review of voltage collapse has been presented in that chapter as well. The objectives and organization of this thesis and specific contributions of the research project have been included also in chapter 1.

An overview of voltage collapse phenomenon is presented in this chapter. Factors affecting voltage collapse and methods to overcome it are included in this chapter as well. Static and dynamic techniques used in voltage collapse analysis including methods based on local measurements are presented.

2.2 Voltage collapse phenomena

Economic considerations have dictated that transmission lines be loaded to their thermal limits. The increased loading of lines, insufficient reactive power generation and transmission of large loads over long distances has resulted in incidents of power system operation at lower than acceptable voltage. When a system is allowed to operate at low voltage and load continues to increase, the voltage decreases further. If the load is reduced, the voltage increases. However, a stage comes when the voltage drops to such a degree that reduction of load does not result in voltage increase, this is called voltage collapse [23].

The following changes in a power system contribute to voltage collapse.

- Increase in load

- Operation of generators, synchronous condensers and / or static VAR compensators (SVC) at their reactive power limits

- Outages of transmission lines and / or generators

2.3 Analysis of power system voltage collapse (a simple example)

The characteristic of voltage collapse is illustrated by considering a two-Bus system shown in Figure 2.1. An energy source is connected to Bus 1; the source is a large capacity power system that is represented by an equivalent generator. Energy is supplied to the load by Bus 2. Bus 1 is connected to Bus 2 by a transmission line. The resistance and capacitance of the source impedance and transmission line are neglected in this discussion to keep the discussion simple. It is assumed that the energy system connected to Bus 1 can supply all the reactive power needed by the load and needed for reactive power losses in the source impedance and transmission line. Now consider that the voltage at Bus 2 decreases because the load increases.

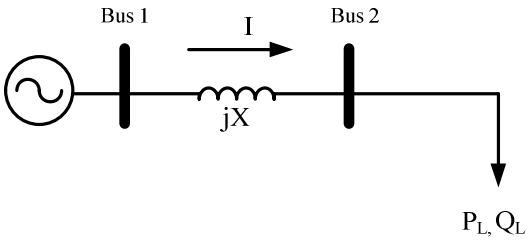

Figure 2.1: A two – Bus system

The complex power supplied to the load can be expressed as

$$P_L + jQ_L = V_L I^* \tag{2.1}$$

where,

P_L is the real power supplied to the load,

Q_L is the reactive power supplied to the load,

$V_L\angle 0^o$ is the voltage at Bus 2, and

I^* is the conjugate of the current phasor.

The current in the transmission line is same as the current in the load. The current flowing in the line can be expressed as a function of the Electro Motive Force (EMF) of the source and voltage of Bus 2 as follows.

$$I = \frac{E_g\cos\delta + jE_g\sin\delta - V_L}{jX} \tag{2.2}$$

where,

$E_g\angle\delta$ is the induced EMF of the equivalent source, and

X is the sum of the reactance of the source and transmission.

Substituting Equation 2.2 in Equation 2.1 provides

$$P_L + jQ_L = V_L\left[\frac{E_g\cos\delta + jE_g\sin\delta - V_L}{jX}\right]^* . \tag{2.3}$$

Rearranging Equation 2.3 provides the following equation.

$$P_L + jQ_L = \frac{V_L E_g\sin\delta}{X} + j\frac{V_L Eg\cos\delta - (V_L)^2}{X} \tag{2.4}$$

Equating the real and imaginary parts of this equation provides the following two equations.

$$\sin\delta = \frac{P_L X}{E_g V_L} \tag{2.5}$$

$$\cos\delta = \frac{Q_L X + V_L^2}{E_g V_L} \tag{2.6}$$

Squaring the left hand sides of these equations and adding them is equal to unity. Therefore, the sum of the squares of the right hand sides of these equations should also be equal to unity. Doing this provides the following equation.

$$(V_L^2)^2 + (2Q_L X - E_g^2)V_L^2 + X^2(P_L^2 + Q_L^2) = 0 \qquad (2.7)$$

Solving this quadratic equation provides

$$V_L^2 = \left[\frac{E_g^2 - 2Q_L X}{2} \pm \frac{1}{2}\sqrt{(E_g^2 - 2Q_L X)^2 - 4X^2(P_L^2 + Q_L^2)} \right]. \qquad (2.8)$$

The real values of $(V_L)^2$ have a physical significance because V_L is a real number. The voltage at Bus 1 is, therefore, given by

$$V_L = \frac{1}{\sqrt{2}}\left[\left(E_g^2 - 2Q_L X\right) \pm \sqrt{(E_g^2 - 2Q_L X)^2 - 4X^2(P_L^2 + Q_L^2)} \right]^{1/2}. \qquad (2.9)$$

This equation provides two values of V_L for a pair of given values of P_L and Q_L (assuming that E_g remains constant) except when $(E_g^2 - 2Q_L X)^2 - 4X^2(P_L^2 + Q_L^2)$ is equal to zero. One solution of V_L has a larger value than the other solution. The voltage at Bus 2 is in a stable state when the voltage is at the larger value given by Equation 2.9. The system is in the voltage collapse mode when the voltage is at the lower value given by Equation 2.9. The voltage collapses when the real and reactive power load at Bus 2 is such that $(E_g^2 - 2Q_L X)^2 - 4X^2(P_L^2 + Q_L^2)$ becomes zero.

The Active Power-Voltage (P-V) curves, when E_g is equal to 400kV and X is equal to $100\,\Omega$, are shown in Figure 2.2. (The ratio of reactive to real power is expressed as tanφ in this figure.) The P-V curves above the knee point represent stable operation and the curves below the knee point represent unstable operation. The knee point represents the load at which voltage collapse occurs.

Figure 2.2 also shows that the real power of load corresponding to voltage collapse increases as the reactive power component of the load decreases. This means that the capability of supplying loads can be increased by providing reactive power compensation at the load. This figure also shows that level of voltage at which it collapses is close to the normal operating level when the reactive power component of the load is compensated at the load Bus. The monitoring of power system security now becomes more complicated because the critical voltage is close to the normal operating range of the voltage.

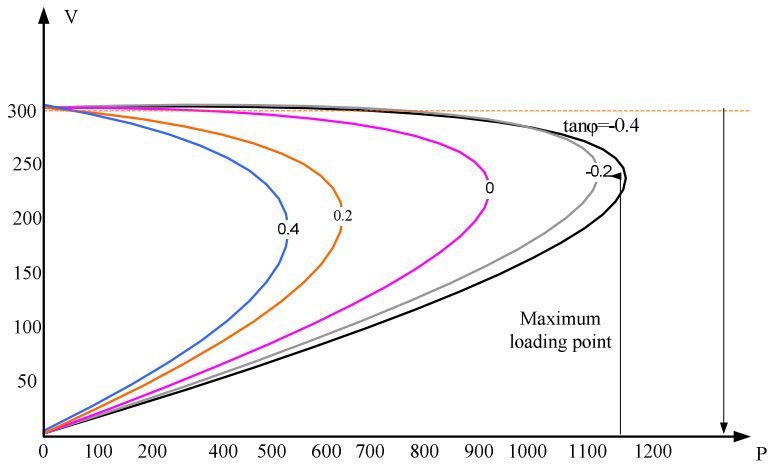

Figure 2.2: P-V curves for different values of real to reactive power ratios

2.4 Factors causing voltage collapse

Voltage collapse is a dynamic and normally large disturbance phenomenon, involving load, transmission and generation subsystems. There are several power system aspects known to contribute to voltage collapse. The following five factors are the major issues causing voltage collapse [24-25].

- Reactive power capability limits of synchronous generators
- Automatic voltage control of synchronous generator
- Loads
- On-line tap changers
- Compensation devices

2.4.1 Reactive power capability of synchronous generators

Voltage regulators of synchronous generators of a power system control their voltages that, in turn, determine the reactive power they provide to the power system. The generators have active and reactive power limits that are commonly displayed in the form of Active Power-Reactive Power (P-Q) diagrams. The active power limits are due to the capacities of their turbines provided enough fuel is available. There is no single value for reactive power limit of a generator; there are different values at different real power outputs. The reactive power limits are usually assumed to be constant values in load flow programs. The non-linear relationship of reactive power with real-power output is, however, an important aspect that should be considered in voltage collapse studies [26,27,28,29].

Reactive power supplied by a generator is normally limited by three considerations: armature current limit, field current limit and end region heating limit. When current flows in the armature, heat is produced due to I^2R losses. This increases the temperature of the armature. The insulation around the winding can withstand the temperature increase up to a certain level without deteriorating. The maximum current that can be carried by the armature is determined by this consideration. Similarly, heat is produced due to current flow in the field winding and the maximum current that can safely flow in the armature is established by its design. When a generator operated in an under-excited mode, localized heating in the end region of the armature occurs; this temperature increase limits the reactive capability of synchronous generators.

When reactive power limiters on generators operate to maintain the machines within their capability, these machines cannot do any more to support system voltages. Thus the operation of the limiters may be good indicators of impending voltage collapse [30, 31, 109].

2.4.2 Automatic voltage control of synchronous generator

Synchronous generators installed during the previous twenty years are equipped with microprocessor based voltage regulators. The voltage regulators try to maintain voltages at set values usually at their terminals. The voltage reduces when the system experiences a fault and during parts of a disturbance [32, 4]. The voltage regulators increase the excitation voltage thus increasing the excitation current for preventing voltage collapse. If the network voltage becomes

sufficiently low, either field current limit or stator current limit is hit. This will change the generator characteristic drastically. Also the condition is much worse if the stator current limit is reached. In this case, the reactive power from generator reduces fast, particularly if the network voltage is further reduced. This ultimately leads to voltage collapse [33, 34, 35, 36].

2.4.3 Loads

The modeling of loads including its dependence on voltage and its dynamics is essential in voltage collapse analysis. The modeling of voltage dependence of loads requires proper consideration of voltage control devices as well. The loads are usually considered to be connected to the system transmission buses. A more accurate model would be to represent voltage dependent loads on the secondary side of step-down transformers along with modeling of the tap changers and their control [37, 38]. Dynamic models for electrical motors are needed when the power system studies include significant motor loads.

2.4.4 On-line tap changers (OLTC)

The action of tap changers affects the voltage dependence of load seen from the transmission network. Typically, a transformer equipped with an on-load tap changer feeds a distribution network and maintains constant secondary voltage. When voltage decreases in the distribution system, the load also decreases. The tap changer operates after a time delay if voltage reduction is large [39].

The action of an on-load tap changer might be dangerous for power system during a disturbance. Following a disturbance, on-load tap changers try to restore the voltage on the secondary side of the distribution transformers at the desired values. Load restoration leads to increased power flow in transmission lines and increase in power losses in the transmission system. This aggravates the situation on the primary side of the transformer particularly when the system is already stressed for reactive power shortage. This is likely to result in voltage collapse. Frequently on-load tap changer blocking is used by electric utilities as a countermeasure to prevent voltage collapse. [40, 41, 42].

2.4.5 Compensation devices

The aim of reactive power compensation is to improve the performance of power system operation. The compensation is needed to control the reactive power balance of the power system. These devices are also used for minimizing reactive power losses and keeping a flat voltage profile in the network. The sources of reactive power are usually located close to the reactive power loads.

The equipment used for compensation is capacitors, reactors, synchronous generators/compensators and static VAR compensators. The reactive power compensation devices should be modeled at the appropriate voltage level including their control logic to ensure that the true effect of these devices is modeled. Switched shunt compensation is used instead of fixed shunts to take into account the voltage control in the network. The static VAR compensators can be modeled as a generator when the reactive power demand is within limits, as a capacitor when the reactive power demand is higher than the maximum limit and as a reactor when the reactive power demand is lower than the maximum limit [43].

2.5 Countermeasures for voltage collapse

Voltage collapse countermeasures have been promoted as a result of major system outages caused by the voltage collapse phenomenon. A number of countermeasures adopted by electric power utilities are presented as follows [44, 45]:

1. Reinforce the power system
2. Improve system controllers
3. Enhance operational practices
4. Monitor the system on the real-time basis
5. Incorporate system-protection systems.

2.5.1 Reinforce the power system

When environmental, political, and other considerations do not permit the building of new transmission lines and/or generating stations near populated load centers, other solutions are sought. One of the approaches is to decrease transmission impedances to decrease voltage drops over long lines. This is done in many different ways. For example, adding series compensation and/or adding additional conductors in transmission line phases are presented [46]. These advantages are, however, weighed against other considerations such as cost, increase of complexity of protection, the impact of bypassing the capacitors and sub synchronous resonance.

Shunt compensation has been the traditional way of providing additional reactive power needed to maintain a good voltage profile. Capacitor banks are located near load centers to improve the power factor and to compensate for reactive losses in sub transmission systems. Excessive shunt compensation, however, has the drawback of bringing the maximum load power point closer to the normal operating values making it difficult to predict voltage collapse [47].

2.5.2 Improve systems controllers

Several options exist for emergency controls that will countermeasure voltage collapse. The emergency controls can be classified as follows according to their cost that includes also the nuisance caused to consumers whose service is disrupted [48].

1. Reactive shunt element switching and special generator voltage controls have no negative impact on consumers or other operational cost and are normally first to be utilized [49].

2. Generation rescheduling, as well as fast unit start-up, do not affect the consumers, but they have a definite impact on the market and thus are controls that are associated with low additional costs.

3. Emergency controls have no direct cost, but affect the load power, as well as the quality of power delivered to consumers. They are thus also classified as intermediate cost countermeasures.
4. Finally, load shedding is a countermeasure to save an unstable system as a last resort if no other alternative is able to stop an approaching collapse.

2.5.3 Operational planning and real-time evaluation

Preventive evaluation of voltage security has been an important issue in operation planning of power systems. Furthermore, security limits frequently require taking into account dynamics of voltage collapse [50,51]. In operational planning, fundamental decisions for security purposes are commitment of thermal units and determination of the best time to use hydro resources to substitute thermal generation units. Deregulation and explicit consideration of fuel stocks are significantly changing the context in which such decisions are taken. Security margins between all power market operators such as transmission system operators and generation companies are checked. The generation companies should also manage their hydro resources so that their water value equals their thermal marginal cost and their marginal revenue in the wholesale electricity market.

Congestion due to voltage security may appear in real-time operation. Preventive control may consist of rescheduling generation and shifting units from cheaper plants located far from load centers to more expensive units that are closer to load centers. In some cases, it may be necessary to shed-load if the voltage security margin is insufficient [52].

2.5.4 Special protection schemes (SPS)

A System Protection Scheme (SPS) is a protection system that is designed to detect abnormal conditions and take, predetermined, corrective actions, other than the isolation of faulted elements, to preserve system integrity and restore acceptable system performances [53, 54, 55]. In recent years, several types of SPS have been proposed and implemented. A decentralized SPS uses local measurements and acts on local devices. On the other hand, a wide-area SPS collects data from several locations and acts on devices located in several places of the system; Figure 2.3 shows the

general structure of a SPS. Decentralized SPS are more reliable, since they do not rely on an extensive telecommunication system. On the other hand, they may lack the system view needed to coordinate competing controls [56, 57, 58].

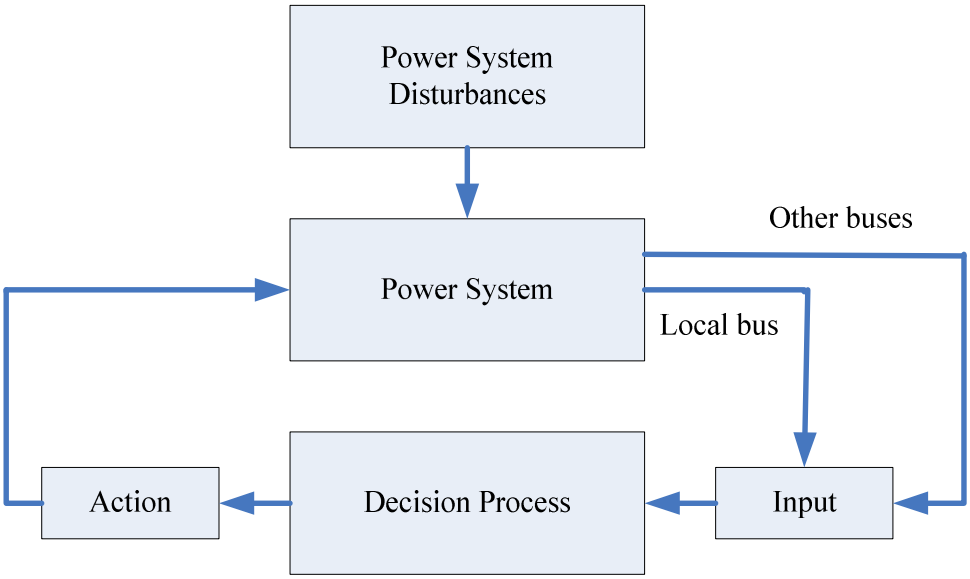

Figure 2.3: Special Protection Scheme (SPS) block diagram

The SPS is classified according to the following criteria.

1. Response-based: A response-based system relies on measurements of electric quantities, such as voltage and frequency, to identify system misoperation [59, 60, 61, 62].

2. Event-based: An event- based systems SPS operates upon the recognition of a particular combination of events. Event-based system is expected to be faster than response-based systems that have to wait for the system response to a specific event before acting. They are appropriate in cases where the threatening disturbances can be clearly identified. However, response-based SPS are more robust, since they work by observing the consequences of disturbances without attempting to identify them [11-24].

3. Rule-based: A rule-based system relies on "if ... then ..." rules, for example comparison of measurements with thresholds. Rule based SPS are comparatively simpler, although the embedded rules have to be properly tuned.

4. Algorithmic decision-based: An Algorithmic decision-based system relies on a more involved analysis of a model of the system. Algorithmic systems rely on a model of the system, they are in principle better prepared to face unforeseen disturbances and adapt their action to the severity of the situation. On the other hand, the more detailed the model, the lower the robustness with respect to modelling and real-time data inaccuracies, and the higher the dependency upon the real-time information system.

5. Closed-loop and open loop: A closed-loop system works in closed loop when it is able to act several times, each action relying on the measured result of the previously taken actions. When the counteracted phenomena make it possible, closed-loop SPS combine selectivity and dependability: since they are allowed to operate as many times as needed, they automatically adapt their action to the severity of the disturbance. Furthermore, this increases the SPS robustness against the inevitable uncertainties in system behaviour. This is particularly important in voltage stability studies, where loads plays a central role while their composition changes with time and their behaviour under large voltage drops may not be known accurately.

2.6 Methods for voltage collapse analysis

The techniques for analyzing voltage collapse can be classified in two categories, static analysis techniques and dynamic analysis techniques. Static analysis techniques consist of solving algebraic equations and, therefore, are computationally more efficient than the dynamic analysis techniques. These techniques are ideal for most studies in which voltage collapse limits for many pre-contingency and post-contingency cases is to be determined [63, 64, 15, 49]. Static voltage-collapse techniques use load flow equations to obtain information on the system operating state. All dynamics are ignored and it is assumed that all controllers have performed their intended functions properly. The results obtained from these studies are usually optimistic compared to the results obtained by dynamic analysis [65, 66, 67, 47].

Dynamic analysis consists of time-domain simulations that solve nonlinear differential equations. The procedure is computationally time consuming and cannot be applied for on-line analysis, monitoring and protection. The time domain simulations, however, capture the events and chronology that lead to voltage collapse when post event analysis is performed but they do not readily provide information regarding the sensitivity or degree of stability [68].

The main disadvantages of dynamic simulations are as follows.

1. They are time-consuming in terms of the time computers take to complete the studies.

2. They require substantial engineering effort for analyzing the results.

Most of the methods used for voltage collapse analysis are evaluated by using load flow study, basic load flow equations are, therefore, discussed in the following section.

2.6.1 Load flow equations

Load flow is normally used to calculate parameters, such as voltage magnitudes and phase angles for all buses in the system and active and reactive powers flowing in each line. The current injected into bus m of a power system represented by N buses is given by the following equations, where $m \neq k$.

$$I_m = \sum_{k=1}^{N} Y_{mk} V_k. \qquad (2.10)$$

where,

Y_{mk} is the mutual admittance between Buses m and k,

V_k is the voltage at Bus k, and

I_m is the current injected into Bus m.

Complex conjugate of the power injected into Bus m is:

$$P_m - jQ_m = V_m^* I_m. \tag{2.11}$$

where,

P_m is active power entering the network at Bus m, and

Q_m is reactive power entering the network at Bus m.

Substituting Equation 2.10 into Equation 2.11 provides,

$$P_m - jQ_m = V_m^* \sum_{k=1}^{N} Y_{mk} V_m. \tag{2.12}$$

The voltage at a typical bus (Bus m) of the system is given in polar co-ordinates as shown in Equation 2.13.

$$V_m = |V_m| \angle \delta_m = |V_m| (\cos\delta_m + j\sin\delta_m). \tag{2.13}$$

where,

δ_m is the phase angle of the voltage V_m with reference to the sewing bus voltage.

Substituting Equation 2.13 into Equation 2.12 provides,

$$P_m - jQ_m = \sum_{k=1}^{N} |Y_{mk} V_m V_k| \angle \theta_{mk} + \delta_k - \delta_m. \tag{2.14}$$

where,

V_k is the magnitude of the voltage at bus k,

δ_k is the phase angle of the voltage V_k with reference to the sewing bus voltage, and

θ_{mk} is the 90 ^{o} impedance angle of the line mk.

Expanding Equation 2.14 provides active and reactive powers as follows,

$$P_m = \sum_{k=1}^{N} \left| Y_{mk} V_m V_k \right| \cos(\theta_{mk} + \delta_k - \delta_m). \tag{2.15}$$

$$Q_m = \sum_{k=1}^{N} \left| Y_{mk} V_m V_k \right| \sin(\theta_{mn} + \delta_k - \delta_m). \tag{2.16}$$

Equations 2.15 and 2.16 are known as static load flow equations. These equations are non-linear and therefore only numerical solution is possible. Load flow equations can be solved using various load flow techniques. Newton-Raphson method is the most widely used power flow calculation methods, which use the above equations as the basis for evaluating unknown parameters at any bus by iterative means.

$$\begin{bmatrix} \Delta P \\ \Delta Q \end{bmatrix} = [J] \begin{bmatrix} \Delta \delta \\ \Delta V \end{bmatrix} \tag{2.17}$$

where,

ΔP is the differences between the specified and calculated values of active power,

ΔQ is represents the differences between the specified and calculated values of reactive power, and

$[J]$ is a square matrix of partial derivatives called the Jacobian matrix.

The elements of the Jacobian matrix defines as, $[J_{PS}]$, $[J_{PV}]$, $[J_{QS}]$ and $[J_{QV}]$,

where,

$[J_{P\delta}]$ is a matrix of partial derivatives of active power with respect to voltage angle,

$[J_{PV}]$ is a matrix of partial derivatives of active power with respect to voltage magnitude,

$[J_{Q\delta}]$ is a matrix of partial derivatives of reactive power with respect to voltage angle, and

$[J_{QV}]$ is a matrix of partial derivatives of reactive power with respect to voltage.

2.6.2 P-V and Q-V curves

Voltage collapse analysis is still widely studied by computing the P-V and Q-V curves at selected buses. A brief introduction to P-V curves are presented in Section 2.3. Q-V curves represent the plot of voltage at a test bus versus reactive power on the same bus for different real power requirements.

Generally, P-V and Q-V curves are generated by executing large number of load flows using conventional methods and models. While such procedures can be automated, they are time-consuming and do not readily insight into the cause of voltage collapse. These procedures focus on individual buses; the stability characteristics are established by stressing each bus independently. The bases selected for P-V and Q-V analysis should, therefore be chosen very carefully and a large number of such curves may be required to obtain all the information needed for power system.

2.6.3 Sensitivity method

Sensitivity analysis gives Voltage-Reactive power (V-Q) sensitivity at a bus for load changes. This method of voltage collapse analysis is also based on load flow simulations. This method uses Jacobian matrix used in Newton-Raphson method to determine the V-Q sensitivity at a bus [69-43].

It is assumed in this method that the system voltage is affected by reactive power requirements only. Incremental changes in the active power are neglected in the formulation. The effects of load changes in the system are taken into account by studying the incremental relationship between Q and V at different operating conditions.

Set, $\Delta P=0$, based on the above considerations, in Equation 2.17; this provides

$$[J_{P\delta}][\Delta\delta]+[J_{PV}][\Delta V]=[0], \tag{2.18}$$

$[\Delta\delta]$ can be obtained from the following equation.

$$[\Delta\delta]=-[J_{P\delta}]^{-1}[J_{PV}][\Delta V], \tag{2.19}$$

and,

$$[\Delta Q]=\left[J_{Q\delta}\right][\Delta\delta]+\left[J_{QV}\right][\Delta V]. \tag{2.20}$$

Substituting Equation 2.19 in Equation 2.20 provides,

$$[\Delta Q]=\left[J_{QV}-J_{Q\delta}[J_{P\delta}]^{-1}J_{PV}\right][\Delta V]$$

$$=[J_R][\Delta V] \tag{2.21}$$

where,

$$[J_R]=\left[J_{QV}-J_{Q\delta}[J_{P\delta}]^{-1}J_{PV}\right]. \tag{2.22}$$

From Equation (2.22),

$$[\Delta V]=[J_R]^{-1}[\Delta Q]. \tag{2.23}$$

The matrix $[J_R]^{-1}$ represents the reduced V-Q Jacobian. The k^{th} diagonal element of $[J_R]^{-1}$ represents the V-Q sensitivity at bus k. A positive V-Q sensitivity is indication of stable operation. As system get closer to voltage collapse, the magnitude of sensitivity increases. It becomes infinite at the point of collapse. The smaller the sensitivity, the more stable the system is. A negative V-Q sensitivity is indication of unstable operation.

2.6.4 Modal analysis

The model analysis computes the eigenvalues and associated eigenvectors of the reduced Jacobian matrix of the power system based on a steady state model of the system. A series of load flow simulations are conducted for load changes in a certain area. The reduced Jacobian matrix is calculated for every study [65,67]. The eigenvalues of the matrix are then calculated. The eigenvalues are associated with voltage and reactive power variation. The system stability can be evaluated by checking the status of those eigenvalues. If all the eigenvalues have a negative real part, the system is asymptotically stable. If one or more of the eigenvalues has a positive real part, the system is unstable. The system is critically stable if all the eigenvalues have negative real part but there is one eigenvalue with a purely imaginary part [70, 71, 72].

2.6.5 Local data based voltage collapse predictor

The local voltage stability monitoring and control is based on a two-bus equivalent system as shown in Figure 2.4. The supply system is represented by its Thévenin equivalent; Thévenin impedance Z_{th} and voltage E_{th} on Bus 1 which is seen from the terminals of the load bus of interest.

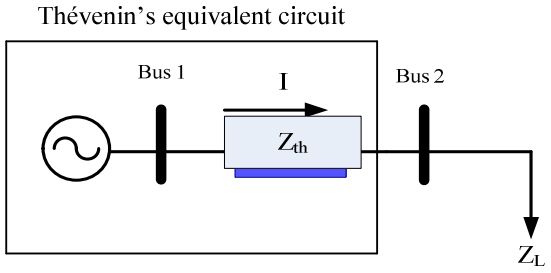

Figure 2.4: Local bus and the rest of the system represented by Thévenin equivalent

From electric circuit theory, it is known that the delivered power to bus 2 is maximized when the load impedance is the complex conjugate of the system impedance. This case however is not suited for power system applications because a high capacitive load would be required to match the

dominantly inductive nature of the system impedance. Half of the energy is consumed in transmission system as losses [73].

The maximum power transfer occurs when,

$$|Z_L| = |Z_{th}|. \tag{2.24}$$

Based on this fact, Khoi Vu has proposed a voltage instability predictor (VIP). In their work the ratio between the voltage and current phasors measured at the load bus is used to calculate the apparent impedance of the load (Z_{app}) [74,7]. Local bus and the rest of the system are treated as Thévenin equivalent circuit. The impedance plane is separated into two regions; the Thévenin impedance circle and the rest of the plane as is shown in Figure 2.5. As load varies, its apparent impedance traces a path in the plane, and voltage collapse occurs when load impedance crosses the Thévenin impedance circle. Indeed, VIP can be viewed as a voltage relay with an adaptive set point. In this work Thévenin equivalent is estimated using only local phasor measurements of voltage and current. The Thévenin equivalent parameters are estimated by the measurements taken at two more different times. It is assumed that source voltage and Thévenin impedance are constant during the estimation process [75].

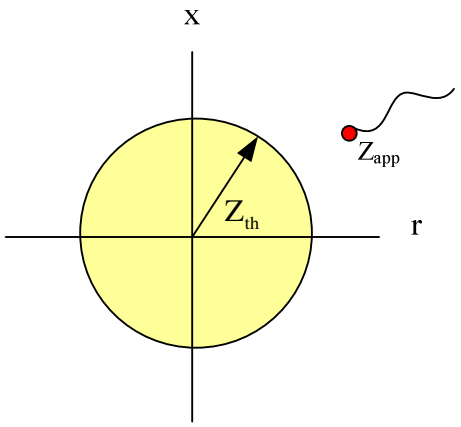

Figure 2.5: Voltage collapse occurs when the apparent impedance of the load bus equals the Thévenin circle

2.6.6 Power margin

The power margin index is used to track the closeness to voltage collapse. Power margin describes the proximity to voltage collapse in terms of power and can be looked upon as the power available before a power system collapses. It is defined as the power differences between the maximum apparent power and the actual system power. Power margin can also be defined as the extra MVA that can be delivered to the load before voltage collapse occurs. When the margin approaches zero, it means that no more power can be increased and system collapse will occurs if additional power is increased [4].

2.6.7 Line index

The line index (L) is simple to calculate because it utilizes information obtained from a normal load flow equation. The line index for a bus is a function of injected complex power, voltage and total impedances connected to the bus. The values of L index vary in the range between zero (no load condition) and one (voltage collapse condition). For a stable situation, the condition $L_j \leq 1$ must be violated at any of nodes.

2.6.8 Voltage collapse prediction index

The calculation of voltage collapse prediction index (VCPI) requires the voltage phasor information of the participating buses in a system and the network admittance matrix. The values of these indices determine the proximity to voltage collapse. The technique is first developed for a two bus system and extended to predict voltage collapse for an N bus system. The value of VCPI values varies between zero and one. If the index is zero, the voltage at the bus is considered to be stable and if the index is unity, the bus voltage is at the edge of collapse [11, 76, 77].

2.7 Summary

In this chapter, the concept of system collapse phenomenon has been discussed. An introduction to static voltage collapse and a simple example that illustrates this phenomenon have been briefly presented. Factors affecting voltage collapse including reactive power capability and automatic

voltage control of synchronous generators, loads, on-line tap changers and compensation devices have been introduced. A number of countermeasures adopted by electric power utilities such as system reinforcement, controllers improvements, operational practice enhancement, real time system monitoring and implementation of system protection schemes have been discussed in this chapter. The most commonly used methods for analyzing voltage collapse have been introduced in section 2.6 including off-line and on-line methods. Since most of the analytical off-line techniques for voltage collapse studies are based on load flow equations, an introduction to load flow analysis and a method of analyzing nonlinear equations have been provided. In addition to off-line methods, voltage collapse predictor and voltage collapse prediction index methods that based on local measurements have been presented in this chapter as well.

3. IDENTIFICATION OF THÉVENIN EQUIVALENT CIRCUIT PARAMETERS

3.1 Introduction

The concept of voltage collapse has been introduced in chapter 2. Factors affecting voltage collapse and methods to countermeasure it have been also discussed. Static and dynamic techniques used in voltage collapse analysis including methods based on local measurements have been presented.

An introduction of the previously proposed techniques for estimating system parameters and limitations of those techniques are discussed in this chapter. Least Square and Delta techniques were enhanced during this research by adding Cumulative Sum Filter. The development of the enhanced Delta and LS methods is also presented in this chapter. The original and enhanced delta and least squares techniques were applied to the IEEE 30-Bus test system. The results obtained from the applications of these techniques are presented in this chapter.

3.2 Overview of estimating system parameters

The Thévenin equivalent of a system at fundamental frequency usually provides enough information on the effects of changes in power system parameters and operating voltage at the load buses. From the knowledge of the Thévenin equivalent, the voltage collapse margin and maximum loadability of the system can be estimated. The published literature focuses primarily on determining the network equivalent impedance. Various proposals have been made ranging from simple models to sophisticated circuits to find the Thévenin equivalent.

The system is at the edge of collapse when the absolute value of load impedance is equal to the absolute value of the estimated Thévenin impedance [7]. This technique is unable to track system

changes and, therefore, is not able to update the Thévenin impedance. As a result, the technique may indicate that the estimated Thévenin impedance and the load impedance are equal, but in reality they are different and the system voltage is not collapsing.

The technique based on constant Thévenin voltage is also not able to track changes in the values of the Thévenin equivalent parameters [78, 79, 80]. In this reference, a time-domain method with tracking capabilities is proposed. The on-line identification procedure proposed with this technique is quite complex and takes considerable time to obtain a final conclusion.

The Constrained Least Squares method proposes an on-line identification procedure to estimate the equivalent impedance and voltage at the fundamental and harmonic frequencies [81,82]. The technique uses Kalman filters to estimate the phasors of voltages and currents as they change with time. The dynamics of the changes and the assumed dynamics in the design of the Kalman filters affect the performance of this technique.

A random load model is used in signal processing technique and the ratio of the cross-correlation of the changes in the load voltage and current with respect to the auto-correlation of the load current changes are used. Another signal processing technique is proposed; this technique is based on processing the data of voltages and currents at the load bus. The cross-correlation of the changes in the load voltage and current with respect to the changes in the load admittance is used to estimate the Thévenin impedance. The technique fail to estimate Thévenin impedance if topology changes due to switching operations initiated by the actions of protection devices or by actions taken by operators. Kalman filtering technique proposed to estimate system reactance and source voltage for out-of-step protection assuming that Thévenin resistance is zero [18].

As a part of research reported in this thesis, Delta and LS techniques were enhanced by Cumulative Sum Filters for estimating system parameters. The developed techniques are based on voltage and current measurements that can be obtained either from load flow simulations during power system planning or operating studies or from on-line measurements taken in real time during the operation of a power system. The techniques process the voltage and current phasors to continuously update the value of the system parameters. Further, this technique is better from the previously used methods because this technique needs smaller data windows compared to the large data windows

required by the previous techniques for suppressing oscillations in current measurements and for tracking system changes. The enhanced Delta and LS techniques are able to change the size of the data window to smoothen the estimates of the system parameters. They are able to track small changes in load and generation without numerical instabilities.

3.3 Thévenin equivalent circuit in voltage collapse studies

Thévenin parameters are the main factors that determine the maximum load that can be supplied at a bus [7]. Voltage collapse analysis methods that take into consideration local measurements are based on the well-known fact that the absolute values of the load impedance and the system Thévenin impedance are equal at the time of voltage collapse; this fact has previously been demonstrated in Chapter 2. The system is represented by a two-bus equivalent where one of the buses is the slack bus that is connected to a load bus by a transmission line as shown in Figure 3.1. The load impedance, Z_L is computed taking the ratio of voltage phasor, V_L, and current phasor, I_L, measured at the load bus. The rest of the system is treated as an equivalent circuit that consists of a Thévenin impedance, Z_{th}, and Thévenin voltage, E_{th}.

A single set of Thévenin parameters may not faithfully represent the rest of the system for the entire operating range. For example, the system shown in Figure 3.1 cannot be represented adequately if it has finite reactive power capability. It is necessary, therefore, to regularly update the Thévenin parameters as the system load or other operating parameters change. The least squares technique was reformulated to make it suitable for updating the Thévenin parameters conveniently. The modified technique is described in the next section.

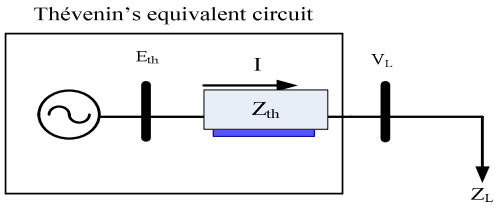

Figure 3.1: Local bus and the rest of the system as represented by Thévenin equivalent

The bus voltage can be expressed as a function of the load current and unknown parameters, E_{th} and Z_{th}, of the system equivalent as follows.

$$V_L = E_{th} - Z_{th} I_L \tag{3.1}$$

Equation 3.2 can be obtained by expanding Equation 3.1 to show the real and imaginary parts of the variables.

$$V_{L_r}(t_j) + jV_{L_i}(t_j) = [E_{th_r}(t_j) + jE_{th_i}(t_j)] - [R_{th}(t_j) + jX_{th}(t_j)][I_{L_r}(t_j) + jI_{L_i}(t_j)] \tag{3.2}$$

where,

V_{L_r} is the real part of load voltage V_L,

V_{L_i} is the imaginary part of load voltage V_L,

I_{L_r} is the real part of current I_L,

I_{L_i} is the imaginary part of current I_L,

E_{th_r} is the real part of Thévenin voltage E_{th}

E_{th_i} is the imaginary part of Thévenin voltage E_{th},

R_{th} is the real part of Thévenin impedance Z_{th}, and

X_{th} is the imaginary part of Thévenin impedance Z_{th}.

This equation can be separated in two linear equations with four unknowns as shown below:

$$\begin{bmatrix} V_{L_r} \\ V_{L_i} \end{bmatrix} = \begin{bmatrix} 1 & 0 & -I_{L_r} & I_{L_i} \\ 0 & 1 & -I_{L_i} & -I_{L_r} \end{bmatrix} \begin{bmatrix} E_{th_r} \\ E_{th_i} \\ R_{th} \\ X_{th} \end{bmatrix} \tag{3.3}$$

Thévenin parameters can be determined by using an identification technique, such as the enhanced Delta or Least Square methods that were developed as a part the research reported in this thesis.

Note that all of the variables in Equation 3.1 are functions of time and are calculated using a sliding window that contains discrete samples of data. The data window is small when the system operating state is changing but is large when the system operating state is stationary [83,84,85].

3.3.1 Trend of Thévenin impedance with increasing P-Q load

This section demonstrates that the Thévenin impedance increases when the P-Q loads supplied by the power system increase. A 3-Bus system shown in Figure 3.2 is used to demonstrate the trend.

Transmission lines impedances used in this example are impedances of typical 230kV line and are shown in Table 3.1 [34]. Transmission lines from Bus 1 to Bus 2 and from Bus 2 to Bus 3 were assumed to be double circuit lines. Line resistances and charging currents were ignored so that the calculations can be quickly verified, Bus 1 was assumed to be an infinite bus whose voltage was maintained at 1.05 pu. Bus 2 and Bus 3 are load buses that supply local P-Q loads. Base voltage, base MVA, base current and base impedance used in these calculations are 230 kV, 100MVA, 251A, and 529 Ω, respectively.

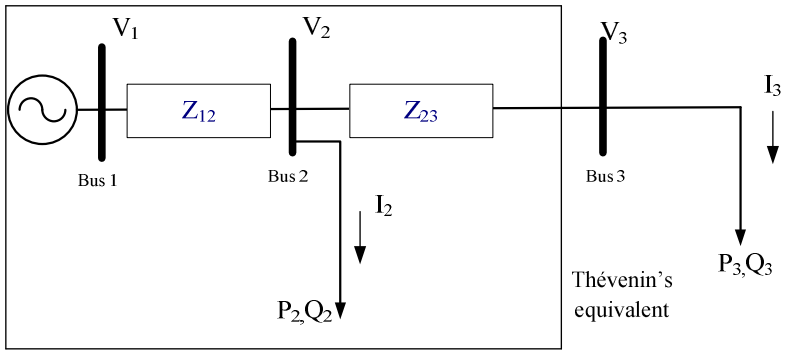

Figure 3.2: A three-Bus System

Table 3.1: 230kV transmission line parameters

r (Ω/km)	x_L (Ω/km)	b_C (μS/km)
0.0500	0.4880	3.3710

Thévenin parameters seen from Bus 3 were calculated for the system shown in Figure 3.2 using open circuit and short circuit tests as described in the following steps.

1. An open circuit test was done at to Bus 3 and Thévenin voltage (E_{th}) was calculated for a condition when there was no load connected to this bus (open circuit condition). Voltages at all buses, current flows in all lines and loads and line reactances used in the calculations are shown in Figure 3.3. The open circuit voltage at Bus 3 is shown in this figure.

2. A short circuit test was done at to Bus 3. Voltages at all buses, current flows in all lines and loads are shown Figure 3.4.

3. Absolute value of Thévenin impedance seen from Bus 3 calculated by substituting open circuit voltage and short circuits current from Figures 3.3 and 3.4 into Equation 3.4 is equal to 0.1249 pu.

$$Z_{th} = \frac{E_{th}}{I_{sc}} \tag{3.4}$$

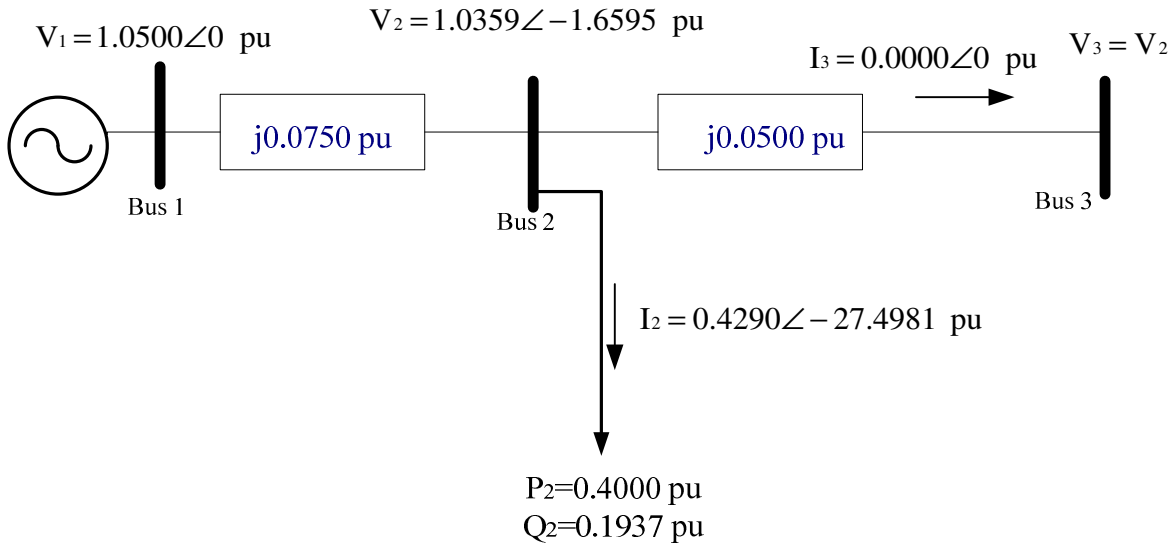

Figure 3.3: Open circuit test on Bus 3

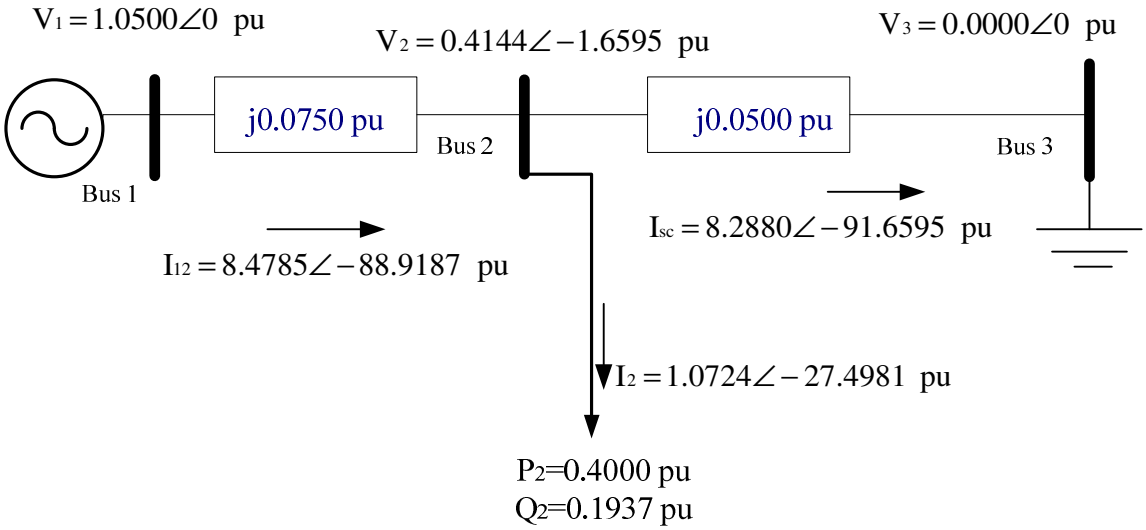

Figure 3.4: Short circuit test on Bus 3

The active and reactive powers on Bus 2 were increased to 0.5000 and 0.2423 pu, respectively and steps 1 and 2 were repeated to calculate the E_{th} and Isc. Voltages and currents for the open circuit and short circuit tests are shown in Figure 3.5 and Figure 3.6 respectively. The absolute value of the Thévenin impedance seen from Bus 3 is now equal to 0.1250 pu.

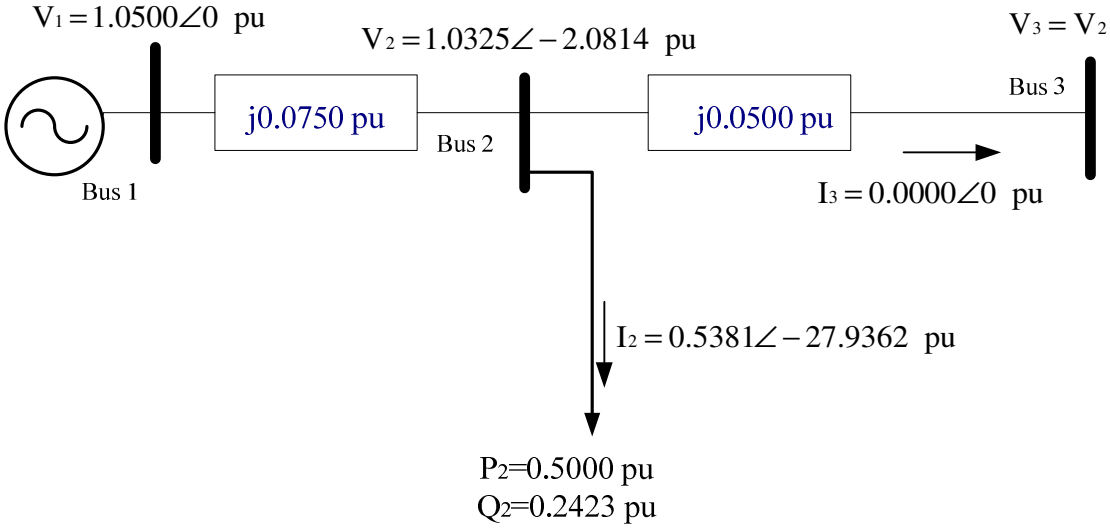

Figure 3.5: Open circuit test on Bus 3

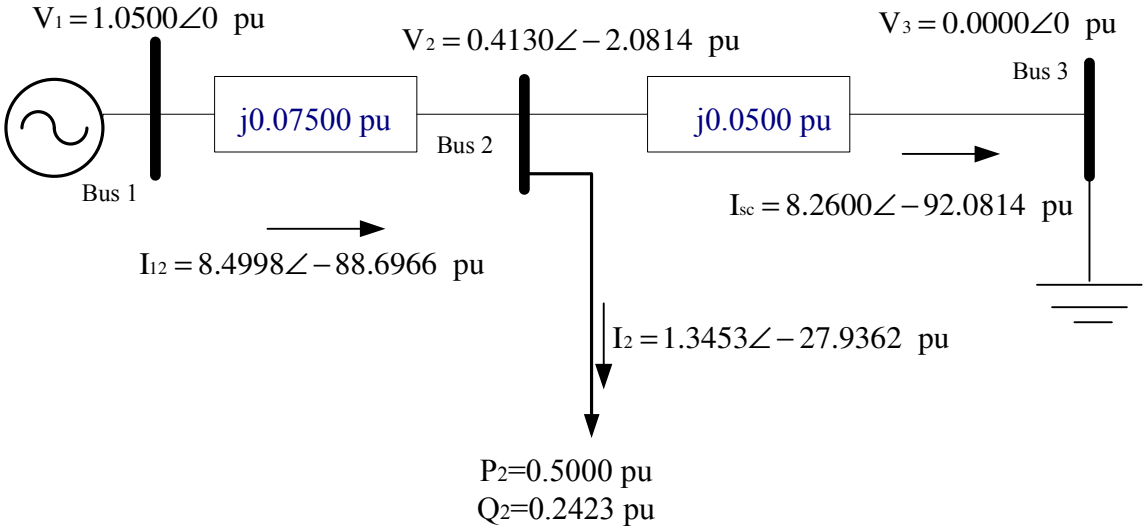

Figure 3.6: Short circuit test on Bus 3

Active and reactive power on Bus 2 were again increased to 0.6000 and 0.2907 pu, respectively and steps 1 and 2 were repeated to calculate the E_{th} and Isc. Voltages and currents for the open circuit and short circuit tests are shown in Figure 3.7 and Figure 3.8 respectively. The absolute value of the Thévenin impedance seen from Bus 3 is now equal to 0.1251 pu.

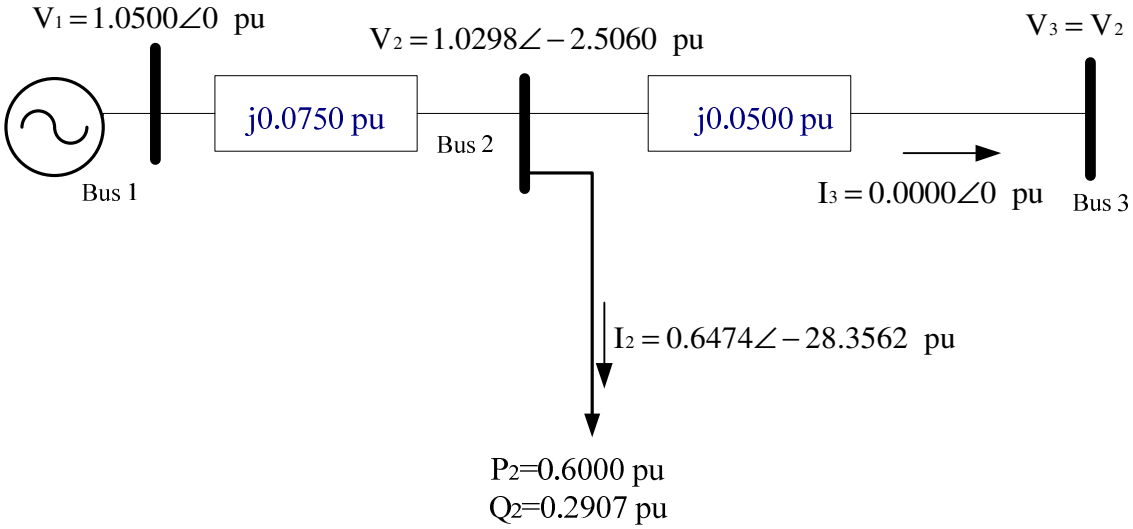

Figure 3.7: Open circuit test on Bus 3

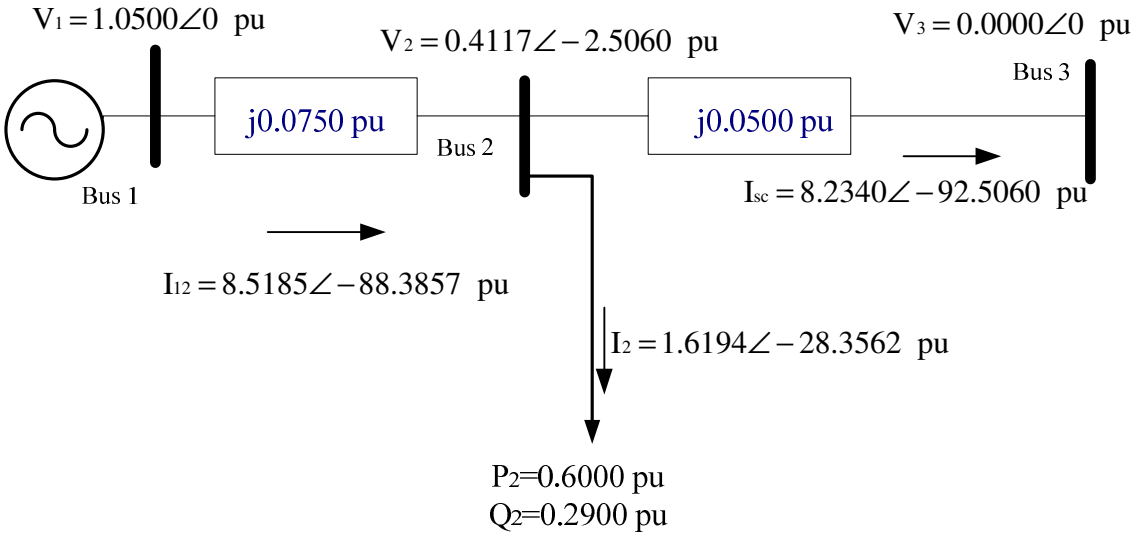

Figure 3.8: Short circuit test on Bus 3

This example demonstrates that increase of P-Q loads in the system results in an increase in the absolute value of the Thévenin impedance seen from a system bus. This finding is consistent with that reported in the published literature [7, 108].

3.4 System parameter estimating techniques

Thévenin parameters are determined by using parameter identification techniques. In this research Delta and Least Squares techniques were enhanced by including Cumulative Sum Filters and were then used for determining the parameters of the Thévenin equivalent. The Delta and Least Squares techniques are described in this section.

3.4.1 Delta technique

The Thévenin equivalent of the system shown in Figure 3.1 can be estimated using changes in measured phasors of the voltage at the load bus and load current by taking two successive measurements at time instances t_1 and t_2. The Thévenin voltages at these instants can be expressed by the following two equations.

$$E_{th}(t_1) = V_L(t_1) + Z_{th}(t_1)\, I_L(t_1) \tag{3.5}$$

$$E_{th}(t_2) = V_L(t_2) + Z_{th}(t_2) I_L(t_2) \tag{3.6}$$

where,

$E_{th}(t_1)$ is the Thévenin voltage E_{th} at time t_1,

$E_{th}(t_2)$ is the Thévenin voltage E_{th} at time t_2,

$V_L(t_1)$ is the phasor of load voltage V_L at time t_1,

$V_L(t_2)$ is the phasor of load voltage V_L at time t_2,

$Z_{th}(t_1)$ is the Thévenin impedance Z_{th} at time t_1,

$Z_{th}(t_2)$ is the Thévenin impedance Z_{th} at time t_2,

$I_L(t_1)$ is the phasor of current I_L at time t_1, and

$I_L(t_2)$ is the phasor of current I_L at time t_2.

Change of voltage can be expressed as a function of change of current as follows.

$$\Delta V_L(t_2) = V_L(t_1) - V_L(t_2)$$

$$\Delta I_L(t_2) = I_L(t_1) - I_L(t_2) \tag{3.7}$$

Equation 3.8 can be obtained by subtracting Equation 3.6 from Equation 3.5 and assuming that the Thévenin equivalent is constant within the data window.

$$0 = \Delta V_L(t_2) + \hat{Z}_{th}(t_2)\, \Delta I_L(t_2) \tag{3.8}$$

where,

$\hat{Z}_{th}(t_2)$ is the estimated Thévenin impedance Z_{th} at time t_2,

$\Delta V_L(t_2)$ is the deviation in voltage measured at the load bus V_L at time t_2 with respect to V_L at time t_1, and

$\Delta I_L(t_2)$ is the deviation in measured current I_L at time t_2 with respect to I_L at time t_1.

Rearranging this equation provides the following equation.

$$\hat{Z}_{th}(t_2) = -\frac{\Delta V_L(t_2)}{\Delta I_L(t_2)} \tag{3.9}$$

N such observation provides the following equation assuming that Thévenin equivalent has not changed while these observations were being taken.

$$\begin{bmatrix} \Delta I_L(t_2) \\ - \\ - \\ \Delta I_L(t_{N-1}) \\ \Delta I_L(t_N) \end{bmatrix} \hat{Z}_{th}(t_N) = -\begin{bmatrix} \Delta V_L(t_2) \\ - \\ - \\ \Delta V_L(t_{N-1}) \\ \Delta V_L(t_N) \end{bmatrix} \tag{3.10}$$

The estimated Thévenin impedance can then be obtained by using the following equation.

$$\hat{Z}_{th}(t_N) = -\frac{\sum_{j=2}^{N} \Delta I_L^*(t_j)\Delta V_L(t_j)}{\sum_{j=2}^{N} \left|\Delta I_L(t_j)\right|^2} \tag{3.11}$$

where,

j is an integer and equal to 1, 2,…, N.

Equation 3.10 shows that if there are no changes in current measurements the denominator is equal to zero, which gives an infinite value for the estimated Thévenin impedance. This problem can be overcome by increasing the number of measurements until the current-changes are observed [86].

It is obvious from the above equations that this technique is based on the changes of voltage at the load bus and changes of the current. Both changes depend on changes in the load, generation and topology. If the operational parameters of the system change slowly and the **c**hanges in the

measurements within the data window are very small, the changes in $\Delta\overline{V}_L$ and $\Delta\bar{I}_L$ will be small as well. It is, therefore, necessary to expand the time window until $\Delta\overline{V}_L$ and $\Delta\bar{I}_L$ increase substantially. Delta technique can be applied in polar coordinates as shown in Appendix D.

3.4.2 Least Square (LS) technique

The voltage at the load bus of the system shown in Figure 3.1 at time t_1 and t_2 can be described by rearranging Equations 3.5 and 3.6.

$$V_L(t_1) = E_{th} - Z_{th} I_L(t_1)$$
$$V_L(t_2) = E_{th} - Z_{th} I_L(t_2) \tag{3.12}$$

It is assumed in this equation that the Thévenin equivalent remains constant with the passage of time. This equation can be expanded as follows by replacing the complex variables and phasors with their real and imaginary components [87].

$$V_{L_r}(t_1) + jV_{L_i}(t_1) = [E_{th_r} + jE_{th_i}] - [R_{th} + jX_{th}][I_{L_r}(t_1) + jI_{L_i}(t_1)]$$
$$V_{L_r}(t_2) + jV_{L_i}(t_2) = [E_{th_r} + jE_{th_i}] - [R_{th} + jX_{th}][I_{L_r}(t_2) + jI_{L_i}(t_2)] \tag{3.13}$$

This equation can be rewritten in the following form.

$$\begin{bmatrix} V_{L_r}(t_1) \\ V_{L_i}(t_1) \\ V_{L_r}(t_2) \\ V_{L_i}(t_2) \end{bmatrix} = \begin{bmatrix} 1 & 0 & -I_{L_r}(t_1) & I_{L_i}(t_1) \\ 0 & 1 & -I_{L_i}(t_1) & -I_{L_r}(t_1) \\ 1 & 0 & -I_{L_r}(t_2) & I_{L_i}(t_2) \\ 0 & 1 & -I_{L_i}(t_2) & -I_{L_r}(t_2) \end{bmatrix} \begin{bmatrix} E_{th_r} \\ E_{th_i} \\ R_{th} \\ X_{th} \end{bmatrix} \tag{3.14}$$

The voltage and current phasors are measured and the Thévenin parameters are the unknowns. Error in each estimate can be expressed as follows.

$$\begin{bmatrix}\varepsilon_{11}\\ \varepsilon_{21}\\ \varepsilon_{31}\\ \varepsilon_{41}\end{bmatrix}=\begin{bmatrix}V_{L_r}(t_1)\\ V_{L_i}(t_1)\\ V_{L_r}(t_2)\\ V_{L_i}(t_2)\end{bmatrix}-\begin{bmatrix}1 & 0 & -I_{L_r}(t_1) & I_{L_i}(t_1)\\ 0 & 1 & -I_{L_i}(t_1) & -I_{L_r}(t_1)\\ 1 & 0 & -I_{L_r}(t_2) & I_{L_i}(t_2)\\ 0 & 1 & -I_{L_i}(t_2) & -I_{L_r}(t_2)\end{bmatrix}\begin{bmatrix}\hat{E}_{th_r}\\ \hat{E}_{th_i}\\ \hat{R}_{th}\\ \hat{X}_{th}\end{bmatrix} \tag{3.15}$$

where,

^ represents the estimated value,

ε_{11} is the error in the estimate of the real part of the voltage phasor at time t_1,

ε_{21} is the error in the estimate of the imaginary part of the voltage phasor at time t_1

ε_{31} is the error in the estimate of the real part of the voltage phasor at time t_2 and

ε_{41} is the error in the estimate of the imaginary part of the voltage phasor at time t_2.

After N measurements are taken, the error vector becomes

$$\begin{bmatrix}\varepsilon\\ 2N\times1\end{bmatrix}=\begin{bmatrix}V\\ 2N\times1\end{bmatrix}-\begin{bmatrix}A\\ 2N\times4\end{bmatrix}\begin{bmatrix}X\\ 4\times1\end{bmatrix} \tag{3.16}$$

Premultiplying both sides of Equation 3.16 with the transpose of the error vector provides the sum of the error squares as follows

$$\begin{bmatrix}\varepsilon^T\\ 1\times2N\end{bmatrix}\begin{bmatrix}\varepsilon\\ 2N\times1\end{bmatrix}=\left[\begin{bmatrix}V\\ 2N\times1\end{bmatrix}-\begin{bmatrix}A\\ 2N\times4\end{bmatrix}\begin{bmatrix}\hat{X}\\ 4\times1\end{bmatrix}\right]^T\left[\begin{bmatrix}V\\ 2N\times1\end{bmatrix}-\begin{bmatrix}A\\ 2N\times4\end{bmatrix}\begin{bmatrix}\hat{X}\\ 4\times1\end{bmatrix}\right] \tag{3.17}$$

The right hand side of this equation can be written as

$$\left[\begin{bmatrix}V^T\\ 1\times2N\end{bmatrix}-\begin{bmatrix}\hat{X}^T\\ 1\times4\end{bmatrix}\begin{bmatrix}A^T\\ 4\times2N\end{bmatrix}\right]\left[\begin{bmatrix}V\\ 2N\times1\end{bmatrix}-\begin{bmatrix}A\\ 2N\times4\end{bmatrix}\begin{bmatrix}\hat{X}\\ 4\times1\end{bmatrix}\right]$$

Expanding this term provides the following as sum of the error squares

$$\begin{bmatrix}\hat{\mathrm{X}}^{\mathrm{T}}\\ 1\times 4\end{bmatrix}\begin{bmatrix}\mathrm{A}^{\mathrm{T}}\\ 4\times 2N\end{bmatrix}\begin{bmatrix}\mathrm{A}\\ 2N\times 4\end{bmatrix}\begin{bmatrix}\hat{\mathrm{X}}\\ 4\times 1\end{bmatrix}-\begin{bmatrix}\mathrm{V}^{\mathrm{T}}\\ 1\times 2N\end{bmatrix}\begin{bmatrix}\mathrm{A}\\ 2N\times 4\end{bmatrix}\begin{bmatrix}\hat{\mathrm{X}}\\ 4\times 1\end{bmatrix}-$$

$$\begin{bmatrix}\hat{\mathrm{X}}^{\mathrm{T}}\\ 1\times 4\end{bmatrix}\begin{bmatrix}\mathrm{A}^{\mathrm{T}}\\ 4\times 2N\end{bmatrix}\begin{bmatrix}\mathrm{V}\\ 2N\times 1\end{bmatrix}+\begin{bmatrix}\mathrm{V}^{\mathrm{T}}\\ 1\times 2N\end{bmatrix}\begin{bmatrix}\mathrm{V}\\ 2N\times 1\end{bmatrix}$$

Taking the derivative of the sum of the error squares and equating it to zero provides the following equation.

$$2\begin{bmatrix}\mathrm{A}^{\mathrm{T}}\\ 4\times 2N\end{bmatrix}\begin{bmatrix}\mathrm{A}\\ 2N\times 4\end{bmatrix}\begin{bmatrix}\hat{\mathrm{X}}\\ 4\times 1\end{bmatrix}-\begin{bmatrix}\mathrm{V}^{\mathrm{T}}\\ 1\times 2N\end{bmatrix}\begin{bmatrix}\mathrm{A}\\ 2N\times 4\end{bmatrix}-\begin{bmatrix}\mathrm{A}^{\mathrm{T}}\\ 4\times 2N\end{bmatrix}\begin{bmatrix}\mathrm{V}\\ 2N\times 1\end{bmatrix}=0 \tag{3.18}$$

In this equation, the term $[V]^T[A]$ is equal to $[A]^T[V]$. Making this substitution in Equation 3.18 and rearranging provides

$$\begin{bmatrix}\mathrm{A}^{\mathrm{T}}\\ 4\times 2N\end{bmatrix}\begin{bmatrix}\mathrm{A}\\ 2N\times 4\end{bmatrix}\begin{bmatrix}\hat{\mathrm{X}}\\ 4\times 1\end{bmatrix}=\begin{bmatrix}\mathrm{A}^{\mathrm{T}}\\ 4\times 2N\end{bmatrix}\begin{bmatrix}\mathrm{V}\\ 2N\times 1\end{bmatrix} \tag{3.19}$$

Premultiplying both sides of Equation 3.19 with the inverse of $[A]^T[A]$ provides the least squares solution of the parameters of the Thévenin equivalent as follows.

$$\begin{bmatrix}\hat{\mathrm{X}}\\ 4\times 1\end{bmatrix}=\left[\begin{bmatrix}\mathrm{A}^{\mathrm{T}}\\ 4\times 2N\end{bmatrix}\begin{bmatrix}\mathrm{A}\\ 2N\times 4\end{bmatrix}\right]^{-1}\begin{bmatrix}\mathrm{A}^{\mathrm{T}}\\ 4\times 2N\end{bmatrix}\begin{bmatrix}\mathrm{V}\\ 2N\times 1\end{bmatrix} \tag{3.20}$$

It should be noted that $[A]^T[A]$ matrix in this equation will be ill conditioned and, therefore, will cause numerical problems if the changes in load currents are small.

3.5 Data window requirements

The main problem in estimating the system parameters by using the Delta and Least Squares techniques is to suppress oscillations in the measurements. In addition, the estimation process succeeds if the following conditions are satisfied:

- There must be a noticeable change in current measurements. This problem can be easily detected by using a large data window or using Cumulative Sum Filter.

- The estimation process in local based measurements algorithm accepts "small" changes in the "actual" Thévenin equivalent in a data window. If a sudden large change occurs, the estimation algorithm of Thévenin impedance postpones the process until the next set of measurements is taken. This problem can be detected by taking into consideration the estimation error when the assumption of constant Thévenin equivalent does not hold, as shown below:

The first requirement can easily be detected by using the differences between voltage and current measurements taken at time t and time t-1.

The second requirement can only be detected by examining the error in the estimates when assumption of constant Thévenin equivalent does not valid. Equation 3.21 can be obtained by applying Equation 3.1 at times t and t-1.

$$\begin{bmatrix} E_{th}(t-1) \\ E_{th}(t) \end{bmatrix} = \begin{bmatrix} V_L(t-1) \\ V_L(t) \end{bmatrix} + Z_{th}(t) \begin{bmatrix} I_L(t-1) \\ I_L(t) \end{bmatrix} + \begin{bmatrix} (Z_{th}(t-1) - Z_{th}(t))\, I_L(t-1) \\ 0 \end{bmatrix} \qquad (3.21)$$

where,

$E_{th}(t)$ is the Thévenin voltage E_{th} at time t,

$E_{th}(t-1)$ is the Thévenin voltage E_{th} at time t-1,

$\Delta Z_{th}(t)$ is the deviation in Thévenin impedance Z_{th} at time t with respect of Z_{th} at time t_0, ,

$V_L(t)$ is the voltage measured at the load bus V_L at time t ,

$V_L(t-1)$ is the voltage measured at the load bus V_L at time t-1,

$I_L(t)$ is the current measured I_L at time t, and

$I_L(t-1)$ is the current measured I_L at time t-1.

By subtracting the second row of Equation 3.21 from the first row the following equation can be obtained.

$$\Delta E_{th}(t) = \Delta V_L(t) + Z_{th}(t)\Delta I_L(t) + \Delta Z_{th}(t)\, I_L(t-1) \tag{3.22}$$

where,

$\Delta E_{th}(t)$ is the deviation in Thévenin voltage E_{th} at time t with respect to E_{th} at time t_0,

$\Delta V_L(t)$ is the deviation in voltage measured at the load V_L bus at time t, and

$\Delta I_L(t)$ is the deviation in measured current I_L at time t.

Equation 3.23 can be obtained by dividing both sides of Equation 3.22 by $\Delta I_L(t)$.

$$\frac{\Delta E_{th}(t)}{\Delta I_L(t)} = \frac{\Delta V_L(t)}{\Delta I_L(t)} + Z_{th}(t) + \frac{\Delta Z_{th}(t)\, I_L(t-1)}{\Delta I_L(t)} \tag{3.23}$$

Rearranging Equation 3.23 provides

$$Z_{th}(t) = -\frac{\Delta V_L(t)}{\Delta I_L(t)} + \frac{\Delta E_{th}(t) - \Delta Z_{th}(t)\, I_L(t-1)}{\Delta I_L(t)}. \tag{3.24}$$

where,

$Z_{th}(t)$ is the estimated Thévenin impedance Z_{th} at time t, and

$\dfrac{\Delta E_{th}(t) - \Delta Z_{th}(t)\, I_L(t-1)}{\Delta I_L(t)}$ is the estimation's error.

Equation 3.24 shows that small changes in load current would result in large errors in the estimated impedances. If the changes in current are small, the estimated Thévenin impedances should be discarded. Load impedance and Thévenin equivalent at time t can be expressed by the following equations when there is a significant change in load and/or system topology from time t-1 to t.

$$E_{th}(t) = \frac{1}{k_{Eth}} E_{th}(t-1)$$

$$Z_{th}(t) = \frac{1}{k_{Zth}} Z_{th}(t-1) \qquad (3.25)$$

$$Z_L(t) = \frac{1}{k_{ZL}} Z_L(t-1)$$

where,

k_{Eth}, k_{Zth}, k_{ZL} are constants

Equation 3.26 shows the deviation in measured current I_L at time t.

$$\Delta I_L(t) = \frac{E_{th}(t)}{Z_{th}(t) + Z_L(t)} - \frac{E_{th}(t-1)}{Z_{th}(t-1) + Z_L(t-1)} \qquad (3.26)$$

The following equation can be obtained by substituting Equations 3.22, 3.23, 3.24 and 3.25 in Equation 3.26.

$$Z_{th}(t) = -\frac{\Delta V_L(t)}{\Delta I_L(t)} + \frac{\left[\Delta E_{th}(t) - \Delta Z_{th}(t)\, I_L(t-1)\right](1-k_{Eth})\left[(1-k_{ZL})(1-k_{Zth})(\Delta Z_{th}(t) + \Delta Z_L(t))\right]}{(1-k_{ZL})(1-k_{Zth})}. \qquad (3.27)$$

Consider the following two types of change in the system.

1. The load changes but the Thévenin equivalent remains unchanged, thus $k_{ZL} \neq 1$, $k_{Eth}, k_{Zth} = 1$ and the deviation in Thévenin equivalent at time t is equal to zero.

2. The Thévenin equivalent changes but the load does not, thus $k_{ZL} = 1$, $k_{Eth}, k_{Zth} \neq 1$. In this case the deviation in current and voltage measurements is equal to zero.

In the first case, the right side of Equation 3.27 is equal to $-\frac{\Delta V_L(t)}{\Delta I_L(t)}$. The Voltage Instability Predictor (VIP) algorithm estimates the correct value of Thévenin impedance based on the assumption of constant Thévenin equivalent within the data window. In the second case the right

side of Equation 3.27 is equal to $\frac{[\Delta Z_{th}(t)]^2 \, I_L(t-1)}{\Delta E_{th}(t)}$. The algorithm in this case estimates the estimation error instead of the Thévenin impedance. The algorithm should recognize and discard this incorrect estimate and delay the estimation process till the next measurement comes to the window.

Figure 3.9 shows a situation where there is a sudden change in the Thévenin equivalent in either the voltage or the impedance. In this case, the technique should recognize the case and discard the estimated values and wait for the new measurements at time t+1.

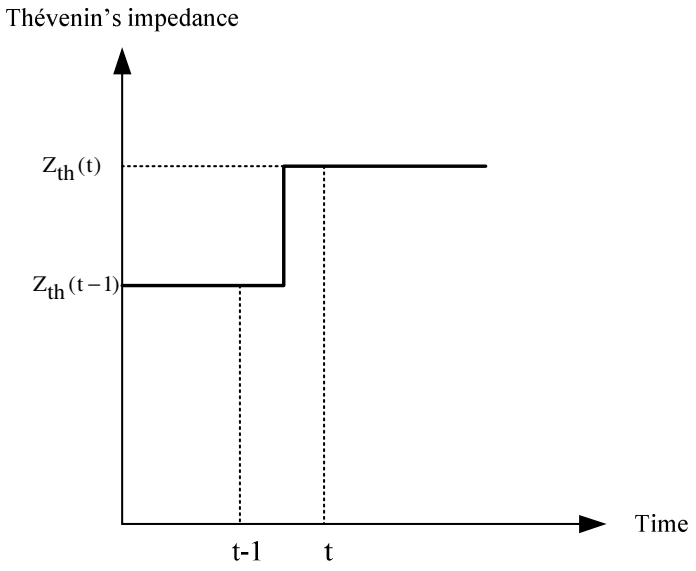

Figure 3.9: Sudden change in Thévenin impedance

3.6 Cumulative Sum Filter (CSF)

Small disturbances and noise can result in the absolute value of the current deviation $|\Delta I_L|$, to become close to zero and this makes the tracking of Thévenin impedance difficult. To overcome this problem, a Cumulative Sum Filter (CSF) was designed and used to monitor current and voltage measurements when the parameters of the Thévenin equivalent were estimated. In the Delta

method, the first step consists of taking the cumulative sum of the absolute values of the variations of bus voltage, $|\Delta V_L|$, and load current $|\Delta I_L|$. The following vectors are defines at time t_n and t_{n-1} using these deviations.

$$[K(t_n)] = \left[|\Delta V_L(t_2)|_2 \quad \sum_{j=2}^{3} |\Delta V_L(t_j)|_3 \quad \ldots \quad \sum_{j=2}^{n} |\Delta V_L(t_j)|_n \right] \tag{3.28}$$

$$[K(t_{n-1})] = \left[|\Delta V_L(t_2)|_2 \quad \sum_{j=2}^{3} |\Delta V_L(t_j)|_3 \quad \ldots \quad \sum_{j=2}^{n-1} |\Delta V_L(t_j)|_{n-1} \right]$$

$$[W(t_n)] = \left[|\Delta I_L(t_2)|_2 \quad \sum_{j=2}^{3} |\Delta I_L(t_j)|_3 \quad \ldots \quad \sum_{j=2}^{n} |\Delta I_L(t_j)|_n \right] \tag{3.29}$$

$$[W(t_{n-1})] = \left[|\Delta I_L(t_2)|_2 \quad \sum_{j=2}^{3} |\Delta I_L(t_j)|_3 \quad \ldots \quad \sum_{j=2}^{n-1} |\Delta I_L(t_j)|_{n-1} \right]$$

In Equations 3.28 and 3.29, n is the last measurement taken within the data estimation window of seven observations. Dividing the difference between the two consecutive elements of [K] and [W] gives the absolute value of the estimated Thévenin impedance at time t_n as follows.

$$\hat{Z}_{th}(t_n) = \frac{K(t_n) - K(t_{n-1})}{W(t_n) - W(t_{n-1})}$$

$$= \frac{|\Delta V_L(t_n)|}{|\Delta I(t_n)|} \tag{3.30}$$

At the present time t_k, a step size $|\Delta x|$ can be defined as follows.

$$\Delta x = \frac{\sum_{i=2}^{k} |\Delta I_L|_i}{\text{number of steps}} \tag{3.31}$$

The absolute value of Thévenin impedance Z_{th} at the present time, t_k, can be found using Equation 3.32.

$$|Z_{th}(t_k)| = \frac{V_L(t_k) - V_L(t_{k-1})}{\Delta x} \tag{3.32}$$

where,

$V_L(t_k)$ is the measured voltage at the load bus at the present time t_k, and

$V_L(t_{k-1})$ is the measured voltage at the load bus at time t_{k-1}.

Figure 3.10 shows that the x-axis, which represents $|\Delta I_L|$, is divided in fixed intervals of $|\Delta x|$ where changes occur in the measured quantity. This approach keeps track of measurements from the present time t_k to when the last measurement was taken at time t_1.

In LS method, the filtering process starts by taking the cumulative sum of the absolute values of the bus voltage, $|V_L|$, and load current $|I_L|$. The following vectors are defined at time t_n and t_{n-1} using the deviations.

$$[K(t_n)] = \left[|V_L(t_2)|_2 \quad \sum_{j=2}^{3} |V_L(t_j)|_3 \quad \ldots \quad \sum_{j=2}^{n} |V_L(t_j)|_n \right] \tag{3.33}$$

$$[W(t_n)] = \left[|\Delta I_L(t_2)|_2 \quad \sum_{j=2}^{3} |\Delta I_L(t_j)|_3 \quad \ldots \quad \sum_{j=2}^{n} |\Delta I_L(t_j)|_n \right]$$

At the present time t_k, a step size $|\Delta x|$ can be defined as follows.

$$\Delta x = \frac{\sum_{i=2}^{k} |I_L|_i}{\text{number of steps}} \tag{3.34}$$

The Thévenin parameters at the present time, t_k, can be found using the Least Square method described in Section 3.4.2.

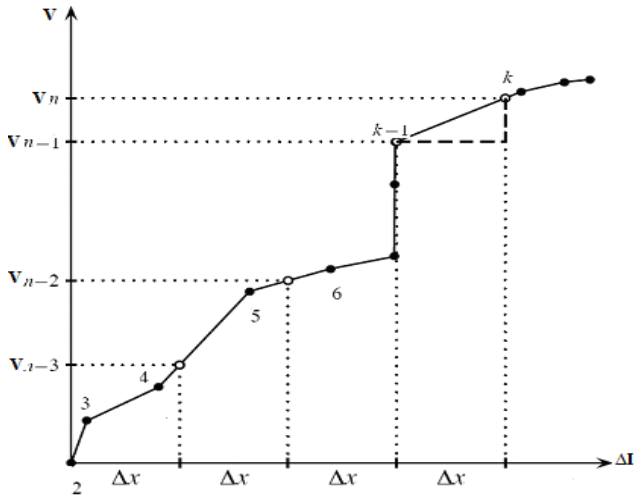

Figure 3.10: Mapping of cumulative sum of |ΔV| to cumulative sum of |ΔI|

3.7 Integration of CSF and Delta method

Voltage and current measurements used to estimate the parameters of the Thévenin equivalent in the Delta method were filtered using CSF to overcome the problem of small disturbances and noise that can cause numerical difficulties in estimating the parameters of the Thévenin equivalent [84].

A flow chart of the Delta technique augmented with CSF is given in Figure 3.11.

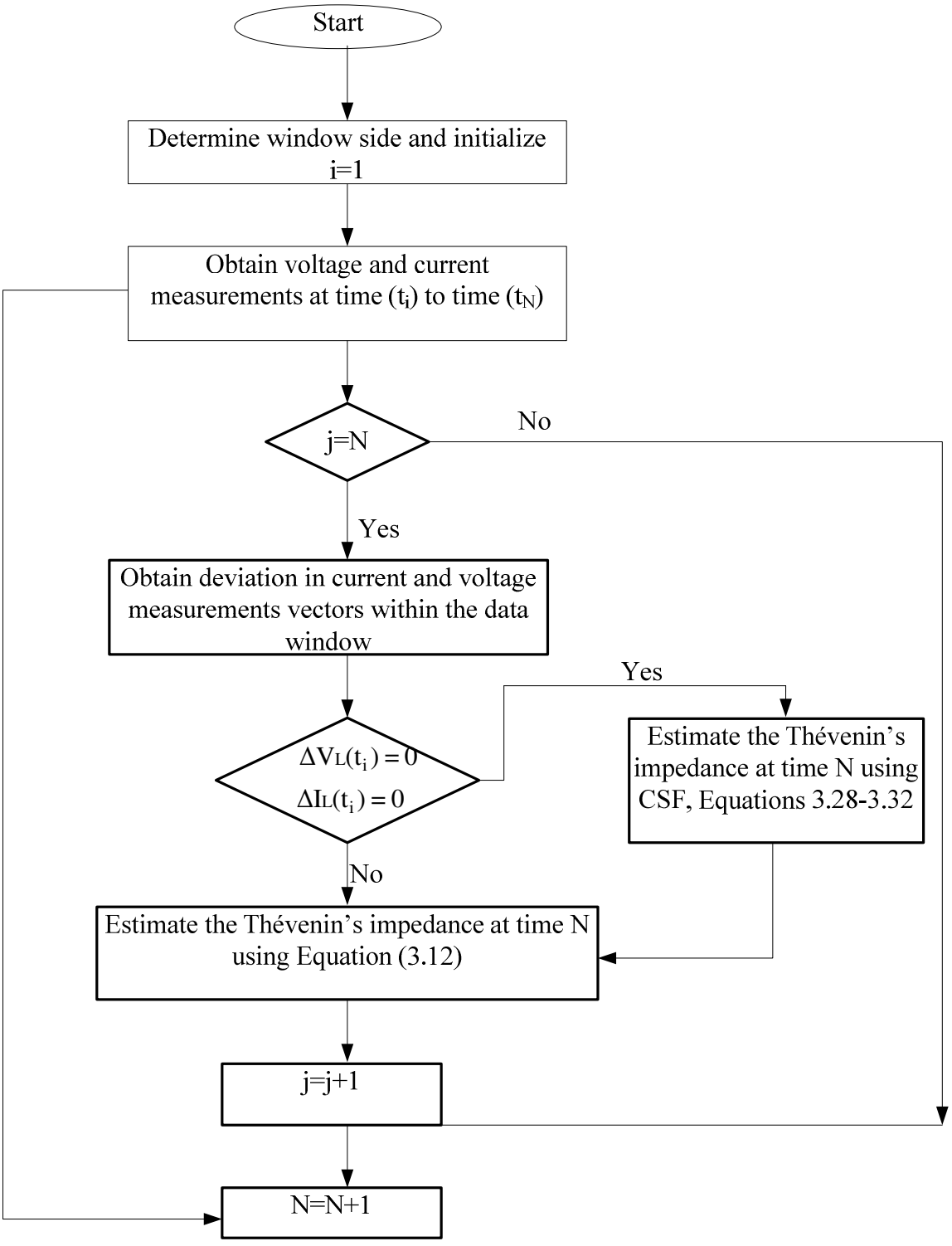

Figure 3.11: Flowchart of the Delta method augmented with the CSF

The performance of the Delta technique augmented with the CSF was evaluated using the IEEE 30-Bus system as shown in Figure 3.12. This system has twenty four load buses, one slack bus, and five voltage controlled buses. The base load of the system is 100 MVA. The connectivity and electrical parameters of the IEEE 30-Bus test system used for studies reported in this thesis are presented in Appendix A. The loads are considered to be P-Q loads and are considered to be changing with time.

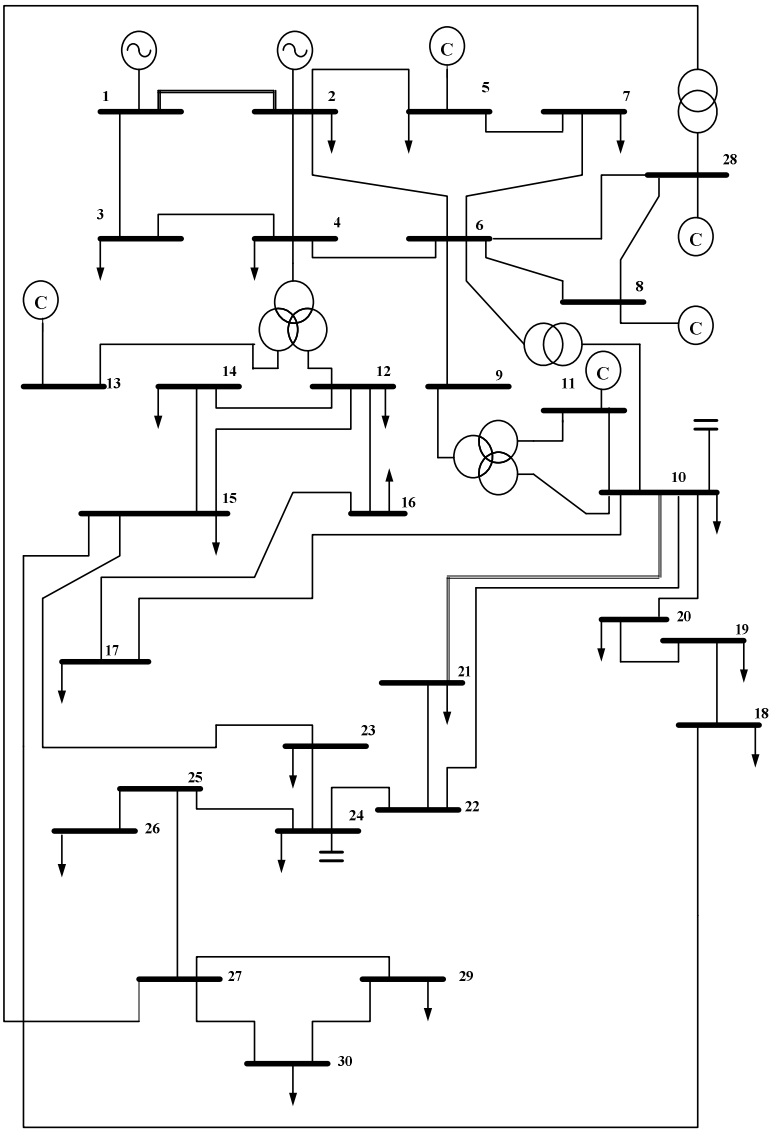

Figure 3.12: IEEE 30-Bus test system

In this study, the required bus voltage and current phasors used in estimating of Thévenin equivalents were obtained using the following steps. All loads in the system are assumed to be P-Q loads.

1. The base-case load flow was conducted and was assigned as load flow at time t=0 assuming that all tap changers, generators, and compensation devices were set at their maximum limits. Voltage calculated on specified bus was identified as $V_L(t_0)$ and the load current was identified as $I_L(t_0)$.

2. The load at the specified bus was increased by one percent and the load flow was conducted again. The load change was considered to have occurred in one minute time. The calculated voltage and current at the specified bus identified as $V_L(t_1)$ and $I_L(t_1)$ respectively.

3. The changes in the bus voltage and load current were calculated as follows

$$\Delta V_L(t_1) = V_L(t_1) - V_L(t_0)$$
$$\Delta I_L(t_1) = I_L(t_1) - I_L(t_0)$$

4. The load at the specified bus was increased by another one percent and the load flow was conducted again. The load change was considered to have occurred in one minute time. The calculated voltage and current at the specified bus identified as $V_L(t_2)$ and $I_L(t_2)$ respectively.

5. $\Delta V_L(t_2)$ and $\Delta I_L(t_2)$ were then calculated.

6. Steps 4 and 5 were repeated to calculate subsequent values of voltage and current changes until $\Delta V_L(t_7)$ and $\Delta I_L(t_7)$ were obtained.

7. If $\Delta V_L(t_i)$ and $\Delta I_L(t_i)$ for j=1, ….7 were equal to zero, CSF were called to estimate Thévenin impedance using Equations 3.28 to Equation 3.30. $\hat{Z}_{th}(t_7)$ was calculated by implementing Equation 3.12 as follows if $\Delta V_L(t_i)$ and $\Delta I_L(t_i)$ for j=1, ….7 were unequal to zero.

$$\hat{Z}_{th}(t_7) = -\frac{\sum_{j=1}^{7} \Delta I_L^*(t_j)\Delta V_L(t_j)}{\sum_{j=1}^{7} \left|\Delta I_L(t_j)\right|^2}$$

8. Steps 4, 5, 7 were repeated to calculate $\hat{Z}_{th}(t_j) \quad j = 8, 9, ..., 24$

Six case studies are presented in this section that evaluate the performance of the Delta method augmented with the developed CSF using the IEEE 30-Bus system. It is assumed in these cases that the load at Bus 26 increases in steps of 1% while the reactive power output of generators, tap changers on transformers, and compensation devices are held at their maximum setting.

In the first case, the Thévenin impedance was calculated using the following three approaches.

1. The actual absolute-value of the Thévenin impedance that was calculated by conducting
    - a load flow with the load on Bus 26 removed and noting down the voltage at Bus 26,
    - conducting a system analysis with a three phase short circuit at Bus 26 and noting donw the short circuit current at Bus 26 and
    - calculating the Thévenin impedance from the open circuit voltage and short circuit current.
2. The Delta technique for each of the load levels at Bus 26.
3. The Delta technique augmented with the developed CSF approach.

The absolute values of the Thévenin's impedances calculated by the three approaches are shown in Figute 3.13. The absolute value of the actual Thévenin's impedance remains constant as shown in

plot (a) in Figure 3.13 because there have been no changes in the system except for the load on Bus 26. However, the absolute values of the Thévenin's impedance calculated by the Delta technique is slightly less than the actual Thévenin's impedance initially but increases gradually with the increase of load on Bus 26 as is shown as plot (b) in Figure 3.13. The absolute value of the Thévenin's impedance calculated by the Delta technique augmented with CSF is shown as plot (c) in Figure 3.13. A comparison of the results shown in Figures 3.13 (b) and (c) shows that the addition of developed CSF to the Delta technique improves the estimates of the Thévenin's impedance.

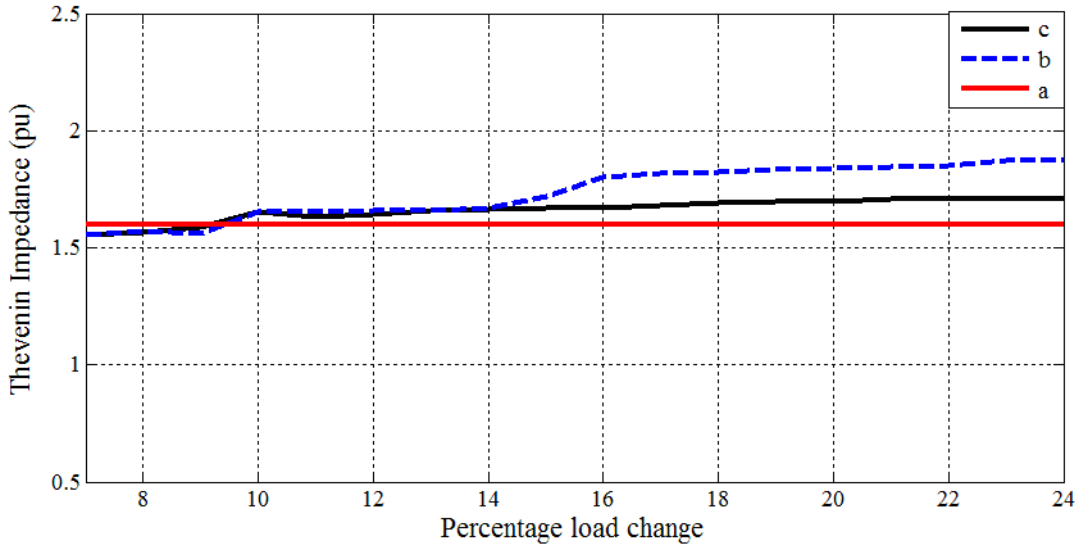

Figure 3.13: Estimated Thévenin impedance at Bus 26 (load at Bus 26 incremented in 1% Steps) using three approaches

The Delta method uses a data window of seven observations and, therefore the Thévenin's impedances from 0% to 6% load increase on Bus 26 are not shown in Figure 3.13 and subsequent figures in this section.

The second case is similar to the first case except that the transmission line from Bus 25 to Bus 24 was taken out of service when the load on Bus 26 reached 15%. The absolute-values of the actual Thévenin's impedance and the Thévenin's impedance estimated by the Delta technique augmented by the CSF filter before and after the disconnection of the line are shown in Figure 3.14. This figure shows that the estimated values of the Thévenin impedance increased gradually from the start of the estimation process and more rapidly after the line was taken out of service.

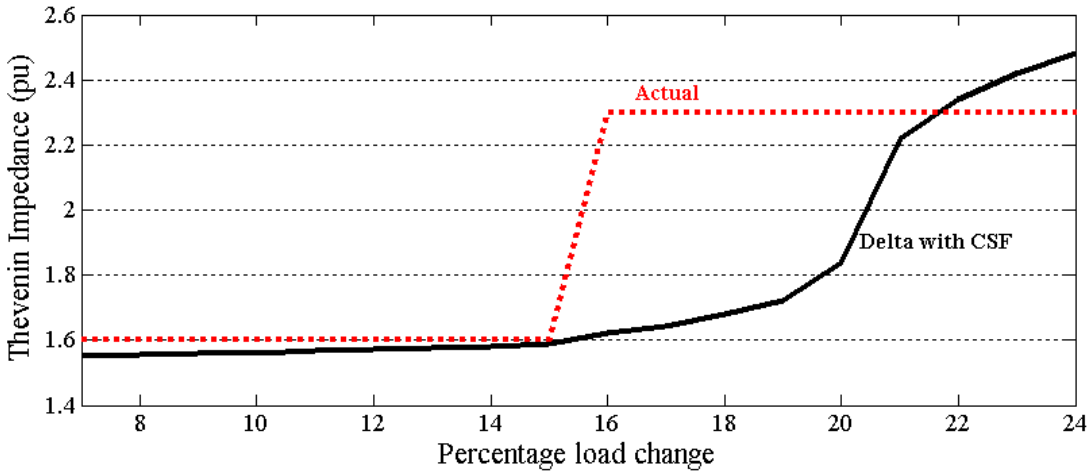

Figure 3.14: Estimated Thévenin impedances at Bus 26 (load at Bus 26 incremented in 1% Steps and transmission line outage applied between Buses 24 and 25)

The third case consists of estimating the values of the Thévenin impedance as seen from Bus 29 while the real power load at Bus 26 increases in steps of 1%. Figure 3.15 shows the estimated values of Thévenin impedance seen from bus 29 as the active power on bus 26 increased in steps of 1%. Figure 3.16 shows the estimated Thévenin impedance seen from bus 29 when load increase on bus 26 is in steps of 2% of the initial load.

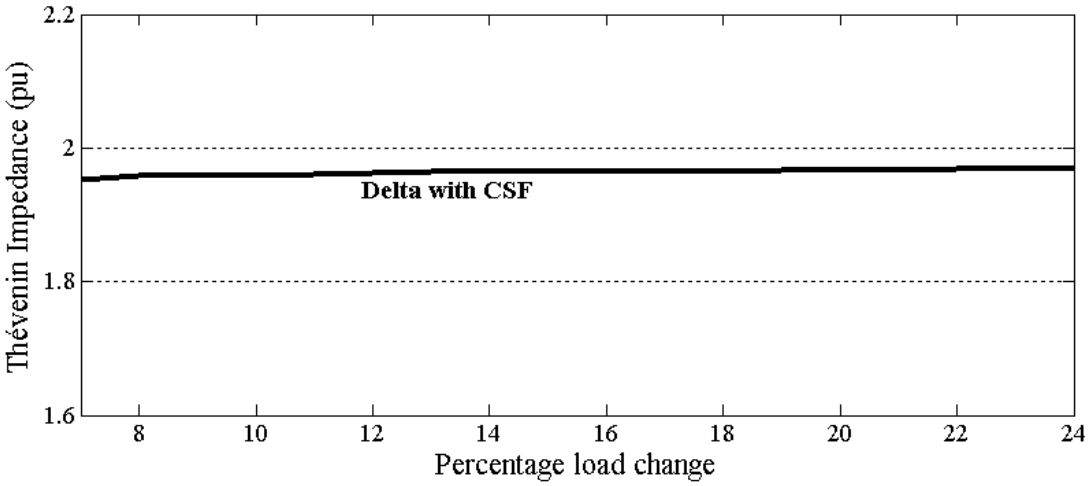

Figure 3.15: Estimated Thévenin impedance at Bus 29 (load at Bus 26 incremented in 1% steps)

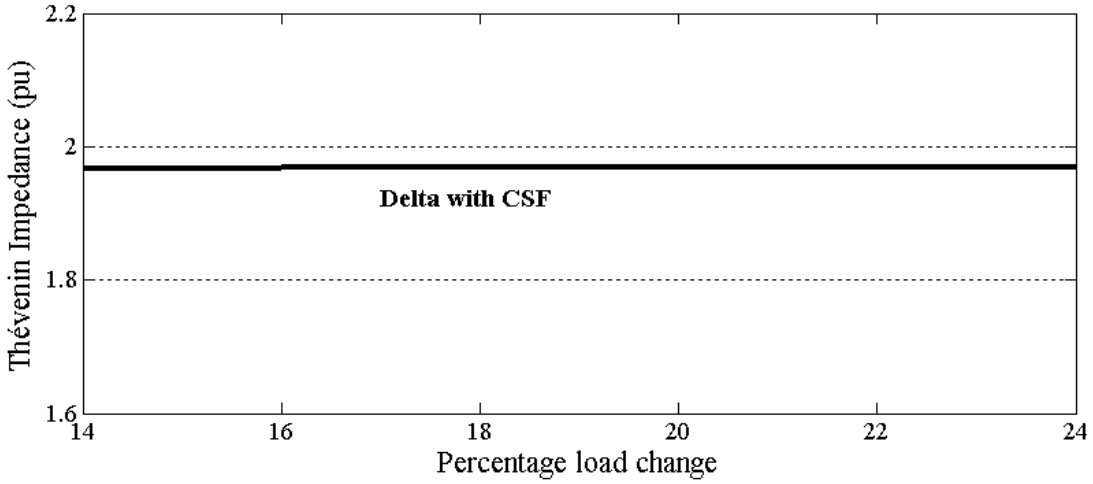

Figure 3.16: Estimated Thévenin impedance at Bus 29 (load at Bus 26 incremented in 2% steps)

The fifth case is similar to the third case except that the values of the Thévenin impedance, as seen from Bus 29, were estimated before and after the transmission line from Bus 24 to Bus 25 was taken out of service. Transmission line from Bus 24 to Bus 25 was taken out of service when load at Bus 26 increased by 15%. The estimated value of the Thévenin impedance is shown in Figure 3.17.

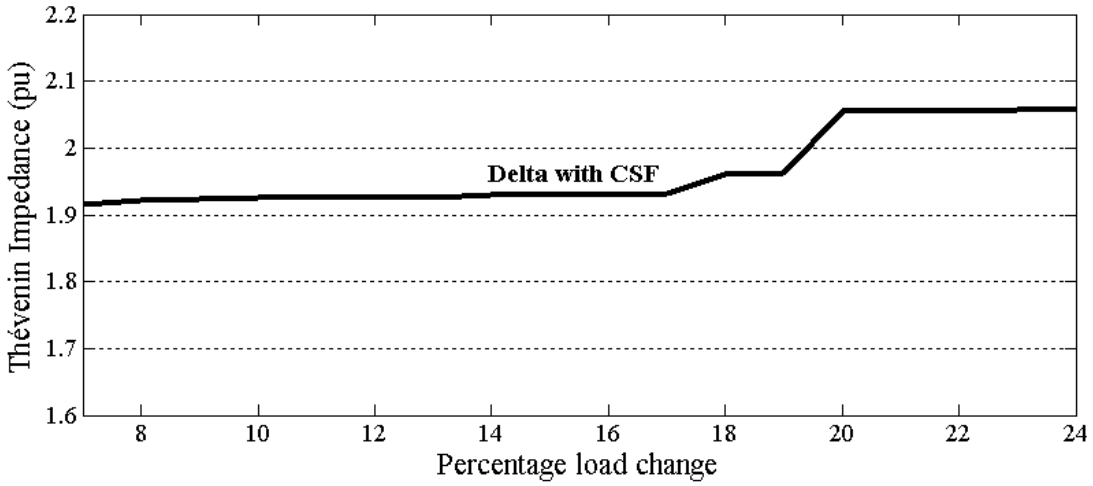

Figure 3.17: Estimated Thévenin impedances at bus 29 (load at bus 26 incremented in 1% steps and transmission line outage is applied between Bus 24 and Bus 25)

The performances of the Delta technique and Delta technique augmented with CSF were evaluated in the sixth case. In this case, loads increased on all buses of the system in steps of 1% per minute

starting from time t=1 minute to time t=15 minutes. Loads were kept constant after the load increase on all buses reached 15%. Plot (a) in Figure 3.18 shows the absolute-value of the Thévenin impedance seen from bus 26 when the estimates were obtained by using the Delta technique. The estimated absolute value of the Thévenin's impedance increased gradually. Plot (b) in Figure 3.18 shows the absolute value of the Thévenin impedance seen from bus 26 when Delta technique augmented with CSF was used. It is obvious from this figure that the absolute value of the estimated Thévenin impedance increased gradually when the loads on all buses increased. Even after the time t=15 the absolute value of the Thévenin's impedance continued to increase but the increase was much less than when the Delta technique was used. The estimates shown in this figure prove that Delta technique augmented with CSF provides more accurate estimates and tracks changes in the power system operating parameters.

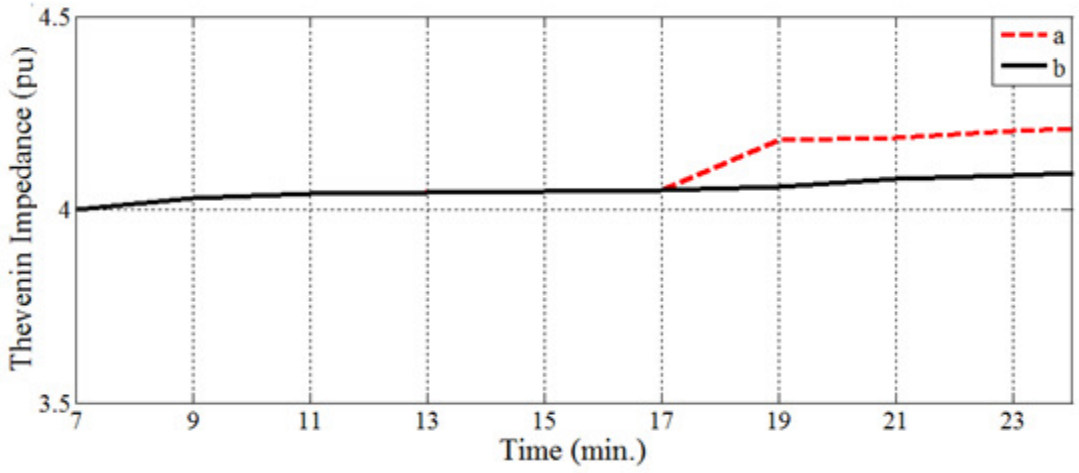

Figure 3.18: Estimated Thévenin impedance at Bus 26 (load on all buses incremented in 1% steps per minute from t= 1 min. to t=15 min. and kept constant from t=16 min. to t=24 min.)

3.8 Integration of CSF into LS method

Voltage and current measurements used to estimate the parameters of the Thévenin equivalent in the LS method were filtered using CSF to overcome the problem of small disturbances and noise that can cause numerical difficulties in estimating the parameters of the Thévenin equivalent [77].

A flow chart of the LS technique augmented with CSF is given in Figure 3.19.

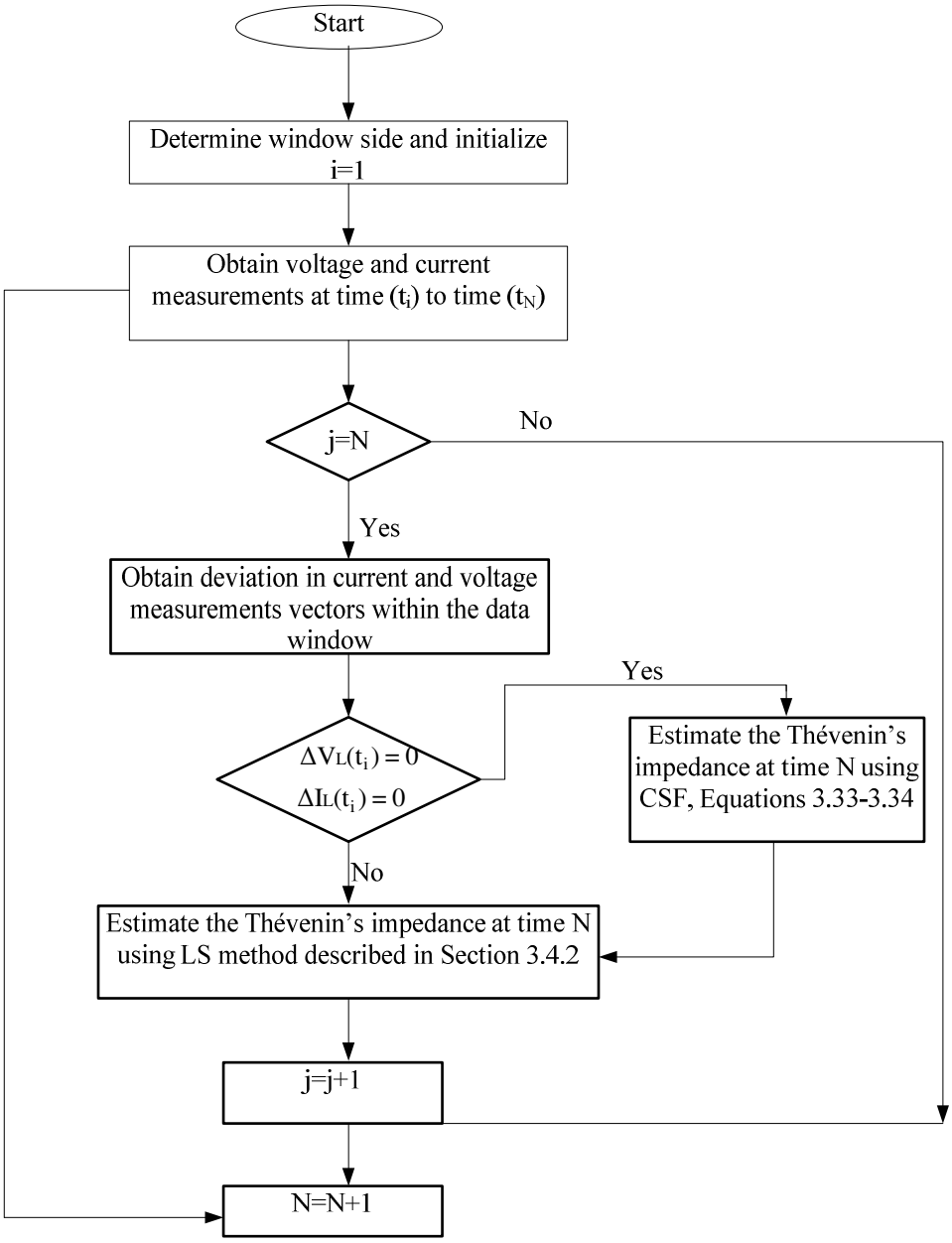

Figure 3.19: Flowchart of LS method augmented with CSF

The performance of the developed LS method augmented with CSF was evaluated using the IEEE 30-Bus system shown in Figure 3.8. All loads in the system were assumed to be P-Q loads.

The developed method was used to identify the Thévenin equivalent circuit and to compare the results with actual Thévenin impedance as seen from the load bus. In this study, the required bus

voltages and current measurements for various load conditions were obtained from load flow simulations.

In this study, the required bus voltage and current phasors used in estimating of Thévenin equivalents were obtained from the following load flow simulations.

1. The base case load flow was conducted and was assigned as load flow at time t=0, assuming that all tap changers, generators, and compensation devices were at their minimum limits. The bus voltage calculated in this case was identified as $V_L(t_0)$ and the load current was identified as $I_L(t_0)$.

2. The load at all buses was increased by one percent and the load flow was conducted again. The load change was considered to have occurred in one minute time. The bus voltage calculated in this case was identified as $V_L(t_1)$ and the load current was identified as $I_L(t_1)$.

3. $\Delta V_L(t_1)$ and $\Delta I_L(t_2)$ were then calculated.

4. Step 2 was repeated to calculate subsequent values of voltage and current until $\bar{V}_L(t_{24})$ and $\bar{I}_L(t_{24})$ were obtained. $\Delta V_L(t_j)$ and $\Delta I_L(t_j)$ were calculated for j=1,….., 24.

5. Voltage vector [V] and current matrix [A] were formed using $V_L(t_j)$ and $I_L(t_j)$, for j=0, 1, 2, 6, as shown below.

$$\begin{bmatrix} V \\ 14\times1 \end{bmatrix} = \begin{bmatrix} V_{L_r}(t_0) \\ V_{L_i}(t_0) \\ V_{L_r}(t_1) \\ V_{L_i}(t_1) \\ \vdots \\ V_{L_r}(t_6) \\ V_{L_i}(t_6) \end{bmatrix} \text{ and,}$$

$$\begin{bmatrix} A \\ 14\times4 \end{bmatrix} = \begin{bmatrix} 1 & 0 & -I_{L_r}(t_0) & I_{L_i}(t_0) \\ 0 & 1 & -I_{L_i}(t_0) & -I_{L_r}(t_0) \\ 1 & 0 & -I_{L_r}(t_2) & I_{L_i}(t_2) \\ 0 & 1 & -I_{L_i}(t_2) & -I_{L_r}(t_2) \\ \vdots & \vdots & \vdots & \vdots \\ 1 & 0 & -I_{L_r}(t_6) & I_{L_i}(t_6) \\ 0 & 1 & -I_{L_i}(t_6) & -I_{L_r}(t_6) \end{bmatrix}.$$

6. If $\Delta V_L(t_i)$ and $\Delta I_L(t_i)$ for j=0, …., 6 were equal to zero, CSF were called to estimate Thévenin impedance using Equation 3.33 and Equation 3.34. Thévenin equivalent vector $[\hat{X}(t_6)]$ was calculated using Equation 3.21 reproduced below if $\Delta V_L(t_i)$ and $\Delta I_L(t_i)$ for j=0, ….,6 were unequal to zero .

$$\begin{bmatrix} \hat{X} \\ 4\times1 \end{bmatrix} = \left[\begin{bmatrix} A^T \\ 4\times14 \end{bmatrix} \begin{bmatrix} A \\ 14\times4 \end{bmatrix} \right]^{-1} \begin{bmatrix} A^T \\ 4\times14 \end{bmatrix} \begin{bmatrix} V \\ 14\times1 \end{bmatrix}$$

7. Step 4 was repeated to form voltage vector [V] and current matrix [A] using $V_L(t_j)$ and $I_L(t_j)$, for j=1, 2, 3,…, 7.

8. The Thévenin equivalent vector $\left[\hat{X}(t_7)\right]$ was calculated using the equation shown in step 6.

9. The procedure was repeated to calculate Thévenin equivalent vectors $\left[\hat{X}(t_{18})\right], \left[\hat{X}(t_{19})\right], \ldots, \left[\hat{X}(t_{24})\right]$.,

Six case studies are presented in this section that evaluate the performance of the developed Least Squares method augmented with the developed CSF using the IEEE 30-Bus system. It is assumed in these cases that the load at Bus 26 increases in steps of 1% while the reactive power output of generators, tap changers on transformers, and compensation devices are held at their maximum setting.

In the first case, the Thévenin impedance was calculated using the following three approaches.

1. The actual absolute-value of the Thévenin impedance that was calculated by conducting

   - a load flow with the load on Bus 26 removed and noting down the voltage at Bus 26,
   - conducting a system analysis with a three phase short circuit at Bus 26 and noting down the short circuit current at Bus 26 and
   - calculating the Thévenin impedance from the open circuit voltage and short circuit current.
2. The developed Least Squares technique for each of the load levels at Bus 26.
3. The developed Least Squares technique augmented with developed CSF approach.

The absolute values of the Thévenin's impedances calculated by the three approaches are shown in Figute 3.20. The absolute value of the actual Thévenin's impedance remains constant as shown in plot (a) in Figure 3.20 because there have been no changes in the system except for the load on Bus 26. However, the absolute values of the Thévenin's impedance calculated by the Least Squares technique initially is slightly less than the actual Thévenin's impedance but increases gradually with the increase of load on Bus 26 as is shown as plot (b) in Figure 3.20. The absolute value of the Thévenin's impedance calculated by the Least Squares technique augmented with CSF is shown as plot (c) in Figure 3.20. A comparison of the results shown in Figures 3.20 (b) and (c) shows that the addition of developed CSF to the Least Squares technique improves the estimates of the Thévenin's impedance.

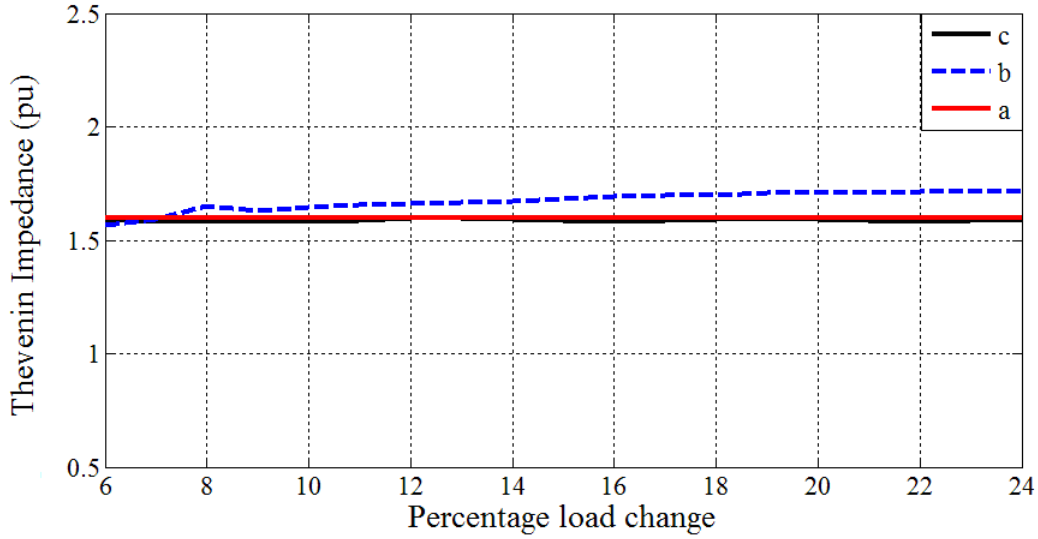

Figure 3.20: Estimated Thévenin impedance Bus 26 incremented in 1% steps)

The Least Squares method uses a data window of seven observations and, therefore the Thévenin's impedances from 0% to 5% load increase on Bus 26 are not shown in Figure 3.20 and subsequent figures in this section.

The second case is similar to the first case except that the transmission line from Bus 24 to Bus 25 was taken out of service when load at Bus 26 increased by 15%. The estimated absolute-values of the Thévenin impedance before and after the disconnection of the line are shown in Figure 3.21. As in the first case, the load was increased in 1% steps. The actual absolute value of the Thévenin's impedance was obtained by using open-circuit and short-circuit simulations with and without the line from Bus 24 to Bus 25 in service. This figure shows that the estimated absolute values of the Thévenin impedance seen from Bus 26 converged to the actual values rapidly from the start of the estimation process and gradually after the line was taken out of service.

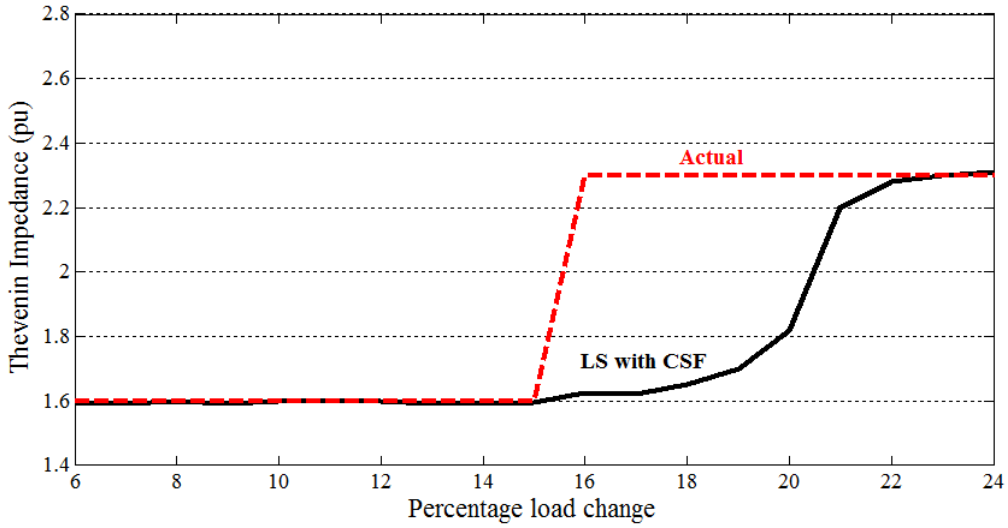

Figure 3.21: Estimated Thévenin impedances at Bus 26 (load at Bus 26 incremented in 1% steps) and transmission line between Bus 24 and Bus 25 taken out of service

The third case consists of estimating the values of the Thévenin impedance as seen from Bus 29 while the real power load at Bus 26 increased in steps of 1%. Figure 3.22 shows the estimated values of Thévenin impedance seen from bus 29 as the active power on bus 26 increased in steps of 1%. Figure 3.23 shows the estimated values of Thévenin impedance seen from bus 29 in a case when load increase on bus 26 was in steps of 2% of the initial load.

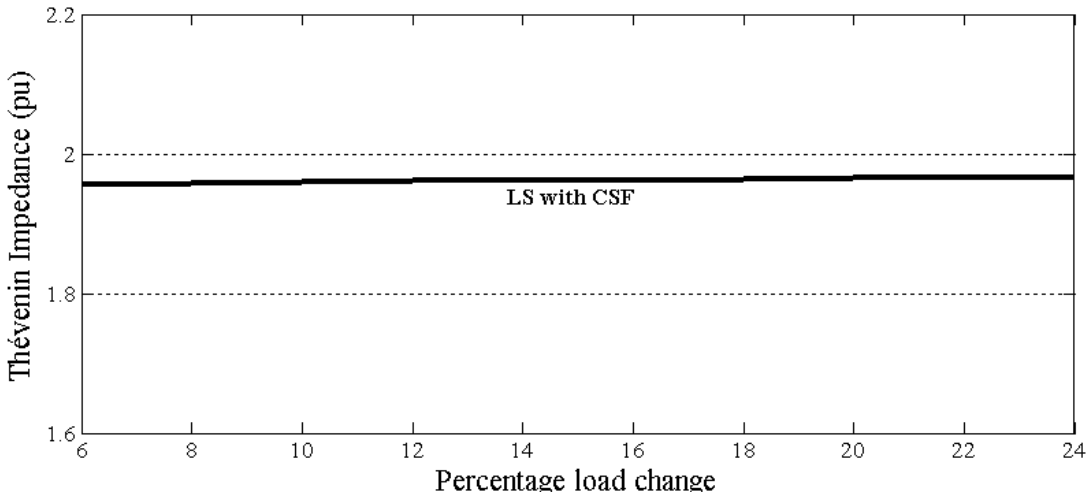

Figure 3.22: Estimated Thévenin impedance at bus 29 (load at bus 26 incremented in 1% steps)

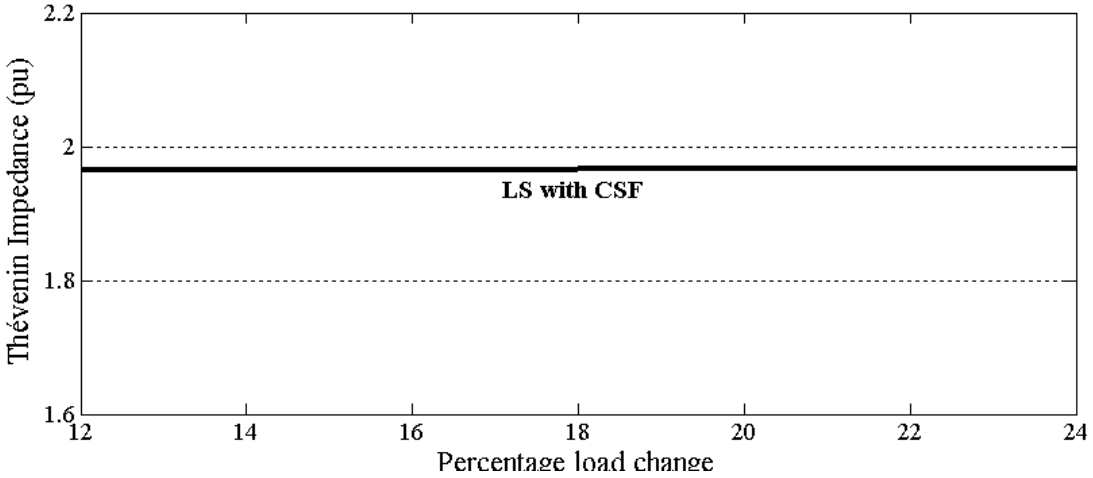

Figure 3.23: Estimated Thévenin impedances at bus 29 (load at bus 26 incremented in 2% steps)

The fifth case is similar to the third case except that the absolute-values of the Thévenin impedance, as seen from Bus 29, were estimated before and after the transmission line from Bus 24 to Bus 25 was taken out of service when load at Bus 26 increased by 14%. The estimated absolute-values of the Thévenin impedance is shown in Figure 3.24.

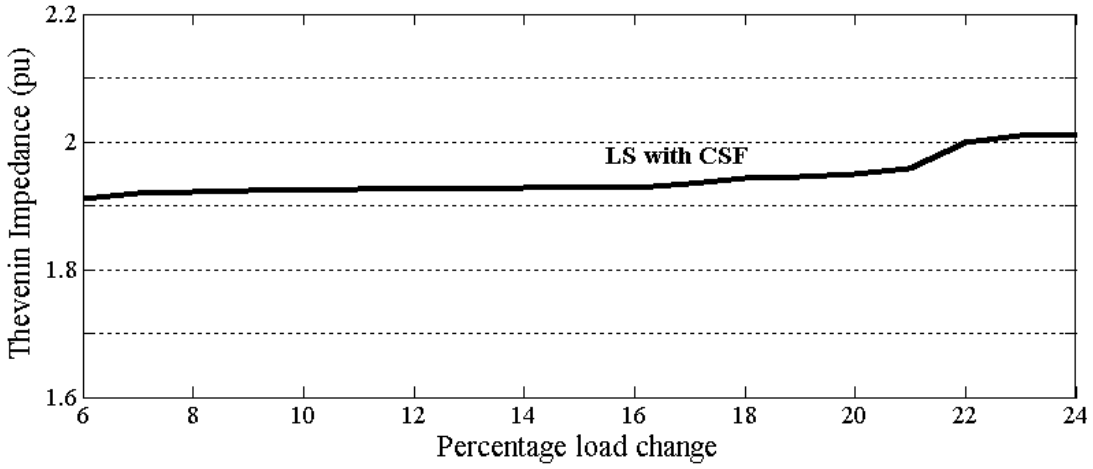

Figure 3.24: Estimated Thévenin impedances at bus 29 (load at bus 26 incremented in 1% steps and transmission line outage is applied between Bus 24 and Bus 25)

The performances of the Delta technique and Least Squares technique augmented with CSF were evaluated in the sixth case. In this case, loads increased on all buses of the system in steps of 1% per minute starting from time t=1 minute to time t=15 minutes. Loads were kept constant after the

load increase on all buses reached 15%. Plot (a) in Figure 3.25 shows the absolute-value of the Thévenin impedance seen from bus 26 when the estimates were obtained by using the Least Squares technique. The estimated absolute value of the Thévenin's impedance increased gradually. Plot (b) in Figure 3.25 shows the absolute value of the Thévenin impedance seen from bus 26 when Least Squares technique augmented with CSF was used. It is obvious from the figure that the absolute value of the estimated Thévenin impedance increased gradually when the loads on all buses increased. Even after the time t=15, the absolute value of the Thévenin's impedance continued to increase but the increase was much less than when the Least Squares technique was used. The estimates shown in this figure prove that Least Squares technique augmented with CSF provides more accurate estimates and tracks changes in the power system operating parameters.

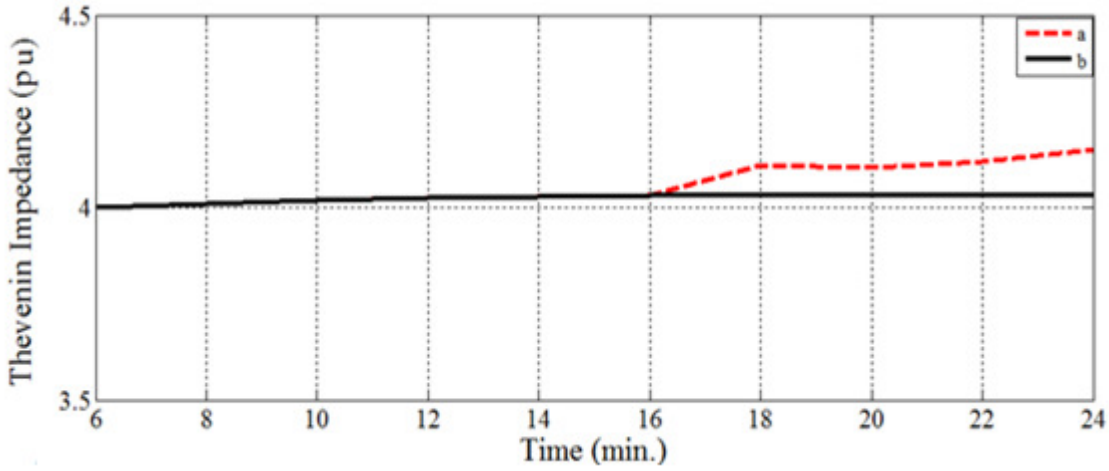

Figure 3.25: Estimated Thévenin impedance at Bus 26 (load on all buses incremented in 1% steps from t=1 min. to t=15 min. and kept constant from t=16 min. to t=24 min.)

3.9 Comparison between results obtained from Delta and LS methods

A comparison of Figure 3.13 and Figure 3.20 show that the absolute values of the Thévenin's impedance, seen from bus 26 for a 1% per minute load increase, estimated using the Delta method augmented with CSF increased gradually while the true value remained constant. These absolute values of these Thévenin's impedances calculated by the Least Squares technique augmented with CSF also increased gradually but to a smaller extent.

Figure 3.21 shows that the estimated absolute values of Thévenin impedance seen from bus 26 for a 1% load increases on Bus 26 and disconnection of a transmission line is effectively tracked by the Least Squares method augmented by CSF. But Figure 3.14 shows that the absolute value of the Thévenin's impedance from Bus 26 for a 1% load increases and disconnection of a line are quite inaccurate.

Figure 3.15 and Figure 3.22 show that the absolute values of Thévenin impedance seen from bus 29 for a 1% load variation on Bus 26 estimated by the Delta and Least Squares techniques augmented with CSF are substantially similar. A comparison of Figure 3.16 and Figure 3.23 show that the absolute values of the Thévenin's impedance, seen from bus 29 for a 2% per minute load increase on Bus 26, estimated using the Delta method augmented with CSF increased gradually. These absolute values of these Thévenin's impedances estimated by the Least Squares technique augmented with CSF also increased gradually but to a smaller extent.

Figure 3.24 shows that the estimated absolute values of Thévenin impedance seen from bus 29 for a 1% load increases on Bus 26 and disconnection of a transmission line is effectively tracked by the Least Squares method augmented by CSF. But Figure 3.17 shows that the absolute value of the Thévenin's impedance seen from Bus 29 gradually increased but to a smaller extent especially after a curtailment of a transmission line.

A comparison of Figures 3.18 and 3.25 shows that the Least Squares technique augmented with CSF provides estimates of the Thévenin's impedance that are closer to the true value compared with the estimates provided by the Delta technique augmented with CSF.

The comparison of the results reveal that the Least Squares method augmented with CSF provides better estimates in all cases compared to the estimates provided by the Delta technique augmented by CSF when the operating parameters change. The performance of the Least Squares method augmented with CSF is much better than the performance of the Delta technique augmented with CSF when the system topology changes are involved.

3.10 Summary

In this chapter a review of the literature on previously used methods for system parameter estimation and details of the developed Delta and LS algorithms have been provided. The main advantages and disadvantages of both developed techniques including data window requirements for implementation of the techniques have been presented in this chapter. In section 3.6, the Cumulative Sum Filter has been introduced to monitor current and voltage measurements while estimating the parameters of the Thévenin equivalent.

The developed Delta and LS techniques can be implemented in off-line as well as in on-line modes. The technique needs measurements of currents and voltages to estimateThévenin equivalentat of the system. The methodologies of both techniques have been explained by applying them on the IEEE 30-Bus test system.

A flowcharts of the developed techniques associated with CSF has been provided to explain the mathematical steps for estimating system parameters. Results obtained the implementation of both techniques have been presented in this chapter as well. The results obtained from Delta and LS techniques have been compared with the actual values of Thévenin impedance. From the comparison between results obtained from developed Delta and LS methods, a conclusion has been made that the LS method with CSF provides accurate estimates in all cases and tracks changes in the power system operating parameters and power system topology.

4. TIME TO VOLTAGE COLLAPSE ALGORITHM

4.1 Introduction

The concept of voltage collapse has been introduced in chapter 2. Factors affecting voltage collapse and countermeasures that can be taken have been also discussed. Static and dynamic techniques used in voltage collapse analysis including methods based on local measurements have been presented in that chapter as well.

The development of modified Delta and Last Squares techniques based on local measurements for estimating system parameters have been introduced in chapter 3. The results obtained from the applications of these techniques have been also presented and discussed.

A technique for estimating time to voltage collapse developed during the course of research conducted for this project is presented in this chapter. The methodology used in the developed technique is also included. The technique was applied to a model of the IEEE 30-Bus test system. The results obtained from the application of this technique are compared with the results obtained from the application of the previously discussed local based measurement techniques.

4.2 Literature review on voltage collapse prediction

A number of methods for analyzing and predicting voltage collapse have been previously proposed. These techniques use continuous mathematical models of system components for finding bifurcation points (points that are common to more than one branch of solutions) in the solution. Unfortunately, many components in the power system cannot be properly described with continuous models. Therefore, analytical approaches have their limitations [6].

Detailed models of system components have been developed and used in dynamic computer simulations of voltage collapse. One problem with this approach is that it works under limited specific conditions. If these conditions are not satisfied, as is often the case in voltage stability studies, these approaches can yield an incorrect solution or provide no solution at all [88,89,90].

Very few on-line methods that predict proximity to voltage collapse and subsequently take corrective actions have been proposed. The first publication used only the voltage phasors at system buses and identified the critical transmission path for real and reactive power flow by computing a transmission path stability index [18]. However, voltage stability evaluation using voltage alone is not likely to always give a correct indication of an impending collapse [3]. In the technique based on power system decomposition, the power system is partitioned into several radial transmission networks, starting at reactive-power source buses and ending at reactive-power load buses [19]. These sub-networks are then transformed into two-bus equivalent systems. Since the analytical solution for maximum power transfer for the two-bus network can be determined, the stability of power transfer along each transmission path is calculated. The technique combines the voltage collapse proximity indicator and the maximum reactive power reserve indicator. Using the two indicators means that the determination of a protection activation threshold is not straightforward. A second drawback of this approach is that the distance of reactive-power sources from the affected load buses is not taken into consideration when the reactive-power reserve of generators is calculated. This method often produces results that are too conservative.

The technique determines the maximum loading of a particular bus in a power system by assuming that the load at the other buses remains constant is not very realistic [19]. Also, the equivalent system used to estimate the maximum load that may be supplied at a bus may not faithfully represent the original system over the entire operating range.

A simple and straightforward technique measures voltages and currents and determines the maximum active and reactive power load that can be supplied. The technique monitors the load and continuously updates the values of the maximum load that can be supplied and calculates the voltage stability margin of the system [21].

The code-named SMART [Stability Monitoring and Reference Tuning] technique uses only local voltage and current measurements and calculates the maximum load that the transmission system can supply to a load bus [7]. According to this technique, the voltage collapse occurs when the local load approaches the system impedance. Although this approach is simple enough to be implemented in numerical relays, it is not capable of tracking load changes caused by voltage drop in nearby buses. Thévenin equivalents seen from other load buses are not observable in this method.

4.3 Local measurements – and subsystem measurements – based methods

Local measurements based techniques use system Thévenin impedance and Thévenin voltage from measurements of local currents and voltages to predict margin to voltage collapse [20,21,7]. The main problem with these techniques is that the number of equations that describe the Thévenin equivalent seen from a bus is less than the number of unknowns. There are, therefore, infinite solutions leading to infinite number of Thévenin equivalents. This problem is resolved by taking measurements at two or more different instants of time and assuming that the Thévenin equivalent has not changed during that period. Problems arise when the Thévenin equivalent changes; the technique provides incorrect prediction of time to voltage collapse. To overcome this problem, the estimation is delayed until the next valid estimation is available. However, the results are often unsatisfactory because the technique is unable to track the system leading towards voltage collapse.

Figure 4.1 shows a system model used in the VIP algorithm. In the case of rapid changes in this system such as loss of a transmission line or generator, the local-based algorithm is able to detect changes in estimates determined from two consecutive sets of measurements. The main weakness in this technique is that any load change on a nearby bus appears as changes in the Thévenin equivalent.

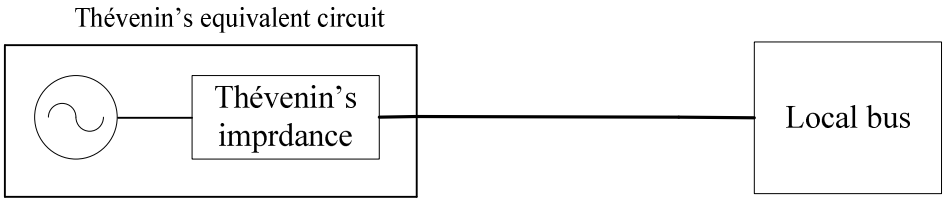

Figure 4.1: VIP algorithm system representation

The model of Figure 4.1 can be extended to include an additional transmission line and station bus as shown in Figure 4.2. Voltage dependant loads are supplied from both buses. These loads respond to voltage drop caused by restoring the loads to pre-contingency levels. The Thévenin equivalent seen from Bus 1 depends on the changes of load on Bus 2. For extreme values of system impedances, if the impedance of load on Bus 2 is equal to zero, the estimated Thévenin impedance seen from bus 1 is equal to the transmission line impedance. If the load impedance on Bus 2 is equal to infinity, the Thévenin impedance seen from Bus 1 is equal to the Thévenin impedance seen from Bus 2 plus the impedance of the transmission line that connects Bus 1 to Bus 2.

The time to voltage collapse technique developed during the work reported in this thesis improves the robustness of the local-based algorithm by taking into consideration local measurements as well as measurements taken at the nearby buses. The developed technique determines not only the lumped system equivalent but also subsets of Thévenin equivalents at different time instances. The technique expands the basic concepts of the local-based protection algorithm to wide-area system protection [91].

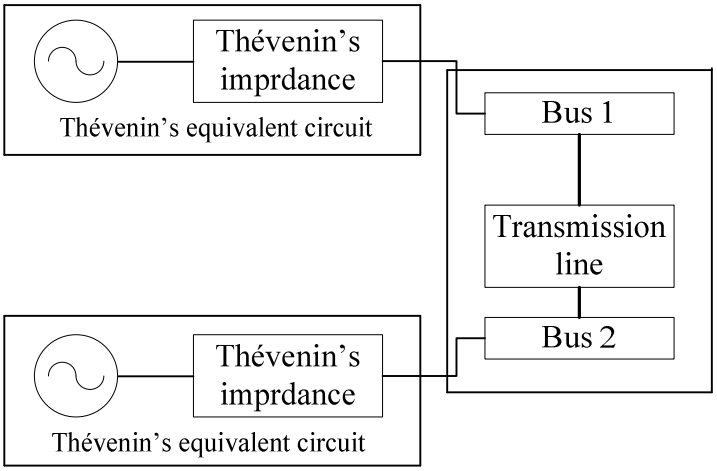

Figure 4.2: Time to voltage collapse system representation

4.4 Method of calculating time to voltage collapse

To clarify the basic concept of time to voltage collapse technique, a simple two-bus system, shown in Figure 4.3, is used as example. It is assumed that the proposed relay that uses the developed time to voltage collapse technique is located on Bus 1. The relay uses two sets of voltage and current measurements taken at Buses 1 and 2 and takes into consideration future load changes on both buses.

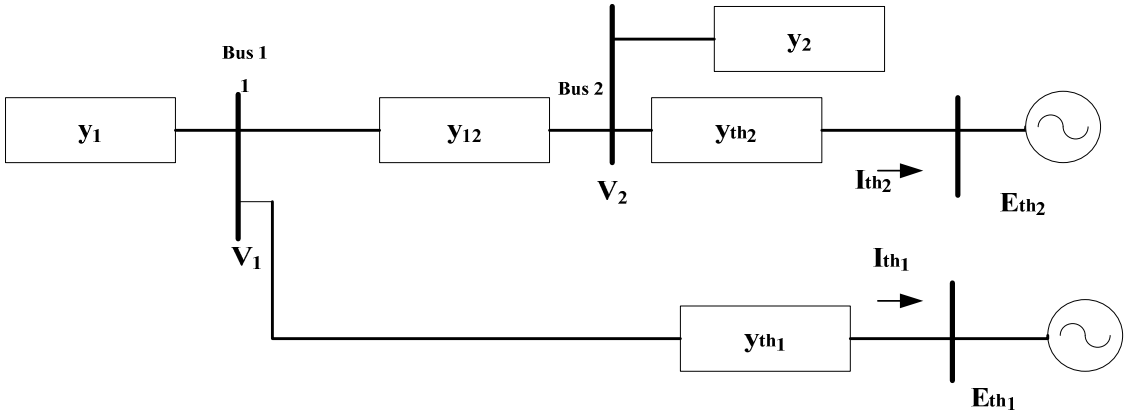

Figure 4.3: Two-Bus model system

The system shown in Figure 4.3 can be described by the following equations.

$$(y_1+y_{th_1}+y_{12})V_1 - y_{12}V_2 - y_{th_1}E_{th_1} = 0$$

$$-y_{12}V_1 + (y_2+y_{th2}+y_{21})V_2 - y_{th2}E_{th2} = 0$$

$$-y_{th1}V_1 + y_{th1}E_{th1} = I_{th1} \qquad (4.1)$$

$$-y_{th2}V_2 + y_{th2}E_{th2} = I_{th2}$$

where,

y_1 is the admittance of the load at Bus 1,

y_2 is the admittance of the load at Bus 2,

y_{th1} is the Thévenin admittance representing the system connected to Bus 1,

y_{th2} is the Thévenin admittance representing the system connected to Bus 2,

y_{12} is the admittance of the transmission line connecting Buses 1 and 2

I_{th1} is the current provided by the Thévenin equivalent of the system connected to Bus 1 , and

I_{th2} is the current provided by the Thévenin equivalent of the system connected to Bus 2.

Equation 4.1 can be written in the matrix form as follows.

$$\begin{bmatrix} y_1+y_{th1}+y_{12} & -y_{12} & -y_{th1} & 0 \\ -y_{12} & y_2+y_{th2}+y_{21} & 0 & -y_{th2} \\ -y_{th1} & 0 & y_{th1} & 0 \\ 0 & -y_{th2} & 0 & y_{th2} \end{bmatrix} \begin{bmatrix} V_1 \\ V_2 \\ E_{th1} \\ E_{th2} \end{bmatrix} = \begin{bmatrix} 0 \\ 0 \\ I_{th1} \\ I_{th2} \end{bmatrix} \qquad (4.2)$$

The first two rows in this equation express the sum of the currents leaving Buses 1 and 2; these Kirchhoff's first law equation can be written as follows.

$$(y_1+y_{th1}+y_{12})V_1 - y_{12}V_2 - y_{th1}E_{th1} = 0$$
$$-y_{12}V_1 + (y_2+y_{th2}+y_{21})V_2 - y_{th2}E_{th2} = 0 \quad (4.3)$$

These equations can be written in a matrix form as follows.

$$\begin{bmatrix} V_1 \\ V_2 \end{bmatrix} = \begin{bmatrix} y_1+y_{th1}+y_{12} & -y_{12} \\ -y_{12} & y_2+y_{th2}+y_{12} \end{bmatrix}^{-1} \begin{bmatrix} y_{th1}E_{th1} \\ y_{th2}E_{th2} \end{bmatrix}$$
$$= \frac{1}{(y_1+y_{th1}+y_{12})(y_2+y_{th2}+y_{12}) - y_{12}^2} \begin{bmatrix} (y_2+y_{th2}+y_{12})y_{th1}E_{th1} + y_{12}y_{th2}E_{th2} \\ (y_1+y_{th1}+y_{12})y_{th2}E_{th2} + y_{12}y_{th1}E_{th1} \end{bmatrix} \quad (4.4)$$

The apparent power, S_1, supplied to the load connected to Bus 1, can be expressed by the following equation.

$$S_1 = \left|V_1(y_1, y_2)\right|^2 |y_1| \quad (4.5)$$

Assuming that Thévenin equivalents are constant during the time when it is being estimated, the voltage V_1 is a function of the admittances y_1 and y_2 as shown in Equation 4.4. Substituting V_1 from Equation 4.4 in Equation 4.5 provides the following equation.

$$S_1 = \frac{\left|A_1 + A_2 y_2\right|^2}{\left|y_1 y_2 + B_1 y_1 + B_2 y_2 + B_3\right|^2} |y_1| \quad (4.6)$$

where,

A_1 represents $[(y_{th2} + y_{12})E_{th1}y_{th1} + y_{12}E_{th2}y_{th2}]$

A_2 represents $[E_{th1}y_{th1}]$

B_1 represents $[y_{th2} + y_{12}]$

B_2 represents $[y_{th1} + y_{12}]$

B_3 represents $[y_{th1}y_{th2} + y_{12}(y_{th1} + y_{th1})]$

The complex parameters A_1, A_2, B_1, B_2, and B_3 are functions of Thévenin impedances y_{th1} and y_{th2}, Thévenin voltages E_{th1} and E_{th2} and the transmission line admittance y_{12}.

Apparent power defined by Equation 4.6 can be plotted in various trajectories as shown in Figure 4.4. This figure shows (i) the maximum power of load at Bus 1 for fixed values of admittance of load at Bus 2 and varying values of admittance of load at Bus 1 and (ii) the maximum power of load at Bus 1 for fixed values of admittance of load at Bus 1 and varying values of admittance of load at Bus 2. These trajectories show that the maximum apparent power that can be supplied to load at Bus 1, shown as "top of the hill", can be different depending on the changes of loads on Bus 2.

This observation can be extrapolated; the maximum reactive power supplied at a bus is affected by changes of loads on other system buses.

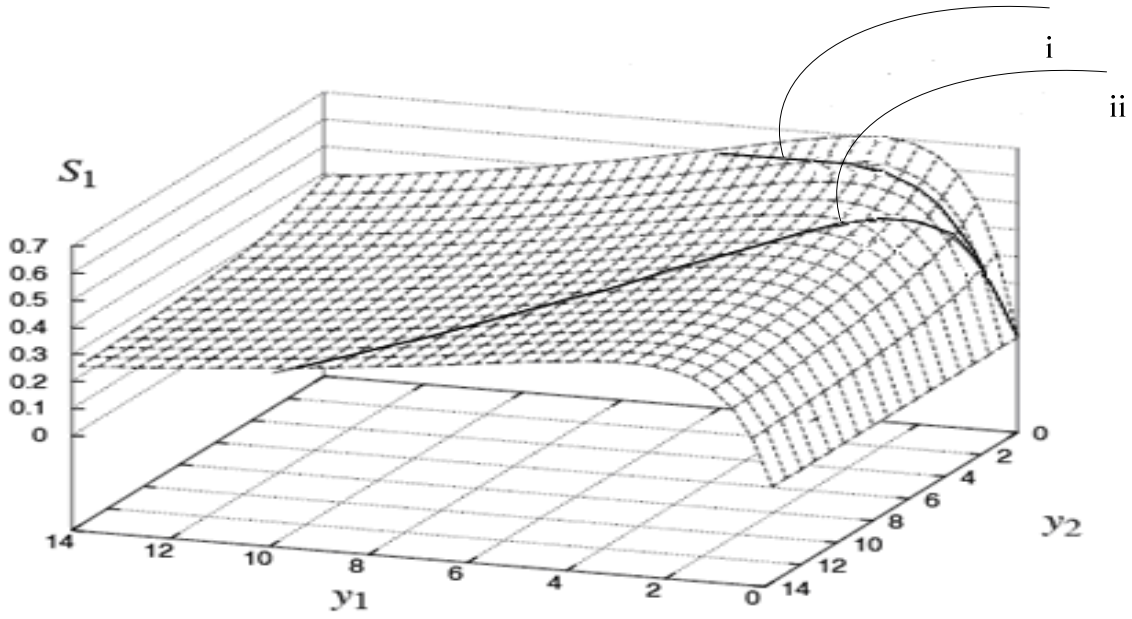

Figure 4.4: Maximum loading point on Bus 1

The time to voltage collapse approach developed in this research depends not only on the present states of both loads but also on expected future load changes. In practical, the expected change in load is obtained from system load forecast. An assumption is made in the work reported in this thesis that all load admittances are functions of present values of load admittances and changes of load admittances expected in future. This yields the following equations:

$$y_1(t) = ym_1(t_0) + \frac{\Delta y_1}{\Delta t}(t - t_0), \text{ and}$$
$$y_2(t) = ym_2(t_0) + \frac{\Delta y_2}{\Delta t}(t - t_0). \tag{4.7}$$

where,

$y_1(t)$ is the admittance of the load at Bus 1 at time t,

$y_2(t)$ is the admittance of the load at Bus 2 at time t,

$ym_1(t_0)$ is the measured admittance of the load at Bus 1 at time t_0,

$ym_2(t_0)$ is the measured admittance of the load at Bus 2 at time t_0,

Δy_1 is the expected incremental change of admittance of load at Bus 1, and

Δy_2 is the expected incremental change of admittance of load at Bus 2.

Separating the imaginary and real parts of the terms on the right-hand side of Equation 4.7 provides the following equations.

$$y_1(t) = gm_{1_r}(t_0) + \frac{\Delta g_{1_r}}{\Delta t}(t - t_0) + j[bm_{1_i}(t_0) + \frac{\Delta b_{1_i}}{\Delta t}(t - t_0)], \text{ and}$$
$$y_2(t) = gm_{2_r}(t_0) + \frac{\Delta g_{2_r}}{\Delta t}t + j[bm_{2_i}(t_0) + \frac{\Delta b_{2_i}}{\Delta t}t]. \tag{4.8}$$

where,

$gm1_r(t_0)$ is the real part of the measured admittance of the load at Bus 1 ym_1 at time t_0,

$gm2_r(t_0)$ is the real part of the measured admittance of the load at Bus 2 ym_2 at time t_0,

$\Delta g1_r$ is the real part of the expected incremental change of admittance of load at Bus 1,

$\Delta g2_r$ is the real part of the expected incremental change of admittance of load at Bus 2,

$bm1_i(t_0)$ is the imaginary part of the measured admittance of the load at Bus 1, ym_1, at time t_0,

$bm2_i(t_0)$ is the imaginary part of the measured admittance of the load at Bus 2, ym_1, at time t_0,

$\Delta b1_i$ is the imaginary part of the expected incremental change of admittance of load at Bus 1, and

$\Delta b2_i$ is the imaginary part of the expected incremental change of admittance of load at Bus 2,

Substituting Equation 4.8 in Equation 4.6 provides an equation for the reactive power load at Bus1. The numerator has two terms; one term of the numerator is as follows.

$$\left|A_1+A_2y2(t)\right|^2 = [A_1 + A_2ym2(t_0) + A_2\frac{\Delta y2}{\Delta t}t][A_1 + A_2ym2(t_0) + A_2\frac{\Delta y2}{\Delta t}t]^*. \quad (4.9)$$

Simplifying Equation 4.9 provides the following equation.

$$\left|A_1+A_2y2(t)\right|^2 = D_0 + D_1t + D_2t^2. \quad (4.10)$$

The variables D_0, D_1, and D_2 are function of the system parameters as shown below.

where,

D_0 represents $\left|A_1 + A_2ym2(t_0)\right|^2$,

D_1 Represents $\{2[Real[(A_1 + A_2 ym2(t_0)][A_2 \frac{\Delta y2}{\Delta t} t]^*\}$, and

D_2 Represents $\left| A_2 \frac{\Delta y2}{\Delta t} t \right|^2$.

Equation 4.11 defines the absolute value of the admittance of the load at Bus 1.

$$|y1| = \sqrt{y1(t)(y1(t))^*} \tag{4.11}$$

Substituting Equation 4.8 in Equation 4.11 provides the following equation.

$$|y1| = \sqrt{[ym1(t_0) + \frac{\Delta y1}{\Delta t} t][ym1(t_0) + \frac{\Delta y1}{\Delta t} t]^*} \tag{4.12}$$

Simplifying Equation 4.12

$$|y1| = \sqrt{Y_0 + Y_1 t + Y_2 t^2}. \tag{4.13}$$

The variables Y_0, Y_1, and Y_2 are function of the system parameters as shown below.

where,

Y_0 represents $|ym1(t_0)|^2$,

Y_1 represents $2\{Real[ym1(t_0)(\frac{\Delta y1}{\Delta t} t)^*]\}$, and

Y_2 represents $\left| \frac{\Delta y1}{\Delta t} t \right|^2$.

As already mentioned, substituting Equation 4.8 in Equation 4.6 provides the equation for the reactive power load at Bus1. The denominator of the resulting equation is as follows.

$$|y1(t)y2(t) + B_1 y1(t) + B_2 y2(t) + B_3|^2 = F_0 + F_1 t + F_2 t^2 + F_3 t^3 + F_4 t^4 \tag{4.14}$$

The variables F_0, F_1, F_2, F_3 and F_4 are function of the system parameters as shown below.

where,

F_0 represents $\left|y_{m1}(t_0)y_{m2}(t_0) + B_1 y_{m1}(t_0) + B_2 y_{m2}(t_0) + B_3\right|^2$,

F_1 represents

$$2\{Real[(y_{m1}(t_0)\frac{\Delta y_2}{\Delta t}t] + y_{m2}(t_0)(\frac{\Delta y_1}{\Delta t}t) + B_1(\frac{\Delta y_1}{\Delta t}t) + B_2(\frac{\Delta y_2}{\Delta t}t)]^* [y_{m1}(t_0)y_{m2}(t_0) + B_1 y_{m1}(t_0) + B_2 y_{m2}(t_0) + B_3]\},$$

F_2 represents

$$\left|y_{m1}(t_0)(\frac{\Delta y_2}{\Delta t}t) + y_{m2}(t_0)(\frac{\Delta y_1}{\Delta t}t) + B_1(\frac{\Delta y_1}{\Delta t}t) + B_2(\frac{\Delta y_1}{\Delta t}t)\right|^2 + 2\{Real\{[(\frac{\Delta y_1}{\Delta t}t)(\frac{\Delta y_2}{\Delta t}t)]^*[(\frac{\Delta y_1}{\Delta t}t)(\frac{\Delta y_2}{\Delta t}t) + B_1 y_{m1}(t_0) + B_2 y_{m2}(t_0) + B_3]\},$$

F_3 Represents

$$2\{Real\{[(\frac{\Delta y_1}{\Delta t}t)(\frac{\Delta y_2}{\Delta t}t)]^*(y_{m1}(t_0)(\frac{\Delta y_2}{\Delta t}t) + y_{m2}(t_0)(\frac{\Delta y_1}{\Delta t}t) + B_1(\frac{\Delta y_1}{\Delta t}t) + B_2(\frac{\Delta y_2}{\Delta t}t)]\}$$, and

F_4 represents $\left|(\frac{\Delta y_1}{\Delta t}t)(\frac{\Delta y_2}{\Delta t}t)\right|^2$.

By substituting Equations 4.10, 4.13, and 4.14 in Equation 4.6, the apparent power delivered to Bus 1 can rewritten as a function of variables D_i, Y_i and F_i as shown below.

$$S_1 = \frac{D_0 + D_1 t + D_2 t^2}{F_0 + F_1 t + F_2 t^2 + F_3 t^3 + F_4 t^4}\sqrt{Y_0 + Y_1 t + Y_2 t^2} \tag{4.15}$$

The derivative of S_1 at the time to voltage collapse, T_c is as follows.

$$\left.\frac{dS_1}{dt}\right)_{t=Tc} = (\sqrt{Y_0 + Y_1T_c + Y_2T_c^2})\frac{(D_1 + 2D_2T_c)(F_0 + F_1T_c + F_2T_c^2 + F_3T_c^3 + F_4T_c^4)}{(F_0 + F_1T_c + F_2T_c^2 + F_3T_c^3 + F_4T_c^4)^2} -$$

$$(\sqrt{Y_0 + Y_1T_c + Y_2T_c^2})\frac{(D_0 + D_1T_c + D_2T_c^2)(F_1 + 2F_2T_c + 3F_3T_c^2 + 4F_4T_c^3)}{(F_0 + FT_{c1} + F_2T_c^2 + F_3T_c^3 + F_4T_c^4)^2} + \qquad (4.16)$$

$$\frac{(D_0 + D_1T_c + D_2T_c^2)(Y_1 + 2Y_2T_c)}{2(\sqrt{Y_0 + Y_1T_c + Y_2T_c^2})(F_0 + F_1T_c + F_2T_c^2 + F_3T_c^3 + F_4T_c^4)^2} = 0$$

Simplifying Equation 4.16 and equating the numerator to zero provides the seventh other polynomial as follows.

$$\sum_{m=0}^{7} G_m T_c^{\,m} = 0. \qquad (4.17)$$

Expanding Equation 4.17 provides

$$G_0 + G_1T_c + G_2(T_c)^2 + G_3(T_c)^3 + G_4(T_c)^4 + G_5(T_c)^5 + G_6(T_c)^6 + G_7(T_c)^7 = 0. \qquad (4.18)$$

where,

G_0 represents $[D_0Y_1F_0 - 2Y_0D_0F_1 + 2Y_0D_1F_0]$,

G_1 represents $[-D_0Y_1F_1 + 2D_0Y_2F_0 + 3D_1Y_1F_0 + 4Y_0D_2F_0 - 4Y_0D_0F_2]$,

G_2 represents $[-3D_0Y_1F_2 + D_1Y_1F_1 + 4D_1Y_2F_0 + 5D_2Y_1F_0 - 2Y_0D_1F_2 + 2Y_0D_2F_1 - 6Y_0D_0F_3]$,

G_3 represents
$[-5D_0Y_1F_3 - 2D_0Y_2F_2 - D_1Y_1F_2 + 2Y_2D_1F_1 + 3D_2Y_1F_1 + 6D_2Y_2F_0 - 4Y_0D_1F_3 - 8Y_0D_0F_4]$,

G_4 represents
$[-7D_0Y_1F_4 - 4D_0Y_2F_3 - 3D_1Y_1F_3 + D_2Y_1F_2 + 4D_2Y_2F_1 - 6Y_0D_1F_4 - 2Y_0D_2F_3]$,

G_5 represents $[-6D_0Y_2F_4 - 5D_1Y_1F_4 - 2D_1Y_2F_3 - D_2Y_1F_3 + 2D_2Y_2F_2 - 4Y_0D_2F_4]$,

G_6 represents $[-4D_1Y_2F_4 - 3D_2Y_1F_4]$, and

G_7 represents $[-2D_2Y_2F_4]$.

This equation can be solved numerically. Positive values of T_c mean that the system is moving towards voltage collapse, while negative values of T_c mean that the system is past the instant of voltage collapse. A complex value of T_c is an unfeasible solution. Thus, the solution is limited to $T_c \in [0, \infty]$. When T_c is equal to zero; the system reaches the moment of voltage collapse. Also note that Equation 4.18 may yield several plausible values, in which case T_c is obtained by picking the minimum value from those solutions.

4.5 Test case

A test simulation is included here to demonstrate the developed approach for tracking time to voltage collapse. The trajectories of load admittances y_1 and y_2 are assumed as defined by Equation 4.19 and are shown in Figure 4.5.

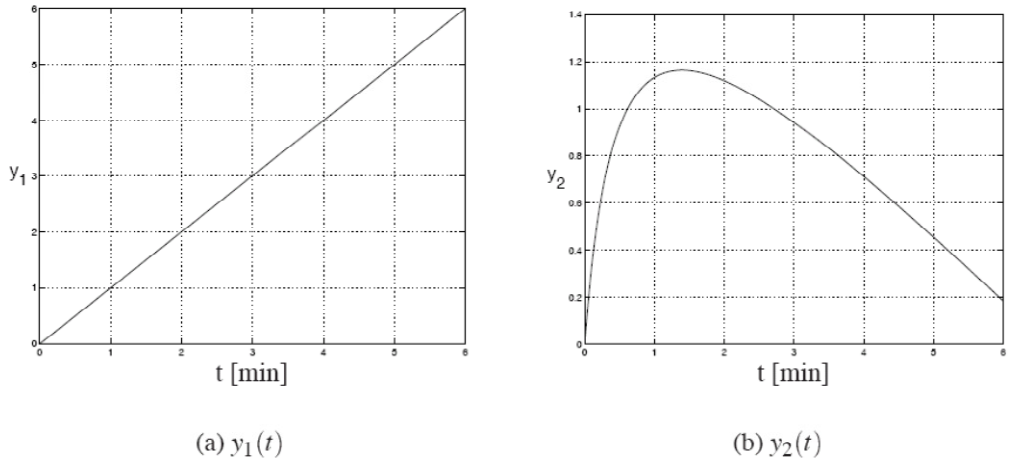

(a) $y_1(t)$ (b) $y_2(t)$

Figure 4.5: Load trajectories

$$y_1(t) = t$$

$$y_2(t) = \frac{4t - 0.6t^2}{1 + 2t} \tag{4.19}$$

These variables as well as the transmission line admittance at any instant are assumed to be known. In real time, the variables will be calculated from voltage and current measurements at every instant.

The time derivatives of Equation 4.19 are:

$$\frac{dy_1}{dt} = 1$$

$$\frac{dy_2}{dt} = \frac{4 - 1.2t - 1.2t^2}{(1 + 2t)^2} \tag{4.20}$$

By substituting Equations 4.19 and 4.20 in Equations 4.10, 4.13, and 4.15 the apparent power can be plotted in various trajectories as shown in Figure 4.6. The trajectory of load changes at Bus 2 only shows maximum reactive power shown as “A” whereas the trajectory of load changes at Bus 1 only shows maximum reactive power shown as “B” . These trajectories show that the maximum reactive power that can be supplied to load at Bus 1, shown as “top of the hill”, is different for two selected patterns of load changes.

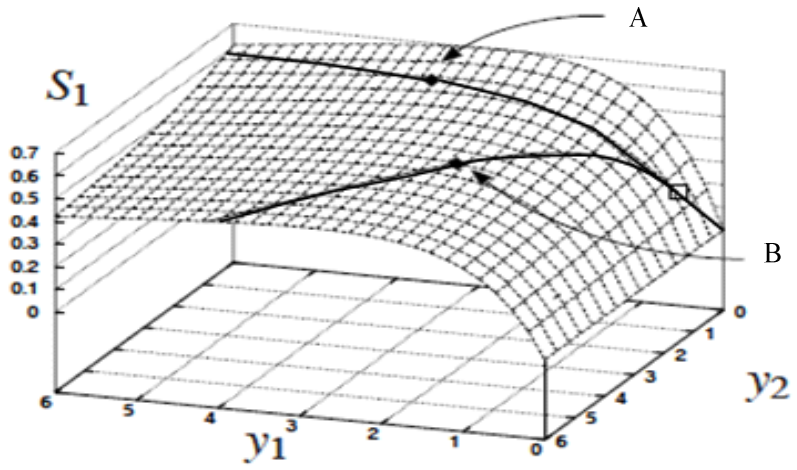

Figure 4.6: Maximum loading point on Bus 1

The two load trajectories reach the maximum point of power transfer "top of the hill". At this point, the time to voltage collapse is zero. Time to voltage collapse can be estimated by applying Equation 4.18. Figure 4.7 shows the estimated time to voltage collapse when load changes are applied on both buses 1 and 2.

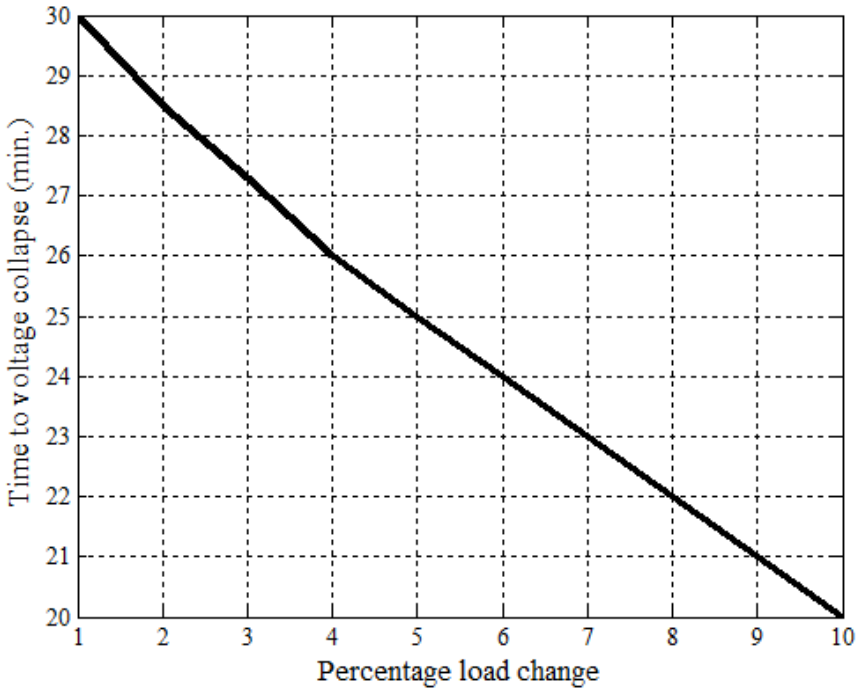

Figure 4.7: Time to voltage collapse

4.6 Generalization to N buses

The main advantage of the developed time to voltage collapse technique is the ability of the technique to take into consideration changes in loads at the local bus as well as loads at the neighbouring buses. The technique can be implemented in any system whose parameters are known and the voltages and currents can be measured in real time. Figure 4.8 shows Bus 1 connected to N-1 known buses.

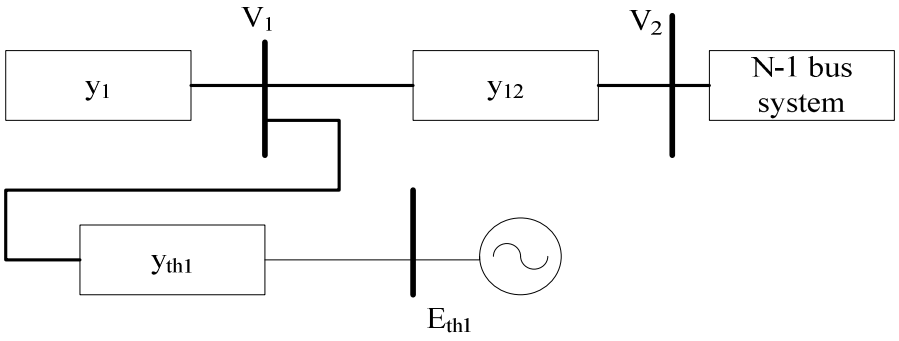

Figure 4.8: N-Bus model system

The voltage and current measurements taken on N buses of the system shown in Figure 4.8 can be written in the following form.

$$\begin{bmatrix} V_1 \\ V_2 \\ \vdots \\ V_N \end{bmatrix} = \begin{bmatrix} (y_1+L_1) & -y_{12} & \dots & -y_{1N} \\ -y_{21} & (y_2+L_2) & \dots & -y_{2N} \\ \vdots & \vdots & \ddots & \vdots \\ -y_{N1} & -y_{N2} & \dots & (y_N+L_N) \end{bmatrix}^{-1} \begin{bmatrix} P_1 \\ P_2 \\ \vdots \\ P_N \end{bmatrix} \qquad (4.21)$$

where,

i is an integer represents the bus number, i= 1, 2, …, N.

V_i is the voltage measured at Bus i,

y_i is the load admittance at Bus i, and

L_i represents sum of Thévenin and transmission line admittances connected to Bus i, and

P_i represents Thévenin voltage on Bus i multiplied by Thévenin admittance connected to Bus i.

In this equation the diagonal elements are function of load admittances and non-diagonal elements are parameter that is calculated using the values of the transmission line admittances.

Voltage on Bus 1 is a function of all admittances connected to the bus as shown in Equation 4.22.

$$V_1 = \frac{M(y_2, ..., y_N)}{N(y_1, ..., y_N)}. \tag{4.22}$$

where,

$M(y_2, ..., y_N)$ represents $A(1)\prod_{I=2}^{N} y_i + \sum_{k=0}^{N-2}\left(\sum_{i_1=1}^{N-k}\sum_{i_2=i_1+1}^{N-k+1}\cdots\sum_{i_{k+1}=i_{k+1}}^{N} A(i,\ldots i_{k+1})\prod_{i\notin(1,i_1,\ldots i_{k+1})} y_i\right)$,

$N(y_1, ..., y_N)$ represents $\prod_{I=2}^{N} y_i + \sum_{k=0}^{N-1}\left(\sum_{i_1=1}^{N-k}\sum_{i_2=i_1+1}^{N-k+1}\cdots\sum_{i_{k+1}=i_{k+1}}^{N} B(i,\ldots i_{k+1})\prod_{i\notin(1,i_1,\ldots i_{k+1})} y_i\right)$.

The apparent power can be expressed as:

$$S_{1(y_1, \text{---}, y_N)} = \left|V_1(y_1, \text{---}, y_N)\right|^2 \left|y_1\right| \tag{4.23}$$

By substituting Equation 4.22 in Equation 4.23, provides the following equation.

$$S_{1(y_1, \text{---}, y_N)} = \frac{\left|M(y_2, ..., y_N)\right|^2}{\left|N(y_1, ..., y_N)\right|^2}\left|y_1\right|. \tag{4.24}$$

An assumption can be made that all future load admittances are functions of the present values of load admittances and changes of load admittances expected in future as shown in Equation 4.25.

$$
\begin{aligned}
y_1(t) &= gm_{1_r}(t_0) + \frac{\Delta g_{1_r}}{\Delta t} t + j\left[bm_{1_i}(t_0) + \frac{\Delta b_{1_i}}{\Delta t} t\right] \\
y_2(t) &= gm_{2_r}(t_0) + \frac{\Delta g_{2_r}}{\Delta t} t + j\left[bm_{2_i}(t_0) + \frac{\Delta b_{2_i}}{\Delta t} t\right] \\
&\vdots \\
y_N(t) &= gm_{N_r}(t_0) + \frac{\Delta g_{N_r}}{\Delta t} t + j\left[bm_{N_i}(t_0) + \frac{\Delta b_{N_i}}{\Delta t} t\right]
\end{aligned}
\tag{4.25}
$$

where,

$gm_{1_r}(t_0)$ is the real part of the measured admittance of the load at Bus 1 ym_1 at time t_0,

$gm_{2_r}(t_0)$ is the real part of the measured admittance of the load at Bus 2 ym_2 at time t_0,

Δg_{1_r} is the real part of the expected incremental change of admittance of load at Bus 1,

Δg_{2_r} is the real part of the expected incremental change of admittance of load at Bus 2,

$bm_{1_i}(t_0)$ is the imaginary part of the measured admittance of the load at Bus 1, ym_1, at time t_0,

$bm_{2_i}(t_0)$ is the imaginary part of the measured admittance of the load at Bus 2, ym_1, at time t_0,

Δb_{1_i} is the imaginary part of the expected incremental change of admittance of load at Bus 1,

Δb_{2_i} is the imaginary part of the expected incremental change of admittance of load at Bus 2,

$gm_{N_r}(t_0)$ is the real part of the measured admittance of the load at Bus N ym_N at time t_0,

Δg_{N_r} is the real part of the expected incremental change of admittance of load at Bus N,

$bm_{N_i}(t_0)$ is the imaginary part of the measured admittance of the load at Bus N, ym_N, at time t_0, and

Δb_{N_i} is the imaginary part of the expected incremental change of admittance of load at Bus N,

Substituting load models shows in Equation 4.25 in Equation 4.24 the following equation can be obtained.

$$S_l = \frac{\sum_{k=0}^{2(N-1)} D_k t^k}{\sum_{j=0}^{2N} F_j t^j} \sqrt{Y_0 + Y_1 t + Y_2 t^2} \tag{4.26}$$

This equation is an expanded form of Equation 4.15. In Equation 4.26 voltage and current measurements from N buses are taken into consideration whereas measurements from two buses are used in Equation 4.15.

Time to voltage collapse, T_c is the minimum value from the solutions of the polynomial obtained by equating the first derivative of Equation 4.26 with respect to time to zero as shown in Equation 4.27 .

$$\left.\frac{dS_l}{dt}\right)_{t=Tc} = \sqrt{Y_0 + Y_1 T_c + Y_2 T_c^2} \left[\frac{(\sum_{j=0}^{2N} F_j T_c^{\,j})(\sum_{k=0}^{2(N-1)} k D_k T_c^{\,k-1}) - (\sum_{j=1}^{2N} j F_j T_c^{\,j-1})(\sum_{k=0}^{2(N-1)} D_k T_c^{\,k})}{(\sum_{j=0}^{2N} F_j T_c^{\,j})^2} \right] +$$

$$\frac{(Y_1 + 2Y_2 T_c)(\sum_{k=0}^{2(N-1)} D_k T_c^{\,k})}{2\sqrt{Y_0 + Y_1 T_c + Y_2 T_c^2}(\sum_{j=0}^{2N} F_j T_c^{\,j})} = 0 \tag{4.27}$$

By multiplying Equation 4.27 by the common denominator, Equation 4.27 can be reduced the following form.

$$\sqrt{Y_0 + Y_1 T_c + Y_2 T_c^{\,2}}\left[\left(\sum_{j=0}^{2N} F_j T_c^{\,j}\right)\left(\sum_{k=0}^{2(N-1)} k D_k T_c^{\,k-1}\right) - \left(\sum_{j=1}^{2N} j F_j T_c^{\,j-1}\right)\left(\sum_{k=0}^{2(N-1)} D_k T_c^{\,k}\right) \right] +$$

$$(Y_1 + Y_2 T_c)\left(\sum_{k=0}^{2(N-1)} D_k T_c^{\,k}\right)\left(\sum_{j=0}^{2N} F_j T_c^{\,j}\right) = 0 \qquad (4.28)$$

Simplifying Equation 4.28 as,

$$\sum_{m=0}^{4N-1} Q_m T_c^{\,m} = 0. \qquad (4.29)$$

Equation 4.29 is a general form of the polynomial that takes into consideration measurements from N buses. As shown in this equation, the order of the polynomial is a function of the number of buses and is equal to 4N-1.

For a two-bus system, the polynomial is of the seventh order, and for a five-bus system it is of the 19^{th} order.

4.7 Size of the model

In the developed time to voltage collapse technique, measurements are taken from the local bus as well as from the neighbouring buses. If the model consists of one bus, this technique behaves like the VIP algorithm.

When load changes at more than one bus are considered, the polynomial becomes complex. The complexity increases with increasing number of buses. If load changes on a large number of buses are considered, the order of the polynomial become large and it becomes difficult to solve which diminishes the effectiveness of the technique.

In this thesis, the maximum number of buses taken into consideration was limited to five. When changes on more than five buses were considered, the effectiveness of the technique did not improve.

4.8 Summary of the methodology of the developed technique

The methodology used for the time to voltage collapse techniques can be summarized as follows:

1. A load flow program is used to simulate various operating conditions of the power system. In this thesis, IEEE 30-Bus test system was used for verifying the effectiveness of the developed technique.

2. The output of the load flow runs is used to estimate the Thévenin equivalents.

3. The results obtained from step 2, the system loads, expected load changes, and transmission line impedances are used as inputs to a MAPLE program. The MAPLE program acts as the front-end for the developed technique.

4. The MATLAB program solves numerically the polynomial given in Equation 4.23 and estimates the system proximity to voltage collapse.

A flow chart of the developed time to voltage collapse technique is given in Figure 4.9.

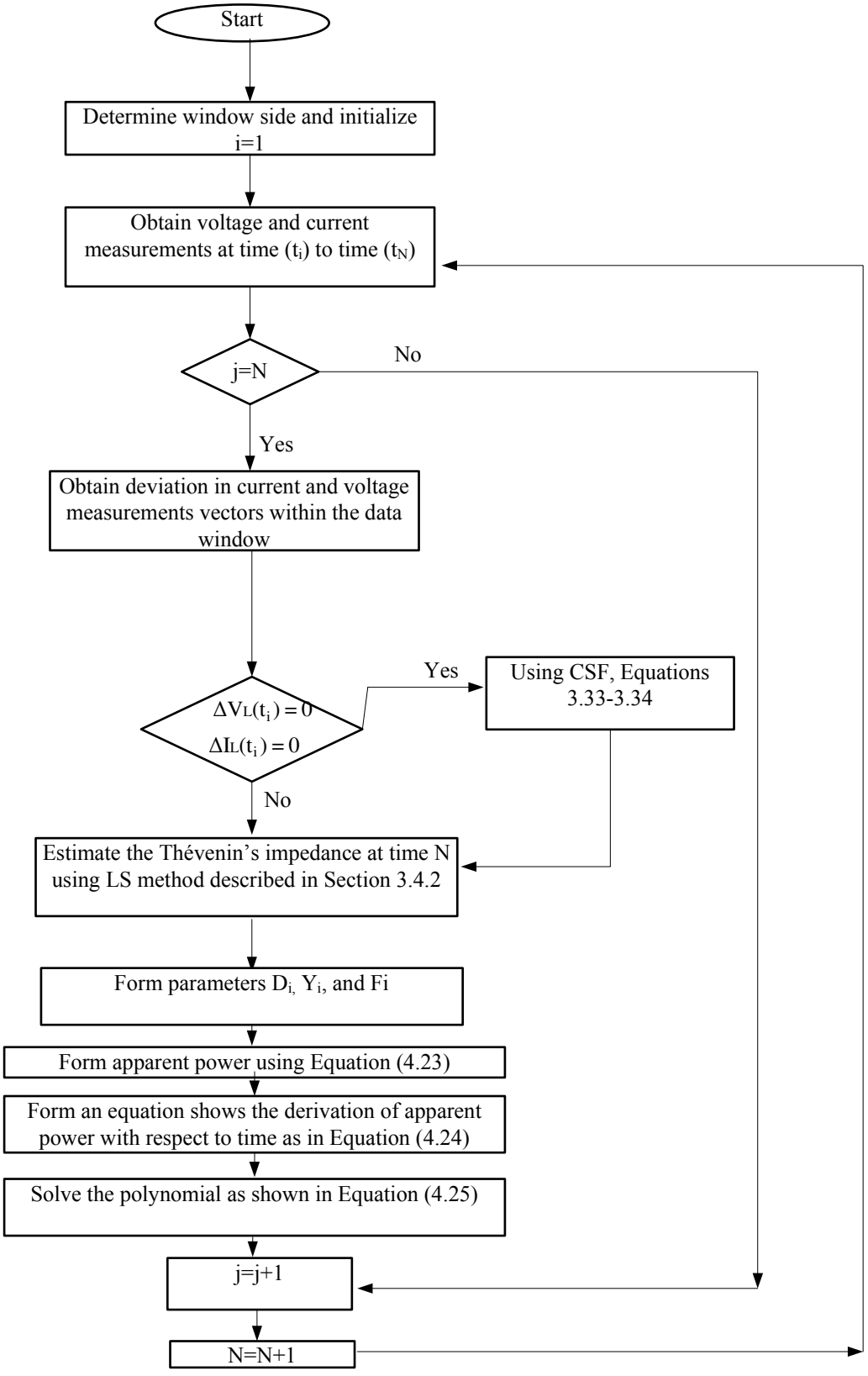

Figure 4.9: Flow chart of time to voltage collapse technique including the CSF and procedure for estimating the Thévenin equivalents

4.9 Summary

In this chapter an overview of the previously used techniques in analyzing voltage collapse and details of the developed time to voltage collapse algorithm have been provided. A review of the literature on previously used methods for predicting voltage collapse has been presented. The main advantages and disadvantages of the local measurements based techniques have been identified. The objective and motivation of the algorithm developed during the work reported in this thesis have been outlined in this chapter as well.

The developed time to voltage collapse technique improves the robustness of the local-based method and can be implemented in off-line as well as in on-line modes. The technique needs measurements of currents and voltages at the heavily loaded buses and the network admittance matrix. Based on this information, time to voltage collapse is calculated considering not only the present loads but also expected load increases in the near future.

The methodology of time to voltage collapse technique has been explained on a simple two bus system in this chapter. A general form of the developed technique that takes into consideration measurements from N buses has also been presented.

A flowchart of the developed technique has been provided to explain the mathematical steps for calculating the time to voltage collapse. The technique requires modest amount of computations to warn from impending voltage collapse.

5. SIMULATION STUDIES AND PSCAD / EMTDC IMPLEMENTATION

5.1 Introduction

The concept of voltage collapse has been introduced in chapter 2. Factors affecting voltage collapse and countermeasures that can be taken have been also discussed. Static and dynamic techniques used in voltage collapse analysis including methods based on local measurements have been presented in that chapter as well.

The development of modified Delta and Last Squares techniques based on local measurements for estimating system parameters have been introduced in chapter 3. The results obtained from the applications of these techniques have been also presented and discussed.

A technique for estimating time to voltage collapse developed during the course of research conducted for this project has been presented in chapter 4. The methodology of time to voltage collapse technique has been explained on a simple two bus system in this chapter. A general form of the developed technique that takes into consideration measurements from N buses has also been presented.

Simulation studies and results obtained from the application of time to voltage collapse technique are presented in this chapter. In addition, the performance of the developed technique is evaluated. PSCAD/EMTDC was extended to include simulation of load changes at specified rates in system performance studies. The cases used for testing the application of the developed technique were simulated on PSCAD/EMTDC. The performance of the developed technique was compared with the results obtained from the PSCAD/EMTDC studies.

5.2 Time to voltage collapse simulation studies

The performance and effectiveness of the developed time to voltage collapse technique was evaluated using the IEEE 30-Bus test system shown in Figure 5.1. The connectivity and electrical parameters of the IEEE 30-Bus test system used for studies reported in this chapter are presented in Appendix A. Time to voltage collapse was calculated for different system operating conditions. Voltage and current phasors of the test system were computed by conducting load flow studies for the selected operating scenarios. All loads in the system were assumed to be P-Q loads except loads connected to the monitored buses. Linear load model as described in Equation 4.7 were used to model loads connected to the monitored buses.

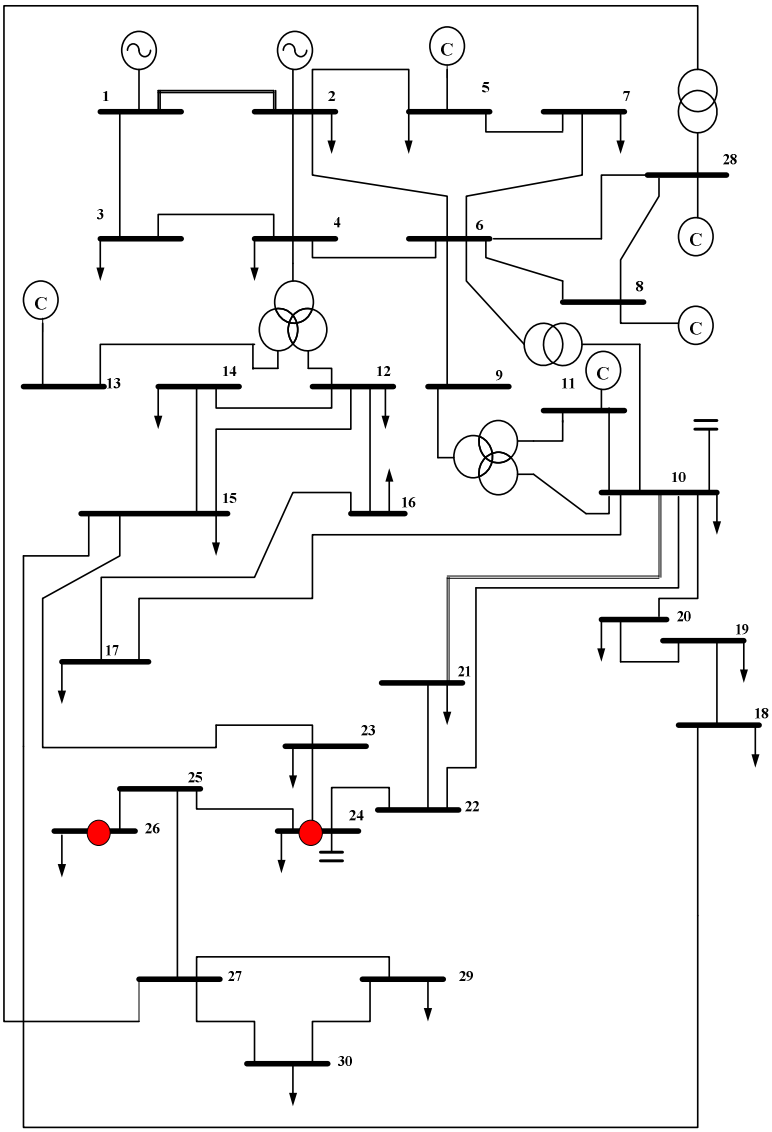

Figure 5.1: Case 1 (Two-Bus System)

The load flow studies and system-parameters identification program were conducted on MATLAB. The results obtained from the programs were used as input to the time to voltage collapse technique was implemented in MAPLE.

The test system were subjected to operating conditions, such as, gradual load increase, transmission line out of service and loss of large block of load. The time to voltage collapse technique was tested for each operating condition using the following four variations of the developed technique [91].

- The technique uses voltages and currents measured at two buses.
- The technique uses voltages and currents measured at three buses
- The technique uses voltages and currents measured at four buses.
- The technique uses voltages and currents measured at five buses.

5.3 Time to voltage collapse studies with data from two buses

It was considered that a time to voltage collapse relay was installed at Bus 26 of the IEEE 30-Bus test system and voltages and currents were monitored at Bus 24 and Bus 26 shown in Figure 5.1. These buses were selected because they are heavily loaded buses.

Performance of the voltage to collapse studies for three system operating scenarios is reported in this section. These include gradual load increase, transmission line taken out of service and load shedding to protect from voltage collapse.

5.3.1 Gradual load increase

The loads at Bus 24 and Bus 26 were considered to have increased gradually. Load flows were conducted and system Thévenin equivalent was estimated using the Least Squares technique with CSF filter described in Section 3.8 of Chapter 3. Voltage and current phasors calculated by the load

flow studies, and the Thévenin equivalent obtained from the application of the Least Squares technique were used as inputs to the time to voltage collapse technique that calculated proximity to voltage collapse.

The base case load flow was conducted and was assigned as load flow at time t=0. The load admittance was calculated and was used to estimate the system admittance to reflect load increases of one percent per minute on all buses. Future loads were then used to conduct load flows at different times until the load flow algorithm failed to converge at t=105 minute. The Thévenin impedances and voltages were calculated for time t_j when j = 1, 2, 3,……., 104 using the procedure described in Section 3.8.1 of Chapter 3.

The Thévenin parameters, voltages and currents at Buses 24 and 26 were provided to the voltage collapse estimation technique that proceeded in the following manner.

1. The technique calculated variables $A_{24}(t = 6,7,8,\ldots\ldots., 104)$ and $A_{26}(t = 6,7,8,\ldots\ldots., 105)$, $B_{26}(t=6,7,8,\ldots.,104)$, and $B_{24}(t=6,7,8,\ldots.,104)$ as defined in Equation 4.6. The application of this equation is reproduced here for ready reference.

$$A_{24}(j) = E_{th26}(j)\, y_{th26}(j)$$

$$A_{26}(j) = \left[y_{th26}(j) + y_{24\text{-}26} \right] \left[E_{th24}(j)\, y_{th24}(j) \right] + y_{24\text{-}26}\, E_{th26}(j)\, y_{th26}(j)$$

$$B_{26}(j) = y_{th26}(j) + y_{24\text{-}26}(j)$$

$$B_{24}(j) = y_{th24}(j) + y_{24\text{-}26}(j)$$

$$B_{26\text{-}24}(j) = y_{th24}(j)\, y_{th26}(j) + y_{24\text{-}26}(j)\,(y_{th24}(j) + y_{th26}(j))$$

2. Variables D(t=6,7,8,…,104), Y(t=6,7,8,…104), and F(t=6,7,8,…104) were calculated by substituting results obtained from steps 1 in Equations 4.10, 4.13, and 4.14 described in Chapter 4. The application of these equations is reproduced here for ready reference.

$$D_0(j) = \left| A_{26}(j) + A_{24}(j)\, ym_{24}(t_0) \right|^2$$

$$D_1(j) = \{2[Real[(A_{26}(j) + A_{24}(j)\, ym_{24}(t_0)][A_{24}(j)\, ym_{24}(t_0)]^*\}$$

$$D_2(j) = \left| A_{24}(j)\, ym_{24}(t_0) \right|^2$$

$$Y_0(j) = \left| ym_{26}(t_0) \right|^2$$

$$Y_1(j) = 2\{Real[ym_{26}(t_0)(\frac{\Delta y_{26}}{\Delta t} j)^*]\}$$

$$Y_2(j) = \left| \frac{\Delta y_{26}}{\Delta t} j \right|^2$$

$$F_0(j) = \left| y_{m26}(t_0) y_{m24}(t_0) + B26(j)\, y_{m26}(t_0) + B_{24}(j)\, y_{m24}(t_0) + B_{26\text{-}24}(j) \right|^2$$

$$F_1(j) = 2\{Real[(y_{m26}(t_0) \frac{\Delta y_{24}}{\Delta t} j] + y_{m24}(t_0)(\frac{\Delta y_{26}}{\Delta t} j) + B_{26}(j)(\frac{\Delta y_{26}}{\Delta t} j) + B_{24}(j)(\frac{\Delta y_{24}}{\Delta t} j)]^*$$

$$[ym_{26}(t_0) y_{m24}(t_0) + B_{26}(j)\, y_{m26}(t_0) + B_{24}(j)\, y_{m24}(t_0) + B_{26-24}(j)]\}$$

$$F_2(j) = \left| y_{m26}(t_0)(\frac{\Delta y_{24}}{\Delta t} j) + y_{m24}(t_0)(\frac{\Delta y_{26}}{\Delta t} j) + B_{26}(j)(\frac{\Delta y_{26}}{\Delta t} j) + B_{24}(j)(\frac{\Delta y_{26}}{\Delta t} j) \right|^2 +$$

$$2\{Real\{[(\frac{\Delta y_{26}}{\Delta t} j)(\frac{\Delta y_{24}}{\Delta t} j)]^*[(\frac{\Delta y_{26}}{\Delta t} j)(\frac{\Delta y_{24}}{\Delta t} j) + B_{26}(j)\, y_{m26}(t_0) +$$

$$B_{24}(j)\, y_{m24}(t_0) + B_{26-24}(j)]\}$$

3. The parameters of the Polynomial, G_0(t=6,7,8,…,104), G_1(t=6,7,8,…104), G_2(t=6,7,8,…104), G_3 (t=6,7,8,…104), G_4(t=6,7,8,…104), G_5(t=6,7,8,…104), G_6(t=6,7,8,…104) and G_7(t=6,7,8,…104) were calculated by substituting results obtained

from steps 2 in Equation 4.18 described in Chapter 4. The application of this equation is reproduced here for ready reference.

$$G_0(j)+G_1(j)T_c(j)+G_2(j)T_c^{\,2}(j)+G_3(j)T_c^{\,3}(j)+G_4(j)T_c^{\,4}(j)+G_5(j)T_c^{\,5}(j)+$$

$$G_6T_c^{\,6}(j)+G_7T_c^{\,7}(j)=0$$

where,

$G_0(j)$ represents $[D_0(j)Y_1(j)F_0(j)-2Y_0(j)D_0(j)F_1(j)+2Y_0(j)D_1(j)F_0(j)]$,

$G_1(j)$ represents

$$[-D_0(j)Y_1(j)F_1(j)+2D_0(j)Y_2(j)F_0(j)+3D_1(j)Y_1(j)F_0(j)+$$
$$4Y_0(j)D_2(j)F_0(j)-4Y_0(j)D_0(j)F_2(j)],$$

$G_2(j)$ represents

$$[-3D_0(j)Y_1(j)F_2(j)+D_1(j)Y_1(j)F_1(j)+4D_1(j)Y_2(j)F_0(j)+$$
$$5D_2(j)Y_1(j)F_0(j)-2Y_0(j)D_1(j)F_2(j)+2Y_0(j)D_2(j)F_1(j)-$$
$$6Y_0(j)D_0(j)F_3(j)],$$

$G_3(j)$ represents

$$[-5D_0(j)Y_1(j)F_3(j)-2D_0(j)Y_2(j)F_2(j)-D_1(j)Y_1(j)F_2(j)+$$
$$2Y_1(j)D_2(j)F_1(j)+3D_2(j)Y_1(j)F_1(j)+6D_2(j)Y_2(j)F_0(j)-$$
$$4Y_0(j)D_1(j)F_3(j)-8Y_0(j)D_0(j)F_4(j)],$$

$G_4(j)$ represents

$$[-7D_0(j)Y_1(j)F_4(j)-4D_0(j)Y_2(j)F_3(j)-3D_1(j)Y_1(j)F_3(j)+$$
$$D_2(j)Y_1(j)F_2(j)+4D_2(j)Y_2(j)F_1(j)-6Y_0(j)D_1(j)F_4(j)-$$
$$2Y_0(j)D_2(j)F_3(j)],$$

$G_5(j)$ represents

$$[-6D_0(j)Y_2(j)F_4(j)-5D_1(j)Y_1(j)F_4(j)-2D_1(j)Y_2(j)F_3(j)-$$
$$D_2(j)Y_1(j)F_3(j)+2D_2(j)Y_2(j)F_2(j)-4Y_0(j)D_2(j)F_4(j)],$$

$G_6(j)$ represents $[-4D_1(j)Y_2(j)F_4(j)-3D_2(j)Y_1(j)F_4(j)]$, and

$G_7(j)$ represents $[-2D_2(j)Y_2(j)F_4(j)]$.

4. The polynomial shown in step 3 was solved and time to collapse T_c (t=6, 7, 8,…, 104), was determined.

Figures 5.2 and 5.3 show the estimated values of Thévenin voltage seen from buses 26 and 24 respectively. It is clear from Figure 5.2 that load increase at all buses caused decrease in estimated values of Thévenin voltage seen from Bus 26. There is also reduction in Thévenin voltage seen from Bus 24 due to load increase at all buses as shown in Figure 5.3.

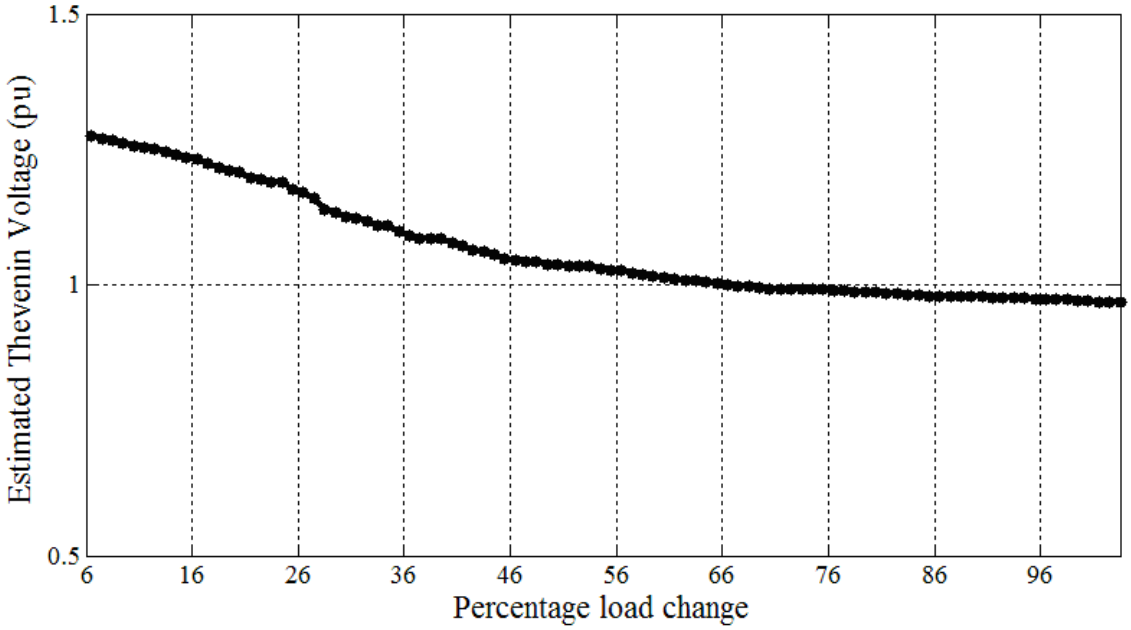

Figure 5.2: Estimated Thévenin voltage seen from Bus 26

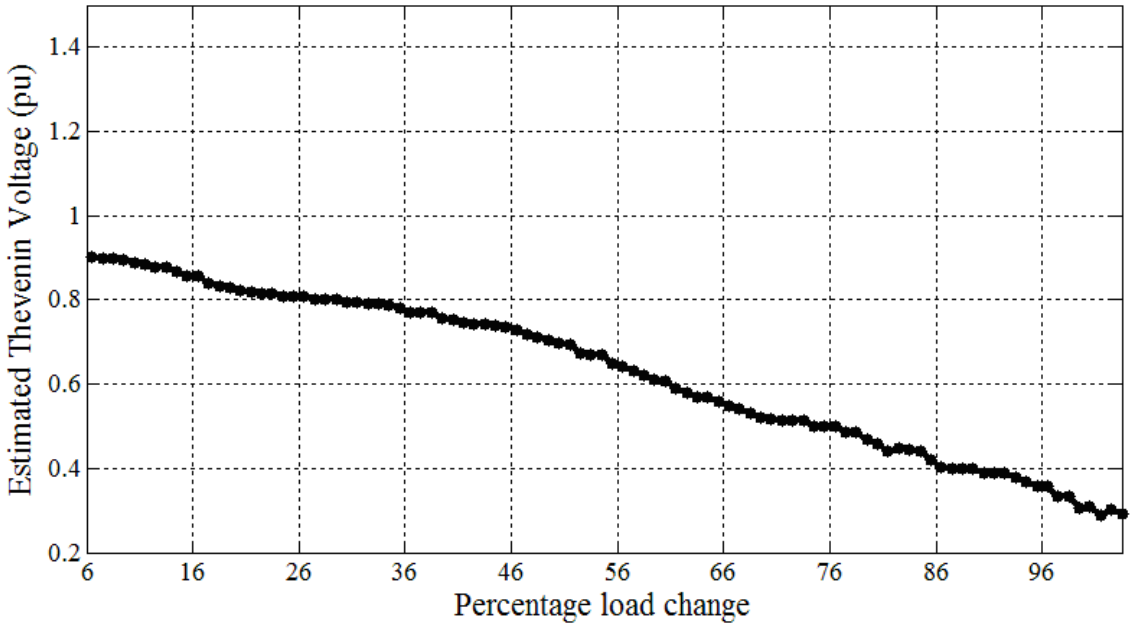

Figure 5.3: Estimated Thévenin voltage seen from Bus 24

The plot of the percentage load increase versus estimated values of Thévenin impedance seen from buses 26 and 24 are shown in Figures 5.4 and 5.5 respectively. It is evident from Figure 5.4 that load increase at all buses caused increase in Thévenin impedance seen from Bus 26. Estimated values of Thévenin impedance seen from Bus 24 increase due to load increase at all buses as shown in Figure 5.5.

Figures 5.4 and 5.5 show the loads on all buses were increased gradually instead of the load increase on Bus 26 only that was done in the case described in Section 3.8.1.

Figure 5.6 shows the time to voltage collapse at Bus 26 for each level of load increase used in this case. It is clear from the figure that any increase in load caused a steep decrease in time to voltage collapse. The figure shows that results obtained from the developed algorithm were consistent with results obtained from the load flow program. Results obtained from the load flow program and the developed algorithm indicated that voltage collapse occurs when load increase on all buses reached 105%.

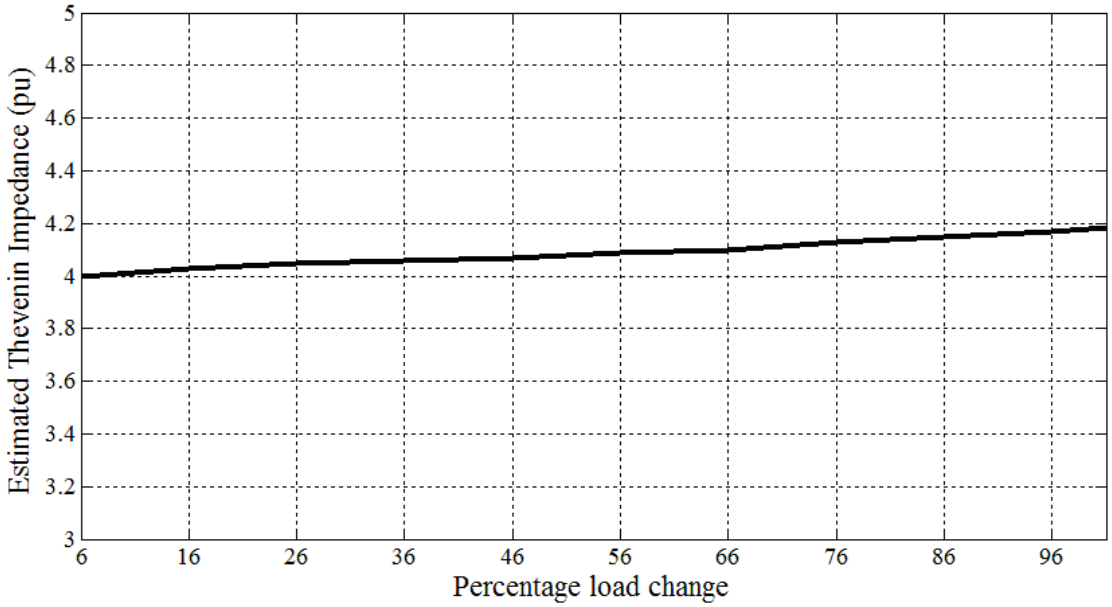

Figure 5.4: Estimated Thévenin impedance seen from Bus 26

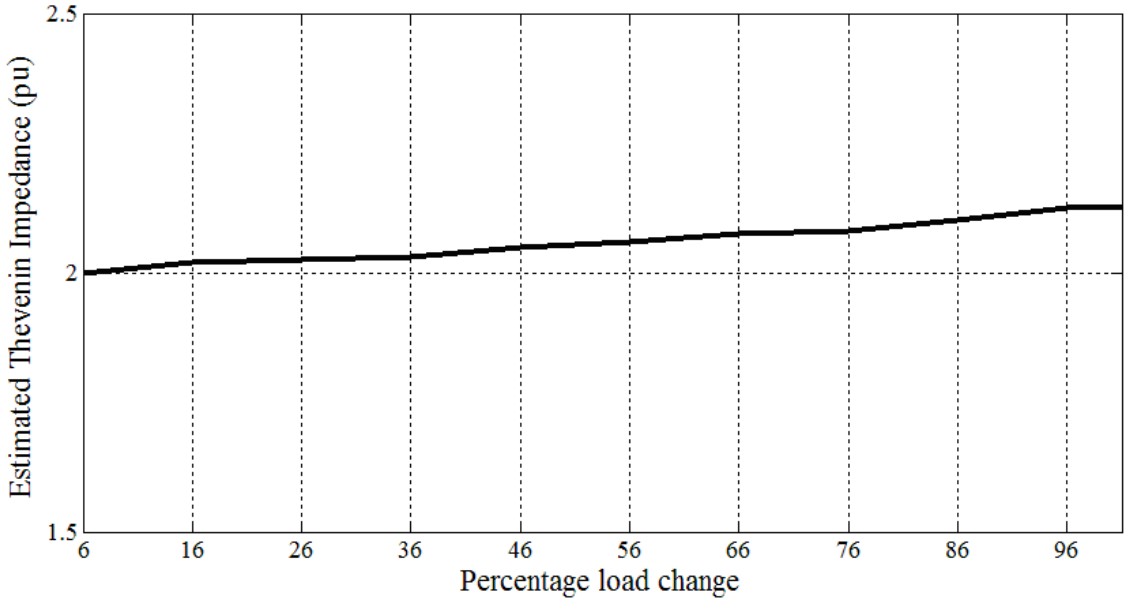

Figure 5.5: Estimated Thévenin impedance seen from Bus 24

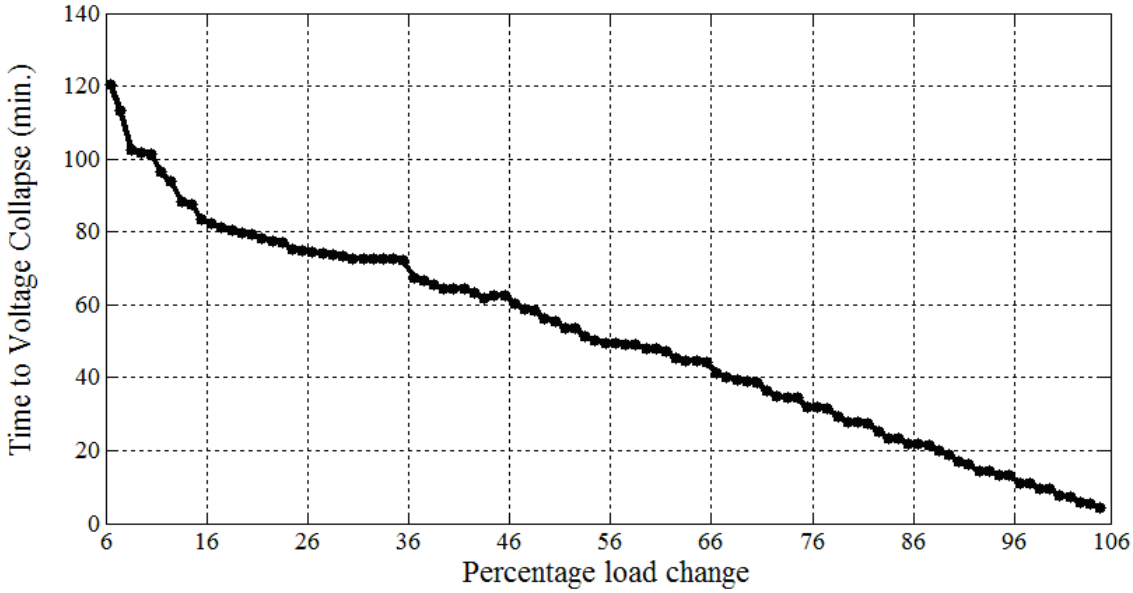

Figure 5.6: Time to voltage collapse

5.3.2 Transmission line outage and gradual load increase

Transmission line from Bus 22 to Bus 24 is one of the vital transmission lines serving loads at Buses 22 and 24. It was considered that loads at all buses increase in this case. Load flows were conducted for every increase in load. The voltage and current phasors on Buses 24 and 26 obtained from load flow studies were given to the system's parameters estimation algorithm. The Thévenin equivalent of the system was estimated using the Least Squares technique with CSF described in Section 3.8. Voltage and current phasors calculated by the load flow studies, and the Thévenin equivalent obtained from the application of the Least Squares technique were used as inputs to the time to voltage collapse technique that calculated proximity to voltage collapse.

The base case load flow was conducted and was assigned as load flow at time t=0. The load admittance was calculated and was used to estimate the load admittances to reflect load increases of one percent per minute. Future loads were then used to conduct load flows at different time until the load flow algorithm fails to converge at t=102 minutes, i.e. t_j, for j = 1, 2, 3, ……., 102. The Thévenin impedances and voltages were calculated for those times using the procedure described in Section 3.8.1.

The Thévenin parameters and phasors of voltages and currents at Buses 24 and 26 were provided to the voltage collapse estimation technique and steps 1, 2, 3, and 4 described in Section 5.3.1 were repeated to determine time to voltage collapse.

The plot of percentage load increase versus time to voltage collapse on Bus 26 is shown in Figure 5.7. A comparison of Figures 5.6 and 5.7 shows that time to voltage collapse at Bus 26 is shorter for each level of load when the transmission line connecting Buses 22 and 24 is out of service. This proves that losing an important transmission line increases the risk of voltage collapse. For example, sixteen percent increase of loads on all buses would result in voltage collapse on Bus 26 in 80 minutes as shown in Figure 5.6. But time to voltage collapse on Bus 26 for the identical load increase decreases to 76 minutes when transmission line from Bus 22 to Bus 24 is out of service.

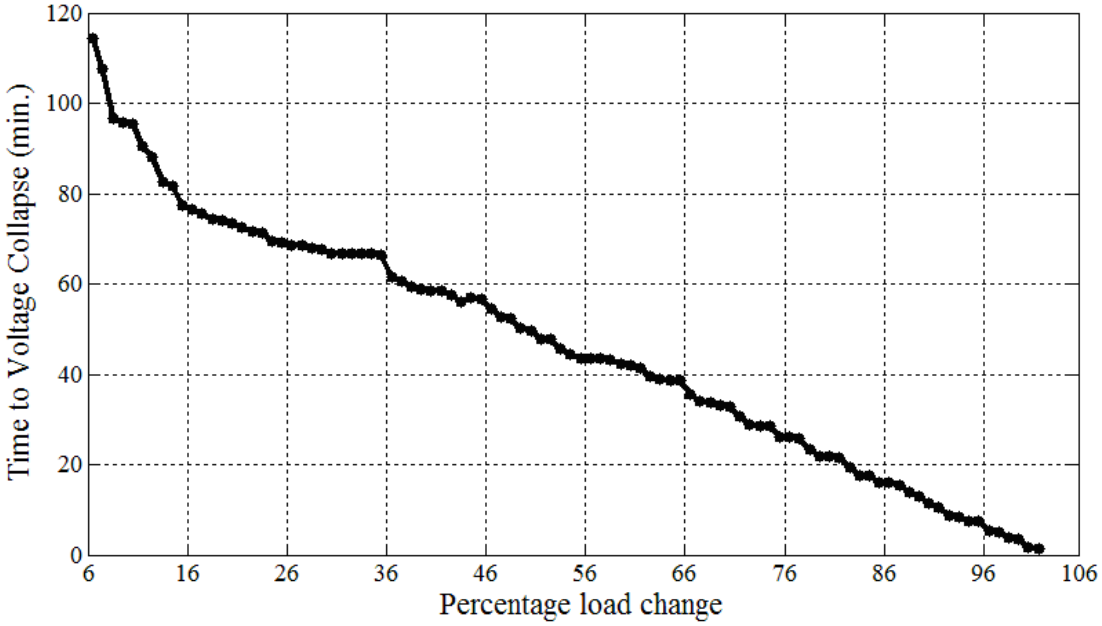

Figure 5.7: Time to voltage collapse when transmission line outage occurs

5.3.3 Load shedding and gradual load increase

System voltage profile can be improved and time to voltage collapse can be increased by implementing a load shedding strategy [58, 92]. A relay that uses time to voltage collapse

algorithm can be easily armed with a local- and/or wide-area control system to activate load shedding when the system is close to the point of voltage collapse.

In the past, many different preventive and corrective remedial measures have been proposed for power system voltage collapse prevention [92]. Load shedding is among the most commonly used remedial measure. In this thesis, it was considered that 10% of load was shed at the buses where the loads were increasing. It is clear that any increase in load caused a steep decrease in time to voltage collapse as shown as plot (a) in Figure 5.8. The results show that when load increase on all buses were equal to 72% time to voltage collapse was 30 minutes. At this time step, load shedding scheme was activated to shed a block of 10% of load in the simulation and relieve the system. Three different locations for load shedding were studied and are reported in the scenarios that follow.

- Scenario 1: 10% load shed at Bus 24 as the loads on all buses increased gradually.

In this scenario, load flows were conducted and system Thévenin equivalent was estimated using the Least Squares technique associated with CSF described in Section 3.8. As before, voltage and current phasors calculated by the load flow studies, and the Thévenin equivalent obtained from the application of the Least Squares technique were used as inputs to the time to voltage collapse technique that calculated proximity to voltage collapse.

The base case load flow was conducted and was assigned as load flow at time t=0. The load admittance was calculated and was used to estimate the load admittance to reflect load increases of one percent per minute. Future loads were then used to conduct load flows at times t_j, for j = 1, 2, 3,……., 104. The Thévenin impedances and voltages were calculated for those times using the procedure described in Section 3.8.1.

The Thévenin parameters, voltages and currents at Buses 24 and 26 were provided to the voltage collapse estimation technique and steps 1, 2, 3, and 4 described in Section 5.3.1 were repeated to calculate time to voltage collapse. The values of time to voltage collapse at Bus 24 as a function of load increase on all buses were determined and are shown as plot (b) in Figure 5.8.

- Scenario 2: 10% load shed at Bus 26 as the loads on all buses increased gradually.

In this scenario, the procedure described in scenario 1 was repeated and the values of time to voltage collapse at Bus 26 as a function of load increase on all buses was determined and shown as plot (c) in Figure 5.8.

A comparison of the time to voltage collapse when load was shed on Bus 24 or Bus 26 indicated that the time to voltage collapse was shorter when the load was shed on Bus 24 instead of shedding load on Bus 26. For example, the time to voltage collapse was 34.5 minutes when the loads on all buses were increased by 72% and 10% load was shed at Bus 26. But the time to voltage collapse was reduced to 33 minutes if 10% load was shed on Bus 24 instead of at Bus 26.

Scenario 3: 10% load shed at Buses 24 and 26 as the loads on all buses increased gradually.

In this scenario, the procedure described in scenario 1 was repeated and the times to voltage collapse at Bus 26 as a function of load increase on all buses were determined and shown as plot (d) in Figure 5.8. These results show that time to voltage collapse on Bus 26 increased substantially when blocks of load were disconnected from Bus24 and Bus 26. For example, voltage collapse time is 36.5 minutes when loads on all buses were increased by 72% and 10% load was shed on Bus 26 and Bus 24. But the time to voltage collapse was reduced to 34 minute if 10% load was shed on Bus 24 instead of both buses.

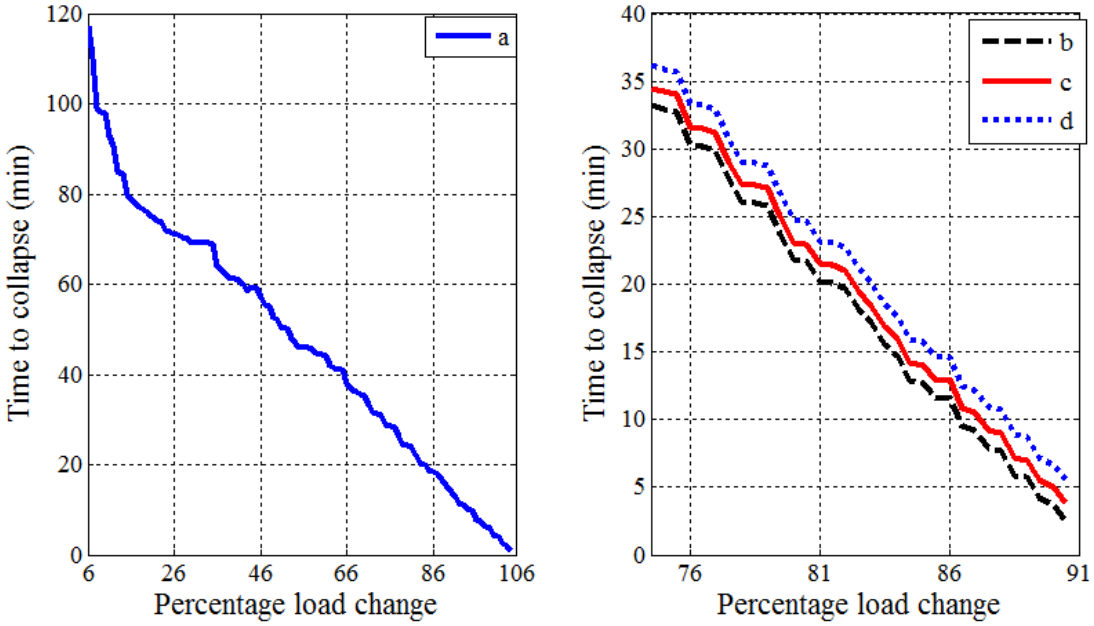

Figure 5.8: Time to voltage collapse when load shedding scheme is activated

5.4 Time to voltage collapse studies with data from three buses

It was assumed in the studies reported in Section 5.3 that data was collected from two buses. This approach was further extended and applied to calculating the time to collapse if the data is collected at three buses. The results are reported in this section.

It was considered in these studies that a time to voltage collapse relay was installed at Bus 26 of the IEEE 30-Bus test system and voltages and currents were monitored at Buses 23, 24, and 26 shown in Figure 5.1. These buses were selected because they are heavily loaded buses.

Performance of the voltage to collapse studies for gradual load increase, transmission line taken out of service and load shedding to protect from voltage collapse were conducted.

5.4.1 Gradual load increase

The loads at all buses were considered to have increased gradually. Load flows were conducted and system Thévenin equivalent was estimated using the Least Squares technique with CSF described in Section 3.8. Voltage and current phasors calculated by the load flow studies, and the Thévenin equivalent obtained from the application of the Least Squares technique were used as inputs to the time to voltage collapse technique that calculated proximity to voltage collapse.

The base case load flow was conducted and was assigned as load flow at time t=0. The load admittance was calculated and was used to estimate the load admittance to reflect load increases of one percent per minute. Future loads were then used to conduct load flows at times t_j, for j = 1, 2, 3, ……., 104. The Thévenin impedances and voltages were calculated for those times using the procedure described in Section 3.8.1.

The Thévenin parameters, voltages and currents at Buses 24, 23, and 26 were provided to the voltage collapse estimation technique and steps 1, 2, 3, and 4 presented in Section 5.3.1 were repeated to determine time to voltage collapse.

Figures 5.2, 5.3 and Figure 5.9 show the estimated values of Thévenin voltage seen from buses 26, 24, and 23 respectively. Estimated values of Thévenin voltage seen from Bus 23 decreased due to load increase at all buses as shown in Figure 5.9.

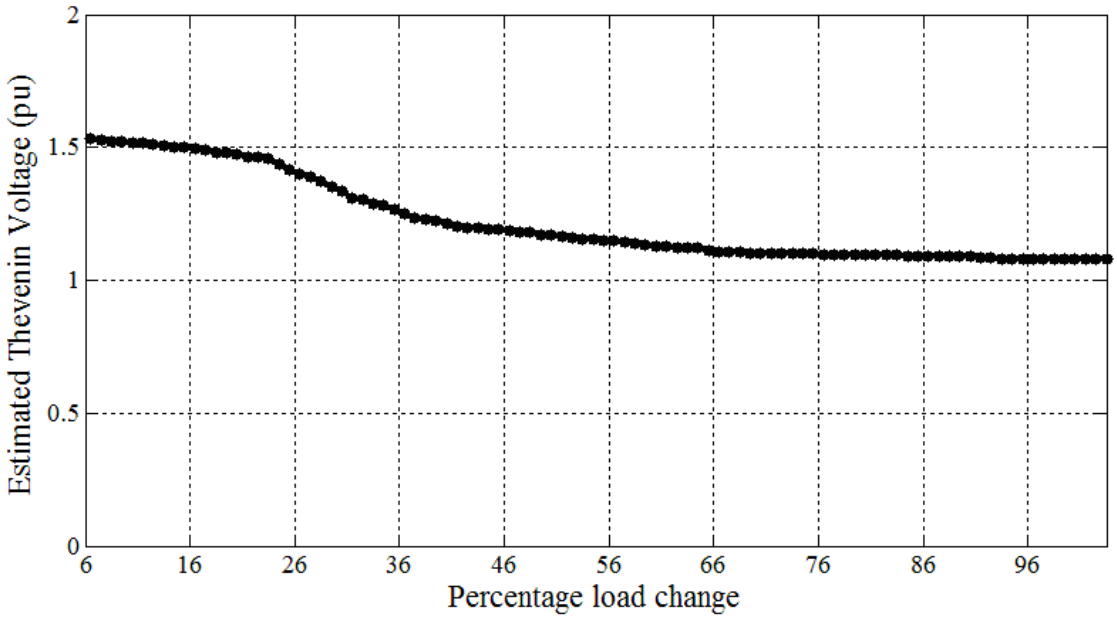

Figure 5.9: Estimated Thévenin voltage seen from Bus 23

The plot of the percentage load increase versus estimated values of Thévenin impedance seen from Buses 26, 24 and 23 are shown in Figures 5.4, 5.5, and 5.10 respectively. It is evident from Figure 5.10 that load increase at all buses caused Thévenin impedance increase seen from Bus 23.

Figure 5.11 shows the time to voltage collapse at Bus 26 for each level of load increase used in this case. It is evident from the figure that, any increase in load caused a steep decrease in time to voltage collapse. The figure shows that time to voltage collapse obtained from the develoed algorithm was consistent with the maximum percent of load increase before system collapse in load flow program.. Both algorithms show that the system collapsed when load increase on all buses was equal to 104%.

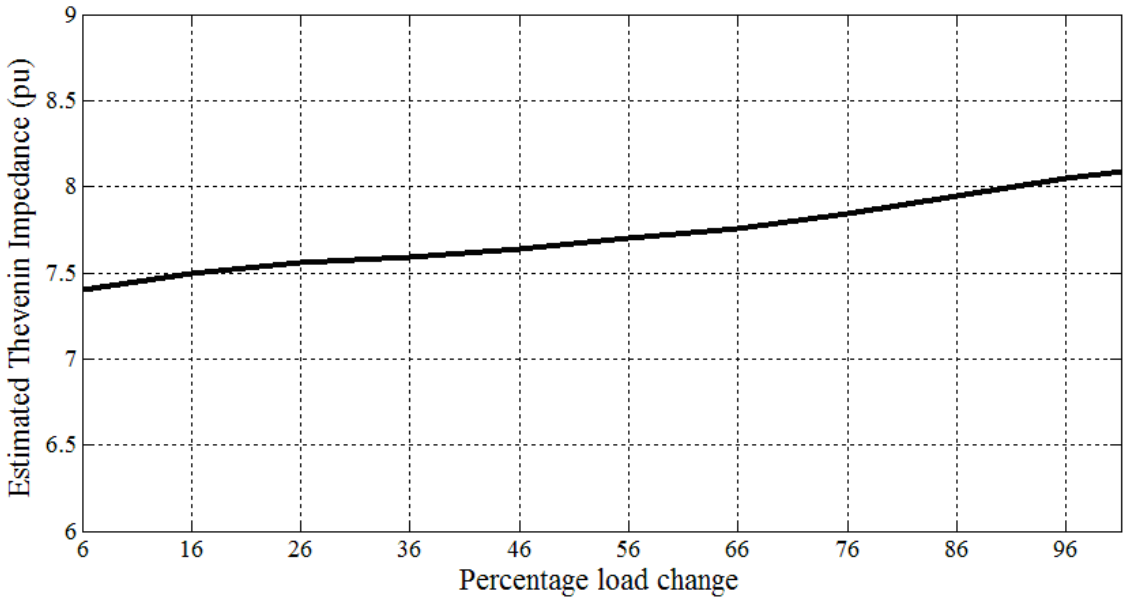

Figure 5.10: Estimated Thévenin impedance seen from Bus 23

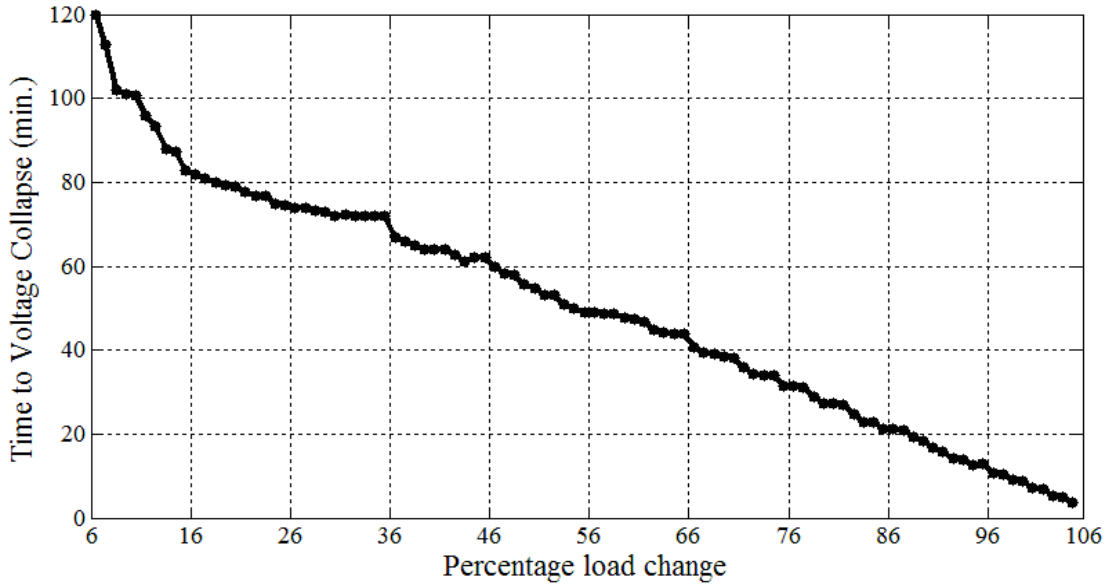

Figure 5.11: Time to voltage collapse

5.4.2 Transmission line outage and gradual load increase

Transmission line from Bus 22 to Bus 24 is one of the vital transmission lines serving loads at Buses 22 and 24. It was considered that loads at all buses increased in this case. Load flows were conducted for every increase in load. The voltage and current phasors on Buses 24, 23, and 26 obtained from load flow studies were given to the system's parameters estimation algorithm. The Thévenin equivalent of the system was estimated using the Least Squares technique with CSF filter described in Section 3.8. Voltage and current phasors calculated by the load flow studies, and the Thévenin equivalent obtained from the application of the Least Squares technique were used as inputs to the time to voltage collapse technique that calculated proximity to voltage collapse.

The base case load flow was conducted and was assigned as load flow at time t=0. The load admittance was calculated and was used to estimate the load admittances to reflect load increases of one percent per minute. Future loads were then used to conduct load flows at times t_j, for j = 1, 2, 3,……., 102. The Thévenin impedances and voltages were calculated for those times using the procedure described in Section 3.8.1.

The Thévenin parameters and phasors of voltages and currents at Buses 24, 23, and 26 were provided to the voltage collapse estimation technique and steps 1, 2, 3, and 4 described in Section 5.3.1 were repeated to determine time to voltage collapse.

The plot of percentage load increase versus time to voltage collapse on Bus 26 is shown in Figure 5.12. A comparison of Figures 5.11 and 5.12 show that time to voltage collapse at Bus 26 was shorter for each level of load when the transmission line connecting Buses 22 and 24 was out of service. This proves that losing an important transmission line increases the risk of voltage collapse. For example, sixteen percent increase of loads on all buses resulted in voltage collapse on Bus 26 in 81 minutes as is shown in Figure 5.11. But time to voltage collapse on Bus 26 for the identical load decreased to 79 minutes when transmission line from Bus 22 to Bus 24 was out of service.

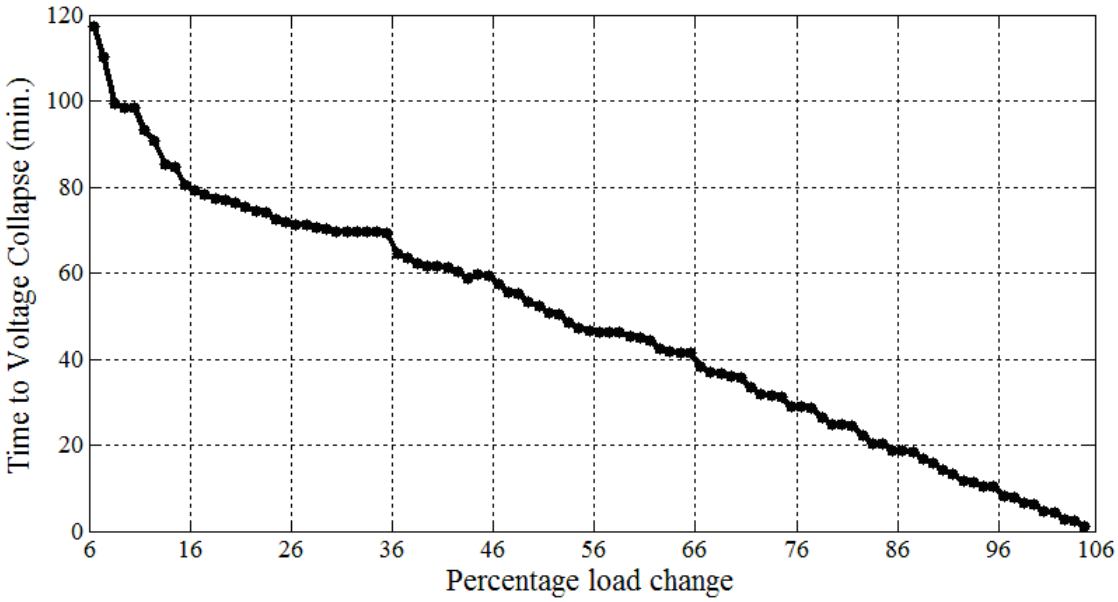

Figure 5.12: Time to voltage collapse when transmission line outage occurs

5.4.3 Load shedding and gradual load increase

System voltage profile can be improved and time to voltage collapse can be increased by implementing a load shedding strategy. A relay that uses time to voltage collapse algorithm can be easily armed with a local-and/or wide-area control system to activate load shedding when the system is close to the point of voltage collapse.

In the past, many different preventive and corrective remedial measures have been proposed to prevent power system voltage collapse. Load shedding is among the most commonly used remedial measures. It is clear that any increase in load caused a steep decrease in time to voltage collapse, as shown as plot (a) in Figure 5.13. The results obtained show that voltage collapse time was equal to or less than 30 minutes when load shedding scheme was activated to shed a block of 10% of load in the simulation and relieved the system. Four different locations for load shedding were studied and are reported in the scenarios that follow.

- Scenario 1: 10% load shed at Bus 26 as the loads on all buses increased gradually.

In this scenario, load flows were conducted and system Thévenin equivalent was estimated using the Least Squares technique with CSF filter described in Section 3.8. As before, voltage and current phasors calculated by the load flow studies, and the Thévenin equivalent obtained from the application of the Least Squares technique were used as inputs to the time to voltage collapse technique that calculated proximity to voltage collapse.

The base case load flow was conducted and was assigned as load flow at time t=0. The load admittance was calculated and was used to estimate the load admittance to reflect load increases of one percent per minute. Future loads were then used to conduct load flows at times t_j, for j = 1, 2, 3,……., 104. The Thévenin impedances and voltages were calculated for those times using the procedure described in Section 3.8.1.

The Thévenin parameters, voltages and currents at Buses 24, 23, and 26 were provided to the voltage collapse estimation technique and steps 1, 2, 3, and 4 described in Section 5.3.1 were repeated to calculate time to voltage collapse. The time to voltage collapse at Bus 26 as a function of load increase at all buses is shown as plot (b) in Figure 5.13.

- Scenario 2: 10% load shed at Bus 24 as the loads on all buses increased gradually.

In this scenario, the procedure described in scenario 1 was repeated and the values of time to voltage collapse at Bus 26 as a function of load increase on all buses was determined as shown as plot (c) in Figure 5.13.

A comparison of the time to voltage collapse when load was shed on Bus 24 or Bus 26 indicated that the time to voltage collapse was shorter when load was shed on Bus 24 instead of shedding load on Bus 26. For example, the time to voltage collapse was 34 minutes when the loads on all buses were increased by 75% and 10% load was shed at Bus 26. But the time to voltage collapse was reduced to 33 minutes if 10% load was shed on Bus 24 instead of Bus 26.

- Scenario 3: 10% load shed at Bus 23 as the loads on all buses increased gradually.

In this scenario, the procedure described in scenario 1 was repeated and the values of time to voltage collapse at Bus 26 as a function of load increase on all buses was determined as shown as plot (d) in Figure 5.13.

A comparison of the time to voltage collapse when load was shed on Bus 23 or Bus 26 indicated that the time to voltage collapse was shorter when load was shed on Bus 23 instead of shedding load on Bus 26. For example, the time to voltage collapse was 34 minutes when load on all buses increased by 75% and 10% load was shed at Bus 26. But the time to voltage collapse was reduced to 32 minutes if 10% load was shed on Bus 23 instead of Bus 26.

- Scenario 4: 10% load shed at Buses 24, 23, and 26 as the loads on all buses increased gradually.

In this scenario, the procedure described in scenario 1 was repeated and the values of time to voltage collapse at Bus 26 as a function of load increase on all buses were determined and shown as plot (e) in Figure 5.13. These results show that time to voltage collapse on Bus 26 increased substantially when blocks of load were disconnected from Buses 24, 23, and 26. For example, time to voltage collapse on Bus 26 was 34 minutes when loads on all buses increased by 75% compared to a time to voltage collapse of 37.5 minutes if load was shed on Buses 23, 24 and 26.

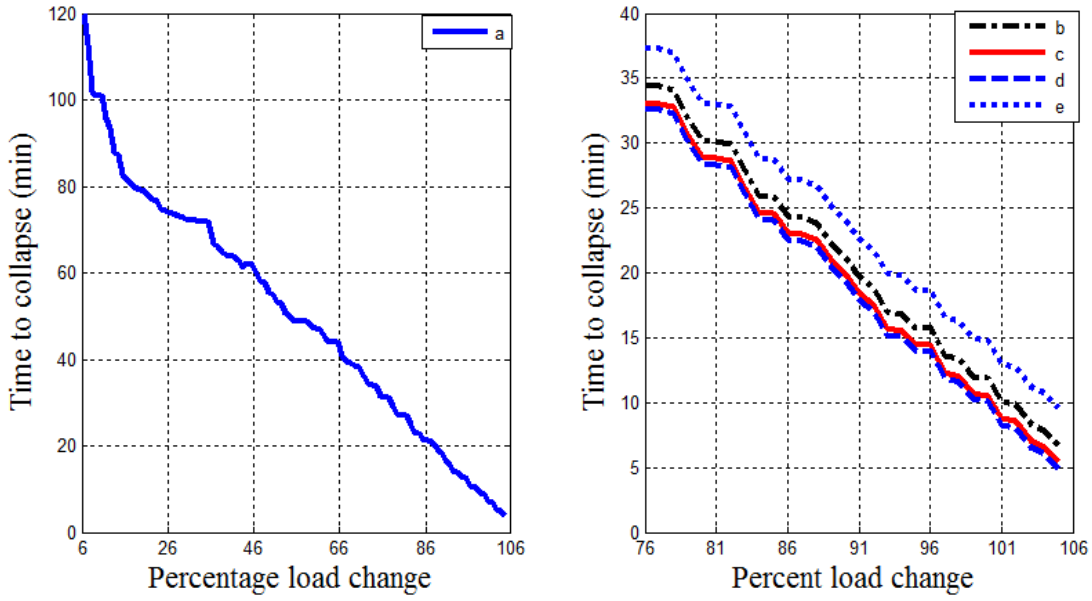

Figure 5.13: Time to voltage collapse when load shedding scheme is activated

5.5 Time to voltage collapse studies with data from four buses

It is assumed in the studies reported in Section 5.4 that data was collected from three buses. This approach was further extended and applied to calculating the time to collapse if the data is collected at four buses. The results are reported in this section.

It was considered in these studies that a time to voltage collapse relay was installed at Bus 26 of the IEEE 30-Bus test system and voltages and currents were monitored at Buses 24, 23, 15, and Bus 26 shown in Figure 5.1. These buses were selected because they are heavily loaded buses.

Performance of the voltage to collapse studies for gradual load increase, transmission line taken out of service and load shedding to protect from voltage collapse were conducted.

5.5.1 Gradual load increase

The loads at all buses were considered to have increased gradually. Load flows were conducted and system Thévenin equivalent was estimated using the Least Squares technique with CSF filter described in Section 3.8. Voltage and current phasors calculated by the load flow studies, and the Thévenin equivalent obtained from the application of the Least Squares technique were used as inputs to the time to voltage collapse technique that calculated proximity to voltage collapse.

The base case load flow was conducted and was assigned as load flow at time t=0. The load admittance was calculated and was used to estimate the load admittance to reflect load increases of one percent per minute. Future loads were then used to conduct load flows at times t_j, for j = 1, 2, 3,……., 104. The Thévenin impedances and voltages were calculated for those times using the procedure described in Section 3.8.1.

The Thévenin parameters, voltages and currents at Buses 24, 23, 15, and 26 were provided to the voltage collapse estimation technique and steps 1, 2, 3, and 4 presented in Section 5.3.1 were repeated to determine time to voltage collapse.

Figures 5.2, 5.3, 5.9, and Figure 5.14 show the estimated values of Thévenin voltage seen from buses 26, 24, 23, and 15 respectively. Results shown in Figure 5.14 proved that load increase at all buses triggered Thévenin voltage decrease at Bus 15.

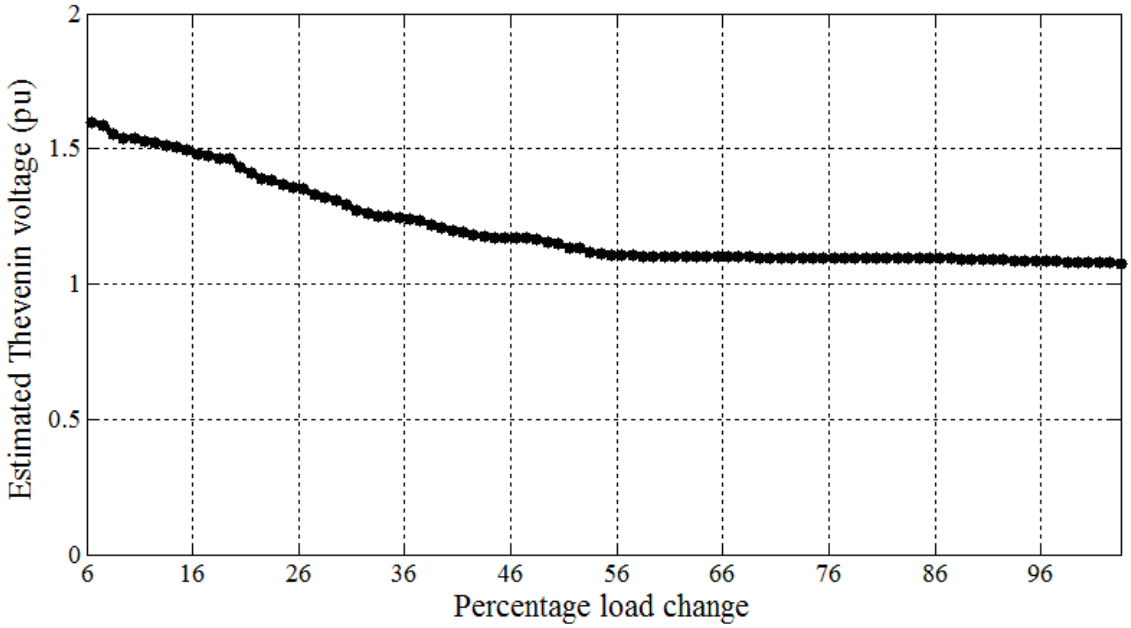

Figure 5.14: Estimated Thévenin voltage seen from Bus 15

The plot of the percentage load increase versus estimated values of Thévenin impedance seen from Buses 26, 24, 23 and 15 are shown in Figures 5.4, 5.5, 5.10, and Figure 5.15 respectively. It is evident from Figure 5.15 that loads increase at all buses caused Thévenin impedance increase seen from Bus 15.

Figure 5.15 shows the time to voltage collapse at Bus 26 for each level of load increase used in this case. It is clear from the figure that, any increase in load caused a steep decrease in time to voltage collapse. The figure shows that time to voltage collapse obtained from the developed algorithm were consistent with maximum power transfer obtained from load flow program.

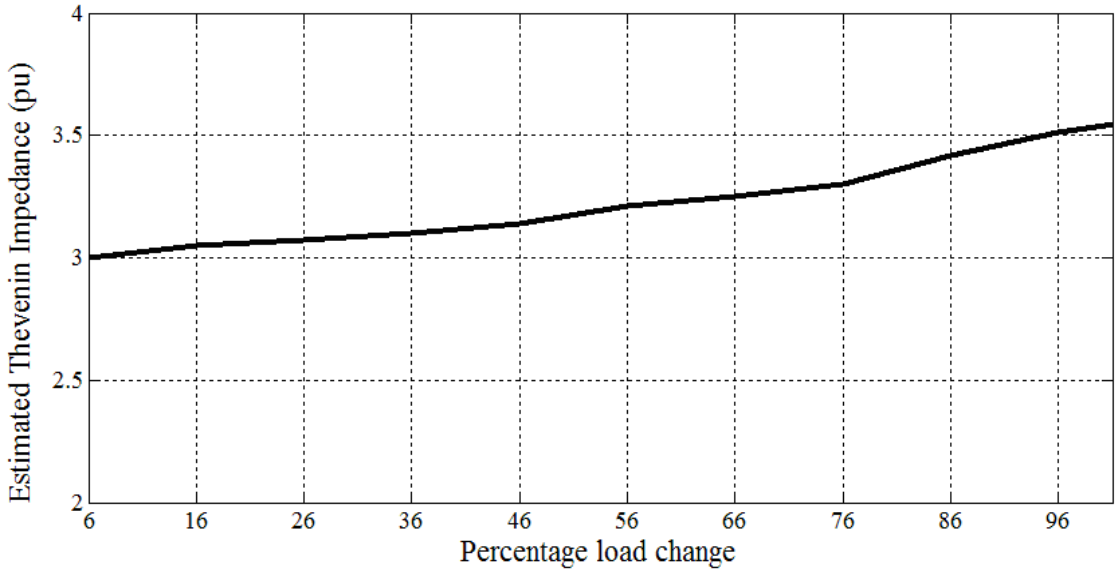

Figure 5.15: Estimated Thévenin impedance seen from Bus 15

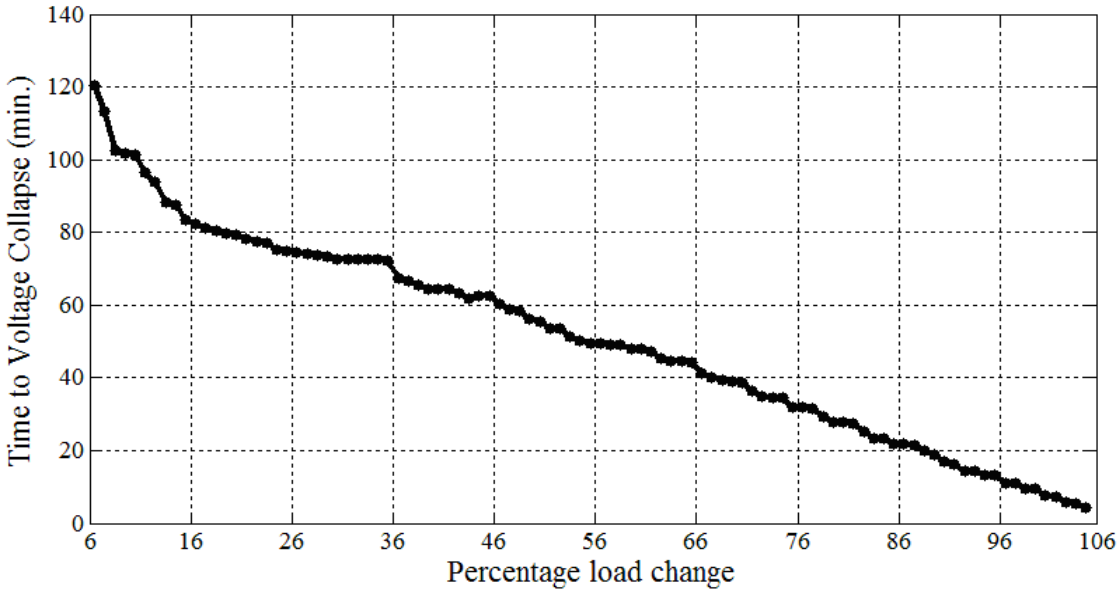

Figure 5.16: Time to voltage collapse

5.5.2 Transmission line outages and gradual load increase

Transmission line from Bus 22 to Bus 24 is one of the vital transmission lines serving loads at Buses 22 and 24, it was considered that loads at all buses increased in this case. Load flows were conducted for every increase in load. The voltage and current phasors on Buses 24, 23, 15, and 26 obtained from load flow studies were given to the system's parameters estimation algorithm. The Thévenin equivalent of the system was estimated using the Least Squares technique with CSF filter described in Section 3.8. Voltage and current phasors calculated by the load flow studies, and the Thévenin equivalent obtained from the application of the Least Squares technique were used as inputs to the time to voltage collapse technique that calculated proximity to voltage collapse.

The base case load flow was conducted and was assigned as load flow at time t=0. The load admittance was calculated and was used to estimate the load admittance to reflect load increases of one percent per minute. Future loads were then used to conduct load flows at times t_j, for j = 1, 2, 3,……., 102. The Thévenin impedances and voltages were calculated for those times using the procedure described in Section 3.8.1.

The Thévenin parameters and phasors of voltages and currents at Buses 24, 23, 15, and 26 were provided to the voltage collapse estimation technique and steps 1, 2, 3, and 4 described in Section 5.3.1 were repeated to determine time to voltage collapse.

The plot of percentage load increase versus time to voltage collapse on Bus 26 is shown in Figure 5.17. A comparison of Figures 5.16 and 5.17 shows that time to voltage collapse at Bus 26 was shorter for each level of load when the transmission line connecting Buses 22 and 24 was out of service. This proves that losing an important transmission line increases the risk of voltage collapse. For example, sixteen percent increase of loads on all buses resulted in voltage collapse on Bus 26 in 81 minutes as shown in Figure 5.16. But time to voltage collapse on Bus 26 for the identical load decreased to 80 minutes when transmission line from Bus 22 to Bus 24 was out of service.

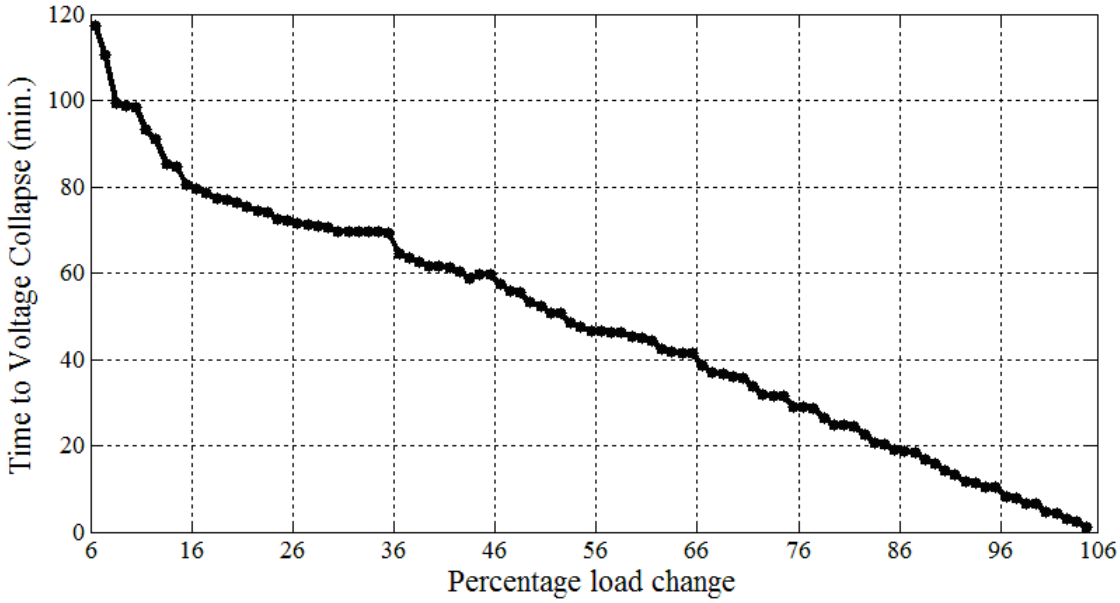

Figure 5.17: Time to voltage collapse when transmission line outages occur

5.5.3 Load shedding and gradual load increase

System voltage profile can be improved and time to voltage collapse can be increased by implementing a load shedding strategy. A relay that uses time to voltage collapse algorithm can be easily armed with a local-and/or wide-area control system to activate load shedding when the system is close to the point of voltage collapse.

In the past, many different preventive and corrective remedial measures have been proposed for preventing power system voltage collapse. Load shedding is among the most commonly used remedial measures. It is clear that any increase in load caused a steep decrease in time to voltage collapse as shown as plot (a) in Figure 5.18. The results show that when time to voltage collapse was equal to or less than 30 minutes load shedding scheme was activated to shed a block of 10% of load in the simulation and relieve the system. Five different locations for load shedding were studied and are reported in the scenarios that follow.

- Scenario 1: 10% load shed at Bus 26 as the loads on all buses increased gradually.

In this scenario, load flows were conducted and system Thévenin equivalent was estimated using the Least Squares technique with CSF filter described in Section 3.8. As before, voltage and current phasors calculated by the load flow studies, and the Thévenin equivalent obtained from the application of the Least Squares technique were used as inputs to the time to voltage collapse technique that calculated proximity to voltage collapse.

The base case load flow was conducted and was assigned as load flow at time t=0. The load admittance was calculated and was used to estimate the load admittance to reflect load increases of one percent per minute. Future loads were then used to conduct load flows at times t_j, for j = 1, 2, 3,……., 104. The Thévenin impedances and voltages were calculated for those times using the procedure described in Section 3.8.1.

The Thévenin parameters, voltages and currents at Buses 24, 23, 15, and 26 were provided to the voltage collapse estimation technique and steps 1, 2, 3, and 4 described in Section 5.3.1 were repeated to calculate time to voltage collapse. The time to voltage collapse at Bus 26 as a function of load increase at all buses is shown as plot (b) in Figure 5.18.. The results show that time to voltage collapse that was 30 minutes when the loads on all buses increased by 73% increased to 33 minutes if 10% load was shed on Bus 26.

- Scenario 2: 10% load shed at Bus 24 as the loads on all buses increased gradually.

In this scenario, the procedure described in scenario 1 was repeated and the values of time to voltage collapse at Bus 26 as a function of load increase on all buses was determined and is shown as plot (c) in Figure 5.18.

A comparison of the time to voltage collapse when load was shed on Bus 26 and load was shed on Bus 24 indicates that the time to voltage collapse was shorter when load was shed on Bus 24 instead of shedding load on Bus 26. For example, the time to voltage collapse was 33 minutes when the loads on all buses increased by 73% and 10% load was shed at Bus 26; but time to voltage collapse reduced to 32.7 minutes if 10% load was shed on Bus 24 instead of on Bus 26.

- Scenario 3: 10% load shed at Bus 23 as the loads on all buses increased gradually.

In this scenario, the procedure described in scenario 1 was repeated and the values of time to voltage collapse at Bus 26 as a function of load increase on Buses 24, 23, 15, and 26 was determined and is shown as plot (d) in Figure 5.18.

A comparison of the time to voltage collapse when load was shed on Buses 26, 23 indicated that the time to voltage collapse was shorter when load was shed on Bus 23 instead of shedding load on Bus 26. For example, the time to voltage collapse was 30.5 minutes when the load on all buses increased by 73% and 10% load was shed on Bus 24 instead of Bus 26.

- Scenario 4: 10% load shed at Bus 15 as the loads on all buses increased gradually.

In this scenario, the procedure described in scenario 1 was repeated and the values of time to voltage collapse at Bus 26 as a function of load increase on Buses 24, 23, 15, and 26 was determined and is shown as plot (e) in Figure 5.18..

A comparison of the time to voltage collapse when load was shed on Buses 26, 15 indicated that the time to voltage collapse was shorter when load was shed on Bus 15 instead of shedding load on Bus 26. For example, the time to voltage collapse was 30 minutes when the load on all buses increased by 73% and 10% load was shed on Bus 15 instead of Bus 26.

- Scenario 5: 10% load shed at 24, 23, 15, and 26 as the load on all buses increased gradually

In this scenario, the procedure described in scenario 1 was repeated and the values of time to voltage collapse at Bus 26 as a function of load increase on all buses were determined and shown as plot (f) in Figure 5.18. These results show that time to voltage collapse on Bus 26 increased substantially when blocks of load were disconnected from Buses 24, 23, 15, and 26. For example, time to voltage collapse on Bus 26 is 36 minutes when loads on all buses increased by 73% compare to a time to voltage collapse of 31 and 30.5 minutes if load was curtailed on Bus 24 and Bus 23 respectively.

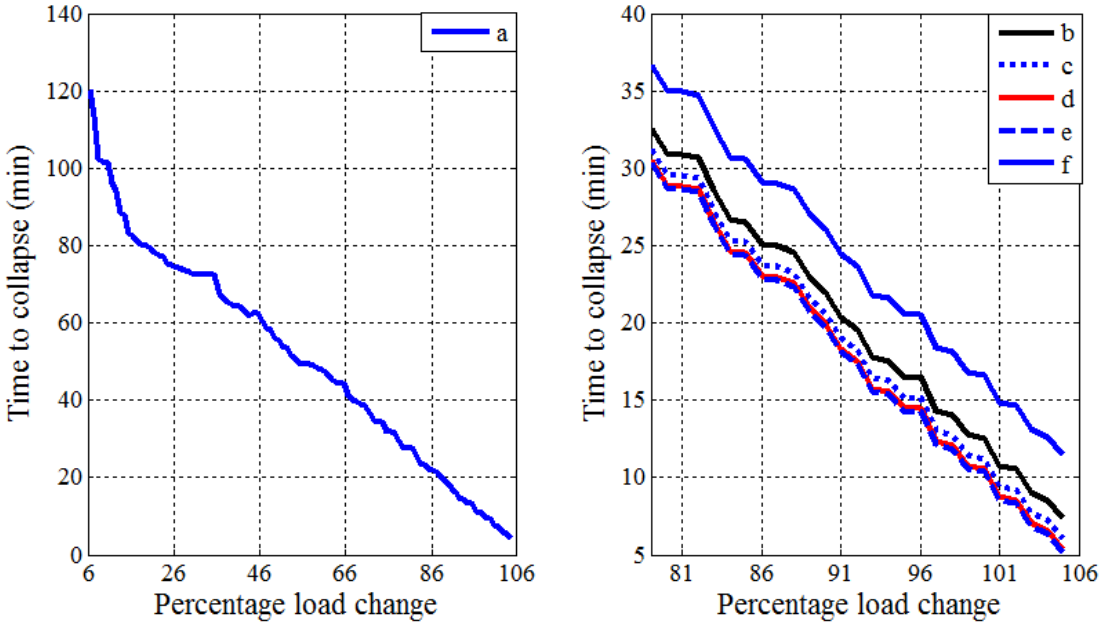

Figure 5.18: Time to voltage collapse when load shedding scheme is activated

5.6 Time to voltage collapse studies with data from five buses

It was assumed in the studies reported in Section 5.5 that data was collected from four buses. This approach was further extended and applied to calculating time to collapse if the data is collected at five buses. The results are reported in this section.

It was considered in these studies that a time to voltage collapse relay was installed at Bus 26 of the IEEE 30-Bus test system and voltages and currents were monitored at Bus 24, 23, 15, 14, and Bus 26 shown in Figure 5.1. These buses were selected because they are heavily loaded buses.

Performance of the voltage to collapse studies for gradual load increase, transmission line taken out of service and load shedding to protect from voltage collapse were conducted.

5.6.1 Gradual load increase

The loads at all buses were considered to have increased gradually. Load flows were conducted and system Thévenin equivalent was estimated using the Least Squares technique with CSF filter described in Section 3.8. Voltage and current phasors calculated by the load flow studies, and the Thévenin equivalent obtained from the application of the Least Squares technique were used as inputs to the time to voltage collapse technique that calculated proximity to voltage collapse.

The base case load flow was conducted and was assigned as load flow at time t=0. The load admittance was calculated and was used to estimate the load admittance to reflect load increases of one percent per minute. Future loads were then used to conduct load flows at times t_j, for j = 1, 2, 3,……., 104. The Thévenin impedances and voltages were calculated for those times using the procedure described in Section 3.8.1.

The Thévenin parameters, voltages and currents at Buses 24, 23, 15, 14, and 26 were provided to the voltage collapse estimation technique and steps 1, 2, 3, and 4 presented in Section 5.3.1 were repeated to determine time to voltage collapse.

Figures 5.2, 5.3, 5.9, 5.14 and Figure 5.19 show the estimated values of Thévenin voltage seen from buses 26, 24, 23, 15, and 14 respectively. It is clear from Figure 5.19 that load increase at all buses caused Thévenin voltage decrease at Bus 26.

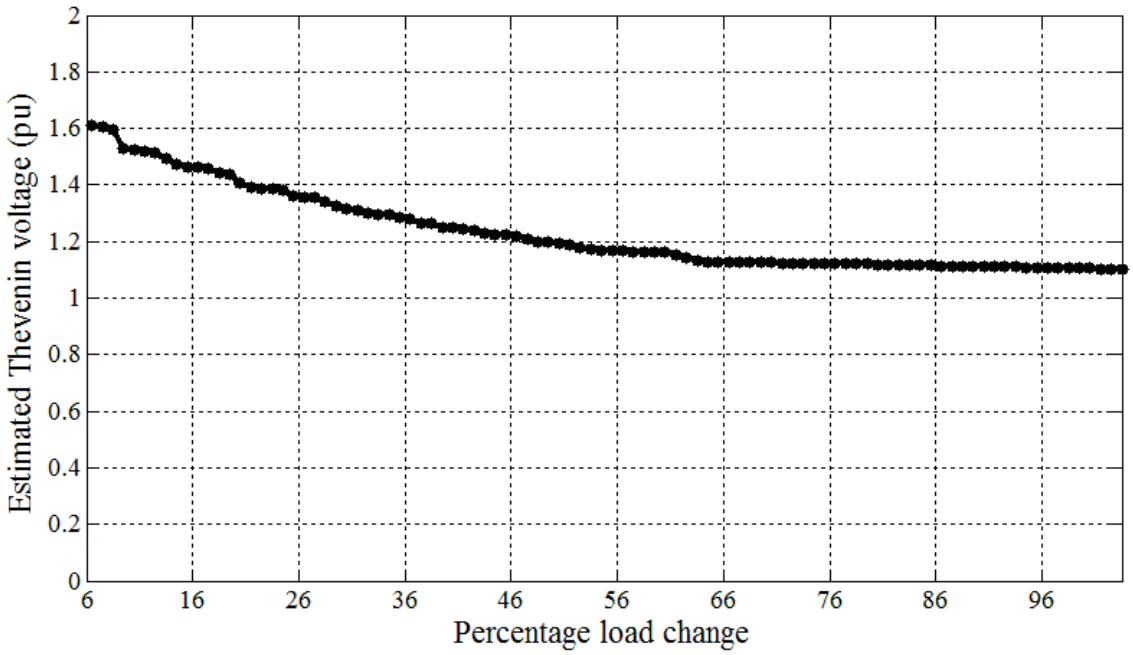

Figure 5.19: Estimated Thévenin voltage seen from Bus 14

The plot of the percentage load increase versus estimated values of Thévenin impedance seen from Buses 26, 24, 23, 15 and 14 are shown in Figures 5.4, 5.5, 5.10, 5.15, and Figure 5.20 respectively. It is evident from Figure 5.20 that load increase at all buses caused increases in Thévenin impedance seen from Bus 26.

Figure 5.21 shows the time to voltage collapse at Bus 26 for each level of load increase used in this case. It is clear from the figure that, any increase in load caused a steep decrease in time to voltage collapse. The figure shows that time to voltage collapse obtained from the developed algorithm were consistent with maximum percent of load increase obtained from load flow program.

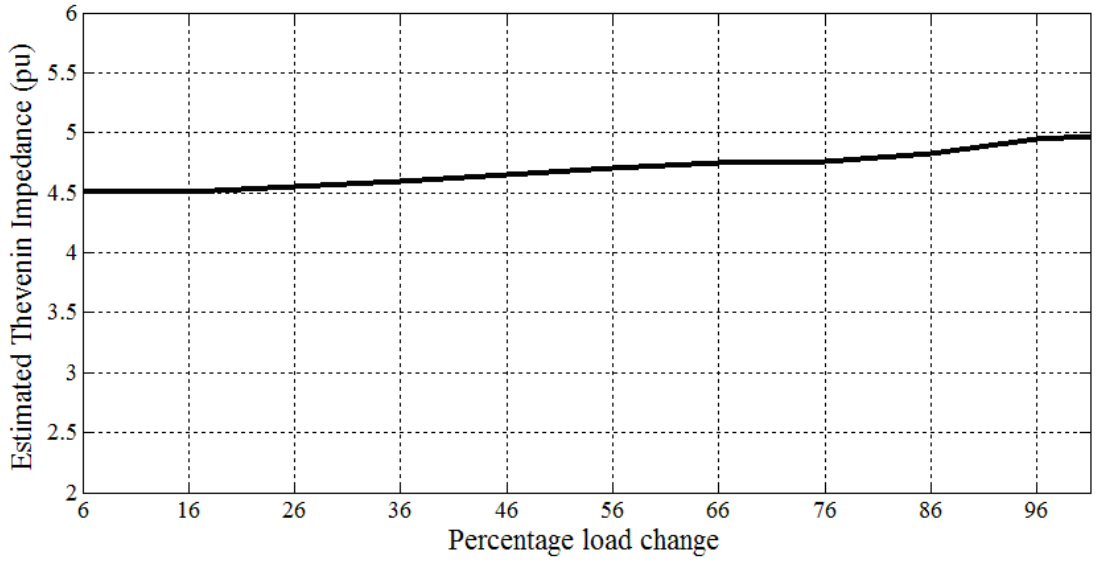

Figure 5.20: Estimated Thévenin impedance seen from Bus 14

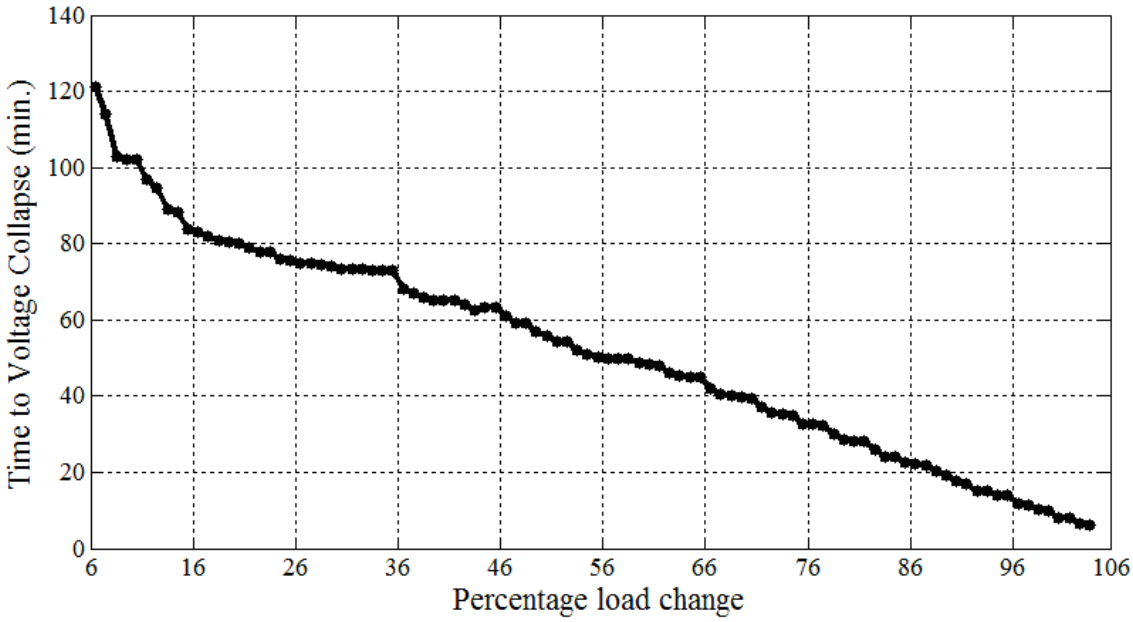

Figure 5.21: Time to voltage collapse

5.6.2 Transmission line outages and gradual load increase

Transmission line from Bus 22 to Bus 24 is one of the vital transmission lines serving loads at Buses 22 and 24, it was considered that loads at all buses increased in this case. Load flows were conducted for every increase in load. The voltage and current phasors on Buses 24, 23, 15, and 26 obtained from load flow studies were given to the system's parameters estimation algorithm. The Thévenin equivalent of the system was estimated using the Least Squares technique with CSF filter described in Section 3.8. Voltage and current phasors calculated by the load flow studies, and the Thévenin equivalent obtained from the application of the Least Squares technique were used as inputs to the time to voltage collapse technique that calculated proximity to voltage collapse.

The base-case load flow was conducted and was assigned as load flow at time t=0. The load admittance was calculated and was used to estimate the load admittance to reflect load increases of one percent per minute. Future loads were then used to conduct load flows at times t_j, for j = 1, 2, 3, ……. , 104. The Thévenin impedances and voltages were calculated for those times using the procedure described in Section 3.8.1.

The Thévenin parameters and phasors of voltages and currents at Buses 24, 23, 15, and 26 were provided to the voltage collapse estimation technique and steps 1, 2, 3, and 4 described in Section 5.3.1 were repeated to determine time to voltage collapse.

The plot of percentage load increase versus time to voltage collapse on Bus 26 is shown in Figure 5.22. A comparison of Figures 5.21 and 5.22 shows that time to voltage collapse at Bus 26 was shorter for each level of load when the transmission line connecting Buses 22 and 24 was out of service. This proves that losing an important transmission line increases the risk of voltage collapse. For example, sixteen percent increase of loads on all buses resulted in voltage collapse at Bus 26 in 83 minutes as is shown in Figure 5.21. But, time to voltage collapse at Bus 26 for identical loads conditions decreased to 80 minutes when transmission line from Bus 22 to Bus 24 was out of service.

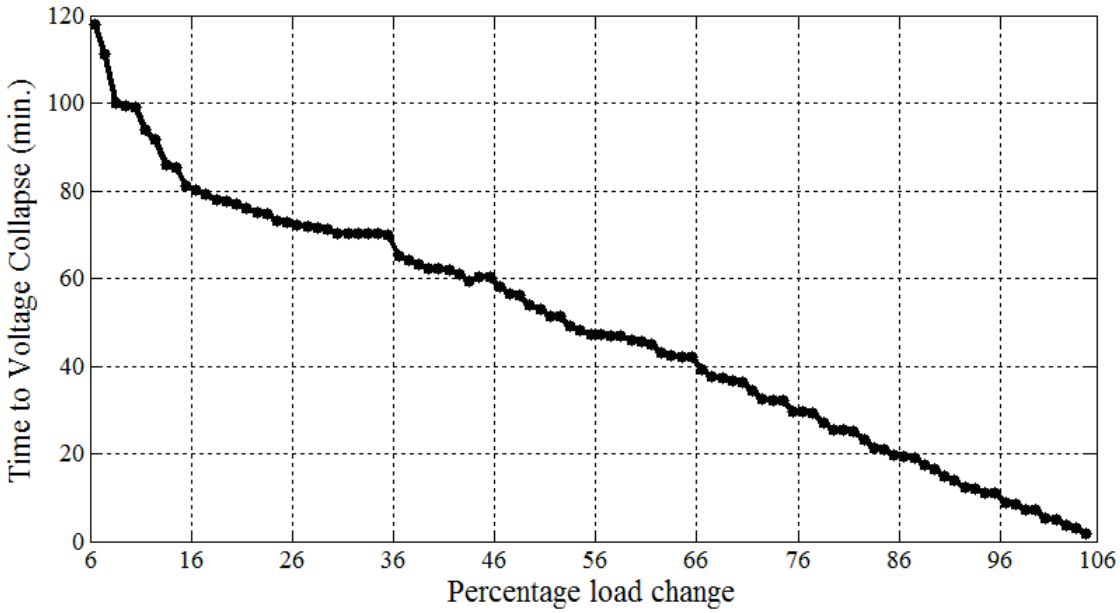

Figure 5.22: Time to voltage collapse when transmission line outages occur

5.6.3 Load shedding and gradual load increase

System voltage profile can be improved and time to voltage collapse can be increased by implementing a load shedding strategy. A relay that uses time to voltage collapse algorithm can be easily armed with a local-and/or wide-area control system to activate load shedding when the system is close to the point of voltage collapse.

In the past, many different preventive and corrective remedial measures have been proposed for power system voltage collapse prevention. Load shedding is among the most commonly used remedial measures. It is clear that any increase in load caused a steep decrease in time to voltage collapse as shown as plot (a) in Figure 5.23. The results show that voltage collapse time was equal or less than 30 minutes when load shedding scheme was activated to shed a block of 10% of load in the simulation and relieved the system. Six different locations for load shedding were studied and are reported in the scenarios that follow.

- Scenario 1: 10% load shed at Bus 26 as the loads on all buses increased gradually.

In this scenario, load flows were conducted and system Thévenin equivalent was estimated using the Least Squares technique with CSF filter described in Section 3.8. As before, voltage and current phasors calculated by the load flow studies, and the Thévenin equivalent obtained from the application of the Least Squares technique were used as inputs to the time to voltage collapse technique that calculated proximity to voltage collapse.

The base case load flow was conducted and was assigned as load flow at time t=0. The load admittance was calculated and was used to estimate the load admittance to reflect load increases of one percent per minute. Future loads were then used to conduct load flows at times t_j, for j = 1, 2, 3, ……. , 104. The Thévenin impedances and voltages were calculated for those times using the procedure described in Section 3.8.1.

The Thévenin parameters, voltages and currents at Buses 24, 23, 15, 14, and 26 were provided to the voltage collapse estimation technique and steps 1, 2, 3, and 4 described in Section 5.3.1 were repeated to calculate time to voltage collapse. The time to voltage collapse at Bus 26 as a function of load increase at all buses is shown as plot (b) in Figure 5.23. The time to voltage collapse was 30 minutes when the loads on all buses increased by 78%. If 10% load were shed on Bus 26, the time to voltage collapse increased to 33 minutes. In practice, more load would be shed so that the time to voltage increases further to avoid voltage collapse due to unexpected increase of load on other buses.

- Scenario 2: 10% load shed at Bus 24 as the loads on all buses increased gradually.

In this scenario, the procedure described in scenario 1 was repeated and the values of time to voltage collapse at Bus 26 as a function of load increase on all buses was determined and is shown as plot (c) in Figure 5.23.

A comparison of the time to voltage collapse when load is shed on Bus 26, and the load is shed on Bus 24 indicates that the time to voltage collapse was shorter when load was shed on Bus 24 instead of shedding load on Bus 26. For example, the time to voltage collapse was 33.5 minutes when the load on all buses increased by 78% and 10% load was shed on Bus 26. But the time to voltage collapse was reduces to 31.9 minutes when10% load was shed on Bus 24 instead of at Bus 26.

- Scenario 3: 10% load shed at Bus 23 as the loads on all buses increased gradually.

A comparison of the time to voltage collapse when load was shed on Buses 26 and 23 indicated that the time to voltage collapse was shorter when load was shed on Bus 23 instead of shedding load on Bus 26. For example, the time to voltage collapse was 33.5 minutes when the load on all buses increased by 78% and 10% load was shed on Bus 26. But the time to voltage collapse reduced to 31.5 minutes when 10% load was shed on Bus 23 instead of at Bus 26 as shown as plot (d) in Figure 5.23.

- Scenario 4: 10% load shed at Bus 15 and gradual load increased at all buses.

A comparison of the time to voltage collapse when load was shed on Buses 26 and 15 indicated that the time to voltage collapse was shorter when load was shed on Bus 15 instead of shedding load on Bus 26. For example, the time to voltage collapse was 33.5 minutes when the load on all buses increased by 78% and 10% load was shed on Bus 26. But, the time to voltage collapse reduced to 30.8 minutes when 10% load was shed on Bus 15 instead of at Bus 26 as shown as plot (e) in Figure 5.23.

- Scenario 5: 10% load shed at Bus 14 and gradual load increased at all buses.

A comparison of the time to voltage collapse when load was shed on Buses 26 and 14 indicated that the time to voltage collapse was shorter when load was shed on Bus 14 instead of shedding load on Bus 26. For example, the time to voltage collapse was 33.5 minutes when the load on all buses increased by 78% and 10% load was shed on Bus 26. But, the time to voltage collapse reduced to 30.5 minutes when 10% load was shed on Bus 14 instead of at Bus 26 as shown as plot (f) in Figure 5.23.

- Scenario 6: 10% load shed at Buses 24, 23, 15, 14, and 26 as the load on all buses increased gradually

In this scenario, the procedure described in scenario 1 was repeated and the values of time to voltage collapse at Bus 26 as a function of load increase on all buses was determined and is shown as plot (g) in Figure 5.23. These results show that time to voltage collapse on Bus 26 increased substantially when blocks of load were shed at Buses 24, 23, 15, 14, and 26. For example, time to

voltage collapse on Bus 26 was 38.2 minutes when loads on all buses increased by 78% and 10% load was shed on those buses compare to a time to voltage collapse of 33.5, 31.9, 31.5, 30.8, and 30.9 minutes when load was curtailed on Buses 26, 24, 23, 15, and 14 respectively.

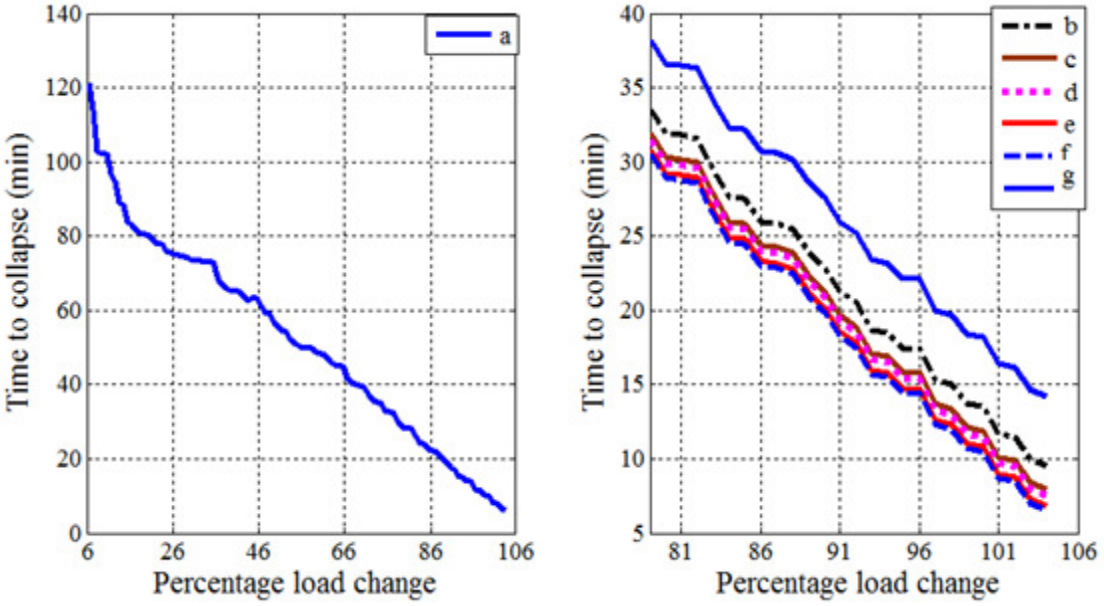

Figure 5.23: Time to voltage collapse when load shedding scheme is activated

5.7 Time to voltage collapse and PSCAD/EMTDC comparison results

The performance of the developed time to voltage collapse algorithm was evaluated and compared with actual time of voltage collapse obtained from PSCAD/EMTDC simulation. PSCAD/EMTDC is an electromagnetic transient analysis program developed by the Manitoba HVDC Research Centre. The program encompasses a wide variety of the steady state and transient power system studies. The primary solution engine is EMTDC that represents and solves differential equations for the entire power system in time domain employing the electromagnetic transient algorithm. The graphical user interface is named PSCAD, and it provides powerful means of visualizing the transient performance of the system. Together PSCAD and EMTDC provide a fast, accurate and flexible solution for the simulation of electrical equipment or systems.

The IEEE 30-Bus test system was modeled using PSCAD/EMTDC library. The only load model available in PSCAD/EMTDC library is a static load model. The static load model is unable to successfully follow gradual load increase required in voltage stability studies. To overcome this difficulty, a new controllable load model was developed during a course of the research presented in this thesis and named "Variable load model". The active and reactive power for the developed model can be easily controlled using a control panel. The control panel was set to increase the developed load model in steps of 1% of initial value per minute. Details for Initializing and developing the developed variable load model are presented in Appendix E.

The variable load model associated with the controller was connected to the monitored buses and load gradually increased on these buses until minimum voltage level on Bus 26 was recorded. The minimum voltage level was considered to be the point of voltage collapse. Time of voltage collapse on Bus 26 was monitored for the following scenario.

Voltage collapse on Bus 26 due to gradual load increase on all buses

The performance of the time to collapse technique using the IEEE 30-Bus test system shown in Figure 5.1 was evaluated and results obtained from the technique were compared with results obtained from load flow simulation studies conducted by using the EMPDC/PSCAD and Matlab softwares.

Voltage profile on Bus 26 for 1% load increment on all buses using load flow program is shown as plot (a) in Figure 5.24. It is clear from this figure that voltage on Bus 26 decreased when loads on other buses in the system increased. Power flow program failed to converge when load increase on all buses was equal to 105% and this point is assumed the point of voltage collapse. Similar results were obtained using the developed time to voltage collapse algorithm as shown in Figures 5.6, 5.11, 5.16 and Figure 5.21.

The developed variable load model was connected to all buses in PSCAD. Controllers were set to change the load model in steps of 1% per minute. Plot (b) in Figure 5.24 shows voltage profile on Bus 26 for 1% load increment on all buses. This figure illustrates that the voltage profile reached

minimum value when load increase on all buses reached 104%. Similar results were obtained using the developed time to voltage collapse algorithm as shown in Figures 5.6, 5.11, 5.16 and Figure 5.21.

It is reasonable to conclude that the developed algorithm was able to accurately detect voltage collapse when the system operating condition was approaching voltage collapse.

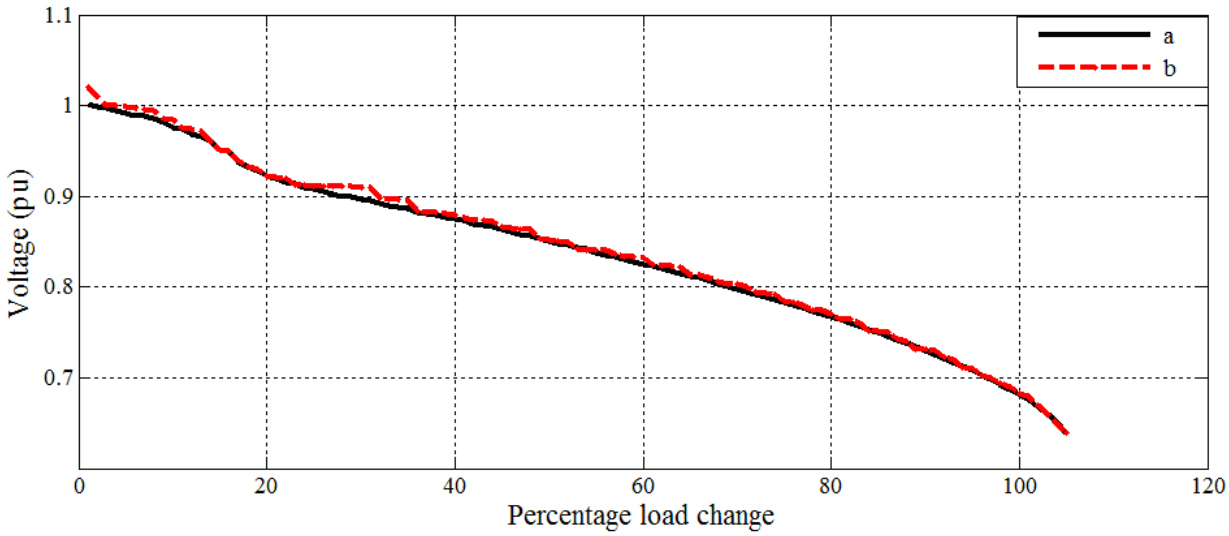

Figure 5.24: Voltage on bus 26 and percentage load increase on all buses

5.8 Summary

The performance of the developed time to voltage collapse algorithm has been evaluated using the IEEE 30-Bus system. Different types of scenarios have been implemented on the test system and time to voltage collapse has been calculated to assess system stability in an on-line mode. From all these studies, calculated time to voltage collapse using the developed algorithm performed satisfactorily. Results from time to voltage collapse algorithm have been compared with actual time of voltage collapse obtained from the PSCAD/EMTDC simulation.. Following these studies, it can be concluded that time to voltage collapse algorithm predicts voltage collapse and signifies that the system is in danger and corrective control action should be initiated to restore the system voltage prior to the actual point of voltage collapse as presented in Section 5.7.

6. CONCLUSIONS

Modern power systems are spread over vast territories and comprise of large number of generators and interconnected transmission lines. Long transmission lines are nowadays operated close to their transmission limits. The loss of an important transmission line or generator as the system load increases in certain areas of the power system can result in voltage collapse. This can result in wide spread outage if no remedial measures are taken in a timely manner.

This thesis proposes a new special protection scheme for predicting impending voltage collapse and initiating control actions to prevent it. The protection scheme uses subsets of measurements and system parameters for calculating time to voltage collapse. The technique used in the protection scheme examines the present state of the system and considers future load increases to determine if the system is approaching a voltage collapse condition.

6.1 Summary

An overview of voltage collapse phenomenon is presented in Chapter 1. Examples of three types of disturbances that lead to system collapse are described in Section 1.2. Literature review on voltage collapse techniques is given in Section 1.3. Objectives of the research conducted for this project, thesis organization and major contributions made by this work are outlined in Chapter 1 as well.

An introduction of voltage collapse phenomenon and a simple example that illustrates this phenomenon are briefly presented in Chapter 2. Factors that affect voltage collapse, such as reactive power capability, loads, on-line tap changers and compensation devices, are reviewed in Section 2.4. A number of countermeasures usually taken by electric power utilities for preventing voltage collapse, such as reinforcing the power system network, using specially designed control systems, enhancing system operation practices, real time monitoring of the system and implementing system protection schemes, are identified in this chapter as well. The most commonly used methods for analyzing voltage collapse that are used in the off-line and on-line modes are

reviewed in Section 2.6. A load flow technique is briefly presented in this chapter because most of the voltage collapse techniques proposed for off-line use are based on the load flow equations. In addition to the off-line techniques, two commonly used on-line techniques, voltage collapse predictor and voltage collapse prediction index, are also presented in Chapter 2.

A review of the literature on previously used methods for system parameter estimation is presented in Chapter 3. Details of the Delta and LS techniques and their enhancements are provided as well. The main advantages and disadvantages of both the enhancements are discussed. The data windows required for implementing those techniques are examined. The Cumulative Sum Filter is introduced in Section 3.6. The filter uses current and voltage measurements while estimating the parameters of the Thévenin equivalent. Flowcharts of these techniques are included. The application of both techniques is demonstrated by their use on the IEEE 30-Bus test system. The results obtained from implementation of both techniques are presented in Sections 3.7 and 3.8.

An overview of the previously used techniques for analyzing the voltage collapse phenomenon and details of the developed time to voltage collapse technique are presented in Chapter 4. A brief description of local-based and subset-based techniques used for detecting voltage collapse is provided. The objective and motivation of the technique developed during the course of this research are reported in Section 4.3. The voltage collapse technique is explained by applying it to a two-bus system. A general form of the developed technique that takes into consideration measurements from N buses is then presented in Section 4.6.

Performance of the time to voltage collapse technique is studied in Chapter 5 by applying the developed technique to the IEEE 30-Bus test system. It is assumed in the first study reported in this chapter that voltage and current measurements are available from two load buses of the system and the load on one of the buses is increasing gradually. Then an outage of a transmission line is considered as part of the disturbance. Impact of load shedding is examined. The studies are then repeated with the assumption that data from three, four and then five load buses is available. The time to voltage collapse is calculated to demonstrate the suitability of the developed technique for implementation in an on-line mode as part of a system protection scheme. A comparison of the off-line results of the developed technique and its application on the PSCAD/EMTDC software is presented in this chapter as well.

6.2 Contributions

The following contributions are made during the research project reported in this thesis:

- Delta and LS techniques have been modified and have been used in conjunction with CSF to monitor current and voltage measurements while estimating the parameters of system's Thévenin equivalent.

- A new technique to predict voltage collapse using subset of measurements has been developed. The developed time to voltage collapse technique is able to track system operation in an on-line mode. A relay that uses the developed technique can process local voltage and current measurements, as well as measurements from surrounding buses and can initiate suitable control action when the system approaching voltage collapse.

- The technique is able to track the system and can include the impact load changes expected in the future.

6.3 Conclusions

Few on-line techniques to predict voltage collapse have been proposed in the past. Those techniques are simple enough for implementing in numerical relays but are not capable of tracking load changes caused by decreasing voltage on nearby buses. Thévenin equivalents seen from other load buses are not observable to the local-based relays. The major objective of the thesis, therefore, was to develop and test a technique for preventing voltage collapse. The technique needs information about the Thévenin parameters of the power system. The impedance of the transmission line and voltage and current measurements at the load buses are used to calculate time to voltage collapse.

Two estimation techniques namely LS and Delta associated with CSF were developed because the most important input to the developed technique is the system's Thévenin parameters. Both techniques monitor voltage and current measurements and limit numerical difficulties. Results obtained from implementation of these techniques indicate that LS method associated with CSF is

able to provide more accurate estimates and is able to track changes in power system operating state and topology. Both techniques assume that Thévenin voltage and impedance remain constant during the data window. It is important to note that, for small changes, Delta method performs almost similar to LS method but the Delta method becomes inaccurate when larger loads are applied.

The time to voltage collapse technique developed during the course of this research was tested using the IEEE 30-Bus test system. The test-results show that the developed technique correctly predicts time to voltage collapse. They also show that the technique can take into consideration future load changes predicted by load forecasting techniques.

The studies further show that the developed technique provides an approximate estimate of time to voltage collapse during the steady state operation of the system. The estimated time in such cases is large. The studies also show that the developed technique presented in this thesis is more stable when there are changes in system measurements. Results obtained from the developed algorithm are consistent with results obtained from the load flow program. Results obtained from load flow program and developed algorithm indicate that voltage collapse occur at 105% of load increase on all buses.

The order of the time to voltage collapse polynomial increases with increasing number of buses from which the measurements of voltages and currents are used in the technique. The polynomials become difficult to solve; this reduces the effectiveness of the proposed technique.

The technique is suitable for implementation in a "System Protection System" for estimating time to impending voltage collapse. The system can alert an operator if there is less than pre-specified time to voltage collapse. If the time is less than the specified value, the system can activate load shedding with the assistance of a local-and/or wide-area control system.

The use of the voltage collapse technique, reported in this thesis, on the PSCAD/EMTDC and simulation studies of voltage collapse on the IEEE 30-Bus system have shown that the developed technique works well under different operating conditions.

REFERENCES

[1] M. Begovic, D. Fulton, M.R. Gonzalez, J. Goossens, E.A. Guro, R.W. Haas, C.F. Henville, G. Manchur, G.L. Michel, R.C. Pastore, J. Postforoosh, G.L. Schmitt, J.B. Williams, K. Zimmerman, and A.A. Burzese, "Summary of System Protection and Voltage Stability", IEEE Transactions on Power Delivery, Vol. 10, No. 2, 1995, pp. 631-638.

[2] IEEE/CIGRE Joint Task Force on Stability Terms and Definitions, "Definition and Classification of Power System Stability", IEEE Transactions on Power Systems, Vol. 19, No. 2, 2004, pp. 1387-1401.

[3] Hassan Ghasemi, "On-line Monitoring and Oscillatory Stability Margin Prediction in Power Systems Based on System Identification", Ph.D. Dissertation, University of Waterloo, ON, Canada, 2006.

[4] J. Bian and P. Rastgoufard, "Power System Voltage Stability and Security Assessment", Electrical Power System Research, Vol. 30, No. 3, 1994, pp. 197-200.

[5] Luis S. Vargas and Claudia A. Canizars, "Time Dependence of Control Avoid Voltage", IEEE Transactions on Power Systems, Vol. 15, No. 4, 2000, pp. 367-1373.

[6] North American Electric Reliability Council, "Survey of the Voltage Collapse Phenomenon", Technical Report, 1991.

[7] Khoi Vu, Miroslav Begovic, Damir Novosel, Murari Mohan Saha, "Use of Local Measurements to Estimate Voltage Stability Margin", IEEE Transactions on Power Systems, Vol. 14, No. 3, 1999, pp. 1029-1034.

[8] Antonio C. Zambroni de Souza, Leonardo M. Honorio, Geraldo L.Torres, and Germano Lambert-Torres, "Increasing the Loadability of Power Systems Through Optimal-Local-Control Actions", IEEE Transactions on Power Systems, Vol. 19, No. 1, 2004, pp. 188-194.

[9] U.S., Canada Power System Outage Task Force, "Final Report on the August 14, 2003 Blackout in the United States and Canada: Causes and Recommendations", 2004.

[10] C. W. Taylor, "Concepts of Under Voltage Load Shedding for Voltage Stability", IEEE Transactions on Power Delivery, Vol. 7, No. 2, 1992, pp. 480-488.

[11] Balamourougan Vinayagam, "A Technique for On-Line Prediction of Voltage Collapse", M.Sc thesis, University of Saskatchewan, SK, Canada, 2002.

[12] J. Chand and D. Tang, "Operational Experience of the Nelson River HVDC System", Second HVDC Operating Conference, 1989, pp. 21-31.

[13] Rüdiger Seydel, "From Equilibrium to Chaos: Practical Bifurcation and Stability Analysis", Elsevier Science Publishing Co., Inc., New York, 1988.

[14] V. Ajjarapu, and B. Lee, "Bifurcation Theory and Its Application on Non-Linear Dynamical Phenomena in an Electrical Power System", IEEE Transactions on Power Systems, Vol. 7, No. 1, 1992, pp. 424-427.

[15] V. Ajjarapu and C. Christ, "The Continuation Power Flow: A Tool for Steady State Voltage Stability Analysis", IEEE Transactions on Power Systems, Vol. 7, No. 1, 1992, pp. 416-423.

[16] H. Glavitsch, "Voltage Stability and Collapse: A Review of Basic Phenomena and Method of Assessment", Proceedings of Bulk Power System Voltage Phenomena – III, Voltage Stability, Security and Control, An International Seminar, Davos, 1994, pp. 9-11.

[17] R. A. Schlueter, A.G. Cost, J.E. Sekerke, and H.L. Forgey, "Voltage Stability and Security Assessment", EPRI Final Report, EL-5967, Project RP-19999-8, 1998.

[18] F. Gubina and B. Strmenil, “Voltage Collapse Proximity Index Determination Using Voltage Phasors Approach”, IEEE Transactions on Power Systems, Vol. 10, No. 2, 1995, pp. 778-794.

[19] F. Gubina and B. Strmenil, “A Simple Approach to Voltage Stability Assessment in Radial Networks”, IEEE Transactions on Power Systems, Vol. 12, No. 3, 1997, pp. 1121-1128.

[20] M. H. Haque, “A Fast Method of Determining the Voltage Stability Limit of a Power System”, Electrical Power System Research, Vol. 32, No. 1, 1995, pp. 35-43.

[21] M. H. Haque, “On-Line Monitoring of Maximum Permissible Loading of a Power System with Voltage Stability Limit”, IEE Proceedings of Generation, Transmission, Distribution, Vol. 150, No 1, 2003, pp. 107-112.

[22] M. Amin, “Toward Self-Healing Energy Infrastructure systems”, IEEE Computer Applications in Power, Vol. 14, No. 1, 2001, pp. 20-28.

[23] CIGRE Task Force Report 38-02-10, “Modeling of Voltage Collapse Including Dynamic Phenomena”, CIGRE publication, 1993.

[24] C.A. Cañizares, “Voltage Stability Assessment: Concepts, Practise and Tools”, IEEE-PES Power System Stability Subcommittee, Special Publications SP101PSS (ISBN 617803786951), 2003.

[25] Carson W. Taylor, Power System Voltage Stability”, McGraw Hill International Editions, 1994.

[26] Capasso and E. Mariani, “Influence of Generator Capability Curves Representation on System Voltage and Reactive Power Control Studies”, IEEE Transactions on Power Apparatus and Systems, Vol. 97, No. 4, 1978, pp. 1036-1040.

[27] P. A. Lőf, “Voltage Dependent Reactive Power Limits for Voltage Stability Studies”, IEEE Transactions on Power Systems, Vol. 10, No. 1, 1995, pp. 220-226.

[28] S. G. Johansson, “Mitigation of Voltage Collapse Caused by Armature Current Protection”, IEEE Transactions on Power Systems, Vol. 14, No. 2, 1999, pp. 591-599.

[29] ANSI/IEEE Std. 37.106, “Guide for Abnormal Frequency Protection for Power Generating Plants”, 1987.

[30] T. Van Gustem and C. Vournas, “Voltage Stability of Electric Power Systems”, Power Electronics and Power Systems, Springer Science, 1998.

[31] Gilles Nativel, Yannick Jacquemart, Vincent Sermanson and Guy Nérin, “Integrated Framework for Voltage Security Assessment”, IEEE Transactions on Power Systems, Vol. 15, No. 4, 2000, pp. 1417-1422.

[32] Allen J. Wood and Bruce. F. Wollenberg, “Power Generation, Operation and Control”, Wiley-Interscience 1996.

[33] M. M. Adibi and D. P. Milanicz, “Reactive Capability Limitation of Synchronous Machines”, IEEE Transactions on Power Systems, Vol. 9, No. 1, 1994, pp. 29-35.

[34] P. Kundur, “Power System Stability and Control”, McGraw-Hill, 1994.

[35] T. J. E. Miller, “Reactive Power Control in Electric Power Systems”, John Wiley Inc., 1982.

[36] Jordi Cabero, Alvaro Baillo and Santiago Cerisola, “A Medium-Term Integrated Risk Management Model for a Hydrothermal Generation Company”, IEEE Transactions on Power Systems, Vol. 20, No. 3, 2005, pp. 1379-1388.

[37] D.J. Hill, I.A. Hiskens and D.H. Popović, "Load Recovery in voltage stability analysis and control" , Proceedings of Bulk Power System Voltage Phenomena – III, Voltage Stability, Security and Control, An international Seminar, Davos, 1994, pp. 579-595.

[38] L. M. Hajagos and B. Danai, "Laboratory Measurements and Models of Modern Loads and Their Effect on Voltage Stability Studies", IEEE Transactions on Power Systems, Vol. 13, No. 2, 1998, pp. 584-591.

[39] Byung Ha Lee and Kwang Y. Lee, "A Study on Voltage Collapse Mechanism in Electrical Power Systems", IEEE Transactions on Power Systems, Vol. 6, No. 3, 1991, pp. 966-974.

[40] J. P. Paul, J. Y. Leost, and J. M. Tesseron, "Survey of the Secondary Voltage Control in France: Present Realization and Investigations", IEEE Transactions on Power System, Vol. 2, No. 2, 1987, pp. 505–511.

[41] J. P. Paul, C. Corroyer, P. Jeannel, J.M. Tesseron, F. Maury, and A. Torra, "Improvements in the Organization of Secondary Voltage Control in France", Proceedings of 33rd International Conference on Large High Voltage Electric Systems, Paper No 38/39-03, 1990. pp. 1-8.

[42] H. Vu, P. Pruvot, C. Launay, and Y. Harmand, "An improved Voltage Control on Large-Scale Power System", IEEE Transactions on Power System, Vol. 11, No. 3, 1996, pp. 1295–1303.

[43] L.Gyugyi and K. K. Sen, "Static synchronous series compensator: A solid-state approach to the series compensation of transmission lines", IEEE Transactions on Power Delivery, Vol. 2, No. 1, 1997, pp. 406-417.

[44] Study Committee 38, CIGRE Task Force 38-02-12, "Criteria and Countermeasures for Voltage Collapse", International Conference on High Voltage Electric Systems, 1995.

[45] CIGRE Working Group 34-08, “Protection Against Voltage Collapse”, Technical Report, CIGRE Publication, 1998.

[46] P. Moore and P. Ashmole, “Flexible AC Transmission Systems, Part 2: Methods of Transmission Line Compensation”, Power Engineering Journal, Vol. 10, No. 6, 1996, pp. 273-278.

[47] Carson W. Taylor, “Power System Voltage Stability”, McGraw Hill, 1994.

[48] M. Adamiak and W. Premerlani, “The Role of Utility Communications in a Deregulated Environment”, Proceedings of the Hawaii’s International Conference on System Sciences, Maui, Hawaii, 1999, pp. 1 - 8.

[49] H. D. Chiang, “CPFLOW: A Practical Tool for Tracing Power System Steady-State Stationary Behaviour Due to Load and Generation Variations”, IEEE Transactions on Power Systems, Vol. 10, No. 2, 1993, pp. 623-630.

[50] B. Ravindranath and M. Chander, “Power System Protection and Switchgear”, Wiley Eastern Ltd., 1977.

[51] IEEE Std. 242 (Buff Book), “Recommended Practice for Protection and Coordination of Industrial and Commercial Power Systems”, 1986.

[52] Y. Mansur, C. D. James and D. N, Patter, “Voltage Stability and Security, BC Hydro’s Operation Practice”, International Symposium on Voltage Stability and Security, Postosi, Missouri, 1998.

[53] E.K. Nielsen, M.E. Coultes, D.L. Gold, J.R Taylor and P.J. Traynor, “An Operations View of Special Protection Systems”, IEEE Transactions on Power Systems, Vol. 3, No. 3, 1988, pp. 1078-1083.

[54] P. M. Anderson and B. K. LeReverend, Industry Experience with Special Protection Schemes", IEEE Transactions on Power Systems, Vol. 11, No. 11, 1994, pp. 1166-1171.

[55] W. R. Lachs, D. Sutanto, and D. N. Logothetis, "Power System Control in The Next Century", IEEE Transactions on Power Systems, Vol. 11, No. 1, 1996, pp. 11–18.

[56] IEEE Power System Relaying Committee Working Group K12, "Voltage Collapse Mitigation", Technical Report, 1996.

[57] Kamwa, R. Grondin and Y. Hebert, "Wide-Area Measurement Based Stabilizing Control of Large Power Systems – A Decentralized/Hierarchical Approach", IEEE Transactions on Power Systems, Vol. 16, No. 1, 2001, pp. 136-153.

[58] W. R. Lachs, "A New Horizon for System Protection Schemes", IEEE Transactions on Power Systems, Vol. 18, No. 1, 2003, pp. 334-338.

[59] M. G. Adamiak, A. P. Apostolov, M. M. Begovic, C. F. Henville, K. E. Martin, G. L. Michel, A. G. Phadke, and J. S. Throp, "Wide Area Protection-Technology and Infrastructures", IEEE Transactions on Power Delivery, Vol. 21, No. 2, 2006, pp. 601-609.

[60] J. Bertsch, C. Carnal, D. Karlsson, J. McDaniel and KH. Vu, "Wide-Area Protection and Power System Utilization", Proceedings of the IEEE, Vol. 93, No. 5, 2005, pp. 997-1003.

[61] P. A. Löf, "New Principles for System Protection Schemes in Electric Power Networks", Bulk Power system Dynamics and Control Conference, Onomichi, Japan, 2001.

[62] CIGRE, Task Force 38.02.19, "System Protection Schemes in Power Networks", CIGRE Tech. Brochure 187, 2001.

[63] Claudio Canizares and Fernando Alvarado, "Point of Collapse and Continuation Methods for Large AC/DC Systems", IEEE Transactions on Power Systems, Vol. 8, No. 1, 1993, pp. 1-8.

[64] J. Bastman, "Comparison of Solution Algorithms in Point of Collapse Method", Proceedings of 13th Power System Computation Conference, Trandheim, Norway, 1999, pp. 451-455.

[65] B. Gao, G. K. Morrison and P. Kundur, "Voltage Stability Evaluation Using Model Analysis", IEEE Transactions on Power Systems, Vol. 7, No. 4, 1992, pp. 1539-1542.

[66] L. Loud, F. Rousseaux, D. Lefebvre and T. Van Cutsem, "A Time-Scale Decomposition-Based Simulation Tool for Voltage Stability Analysis", Proceedings of IEEE Porto (Portugal), Power Tech Conference, 2000, pp. 6-9.

[67] B. Gao, G. K. Morison and P. Kundur, "Voltage Stability Evaluation Using Model Analysis", IEEE Transactions on Power Systems, Vol. 7, No. 4, 1992, pp. 1529-1542.

[68] B. Gao, G. K. Morison, and P. Kundur, "Towards the Development of a Systematic Approach for Voltage Stability Assessment of Large-Scale Power Systems", IEEE Transactions on Power Systems, Vol. 11, No. 3, 1996, pp. 1314-1324.

[69] GE Power Systems Engineering, "Assessment of Applications and Benefits of Phasor Measurement Technology in Power Systems", EPRI Final Report, 1997.

[70] Magnus Gustafsson and Niclas Krantz, "Voltage Collapse in Power Systems Analysis of Component Related Phenomena Using a Power System Model", Technical Report No. 215L, Department of Electrical Power Engineering, Chalmers University of Technology, 1995.

[71] E. S. Cate, K. Hemmaplardh, J.W. Manke and D.P. Gelopulos, "Time Frame Notion and Time Response of the Models in Transient, Mid-term and Long-term Stability Programs", IEEE Transactions on Power Apparatus and Systems, Vol. 103, No. 1, 1984, pp. 143-151.

[72] R. Lind and D. Karlsson, "Distribution System Modelling For Voltage Stability Studies", IEEE Transactions on Power Systems, Vol. 11, No. 4, 1996, pp. 1677-1682.

[73] G. Phadke and J. S. Thorp, "Computer Relaying for Power Systems", Research Studies Press Ltd.,1988.

[74] T. W. Cease and B. Feldhaus, "Real-time Monitoring of The TVA power System", IEEE Computer Applications in Power, Vol. 7, No. 3, 1994, pp. 47-51.

[75] Tara Alzahawi, Mohindar S. Sachdev and G. Ramakrishna, "Online Prediction of Voltage Collapse Using Local System Measurements", 5th International Conference on Power System Automation and Protection, 2010.

[76] Borka Milovevic and Miroslav Begovic, "Voltage-stability Protection and Control Using Wide-Area Network of Phasor Measurements", IEEE Transactions on Power Systems, Vol. 18, No. 1, 2003, pp. 121-127.

[77] C. Rehtanz, "Online Stability Assessment and Wide Area Protection Based on Phasor Measurements", Bulk Power System Dynamics and Control Conference, Onomichi, Japan, 2001.

[78] A. G. Phadke, J. S. Thorp and M. G. Adamiak, "A New Measurement Technique for Tracking Voltage Phasors, Local System Frequency, and Rate of Change of Frequency", IEEE Transactions on Power Apparatus and Systems, Vol. 102, No. 5, 1983, pp. 1025-1038.

[79] T. L. Baldwin, "Real-Time Phasor Measurements for Improved Monitoring and Control of Power System Stability", Ph.D. Dissertation, Virginia Polytechnic Institute and State University, 1993.

[80] R. F. Nuqui, A. G. Phadke, R. P. Schulz and N. B. Bhatt, "Fast On-Line Voltage Security Monitoring Using Synchronized Phasor Measurements and Decision Trees", Proceedings of the IEEE-Power Engineering Society Winter Meeting, Vol. 3, 2001, pp. 1347-1352.

[81] De Oliveria, J.C. De Oliveira, J.W. R esende, and M.S. Miskulin, "Practical Approaches for AC System Harmonic Impedance Measurements", IEEE Transactions on Power Delivery, Vol. 6, No. 4, 1991, pp. 1721-1726.

[82] A.A. Girgis, W.H. Quaintance, J.Qiu, and E.B. Makram , "A Time Domain Three-Phase Power System Impedance Modeling Approach for Harmonic Filter Analysis", IEEE Transactions on Power Delivery, Vol. 8, No. 2, 1993, pp. 504-510.

[83] M. Bahadornejad and G. Ledwich, "Studies in System Thévenin Impedance Estimation from Normal Operational Data", The 6th International Power Engineering Conference, IPEC, 2003 pp. 22-24.

[84] M. Bahadornejad and G. Ledwich, "System Thevenin Impedance Estimation Using Signal Processing on Load Bus Data", Proceedings of the 6th International Conference on Advances in Power System Control Operation and Management, APSCOM, 2003, pp. 274-279.

[85] K. Ohtsuka, "An Equivalent of Multi-Machine Power Systems and Its Identification for On-Line Application to Decentralized Stabilizers", IEEE Transactions on Power Systems, Vol. 4, No. 2, 1989, pp. 687-693.

[86] Tara Alzahawi, Mohindar S. Sachdev and G. Ramakrishna, "Thévenin Equivalent Circuit Tracking During Power System Steady-State Operation", International Conference on Advance Power System Automation and Protection, 2007.

[87] Giuseppe Fusco, Arturo Losi and Mrio Russo, "Constrained Least Square Methods for Parameter Tracking of Power System Steady-State Equivalent Circuit", IEEE Transactions on Power Delivery, Vol. 15, No. 3, 2000, pp. 1073-1080.

[88] P. W. Sauer and M. A. Pai, "Power System Dynamics and Stability", Prentice Hall, 1998.

[89] R. O. Burnett, M. M. Butts and S. S. Sterlina, “Power system Applications for Phasor Measurement Units”, IEEE Computer Applications in Power, 1994, pp. 8-13.

[90] H. K. Clark, R. K. Gupta, C. Loutan and D. R. Sutphin, “Experience with Dynamic System Monitors to Enhance System Stability Analysis”, IEEE Transactions on Power Systems, Vol. 7, No. 2, 1992, pp. 693-701.

[91] Tara Alzahawi, Mohindar S. Sachdev and G. Ramakrishna, “A Special protection scheme for voltage instability prevention”, Proceedings of IEEE Canadian Conference on Electrical and Computer Engineering, 2005, pp. 545-548.

[92] D. Prasetijo, W. R. Lachs, and D. Sutanto, “A New Load Shedding Scheme for Limiting Underfrequency”, IEEE Transactions on Power Systems, Vol. 9, No. 3, 1994, pp. 1371–1378.

[93] A.G. Phadke, “Synchronized Sampling and Phasor Measurements for Relaying and Control”, IEEE Transactions on Power Delivery, Vol. 9, No. 1, 1994, pp. 442-452.

[94] IEEE Std. C37-118, “IEEE Standard for Synchrophasors for Power Systems”, IEEE Transactions on Power Delivery, Vol. 13, No. 1, 1998, pp. 73-77.

[95] T. L. Baldwin, L. Mili, M. B. Boisen and R. Adapa, “Power System Observability with Minimal Phasor Measurement Placement”, IEEE Transactions on Power Systems, Vol. 8, No. 2, 1993, pp. 701-715.

[96] A.F. Snyder, A.E. Mohammed, D. Georges, T. Margotin, N. Hadjsdid, L. Mili, and A. Robust “Damping Controller for Power Systems Using Linear Matrix Inequalities”, Proceedings of the IEEE-Power Engineering Society Winter Meeting, 1999, pp. 519-524.

[97] A.F. Snyder, D. Ivanescu, N. HadjSaid, D. Georges and T. Margotin, “Delayed-Input Wide-Area Stability Control with Synchronized Phasor Measurements and Linear Matrix

Inequalities", Proceedings of the IEEE-Power Engineering Society Summer Meeting, 2000, pp. 1009-1014.

[98] R. P. Schulz, L. S. Van Slyck and S. H. Horowitz, "Applications of Phasor Measurements on Utility Systems", Power Industry Computer Application Conference, PICA 89, 1989, pp. 49-55.

[99] J. De La Ree, V. Centeno, J.S. Thorp and A. G. Phadke, "Synchronized Phasor Measurements Applications in Power Systems", IEEE Transactions on Smart Grid, Vol. 1, No. 1, 1993, pp. 20-27.

[100] Siok Mak, and Denny Radford, "Communication System Requirements for implementation of Large Scale Demand Side Management and Distribution Automation", IEEE Transactions on Power Delivery Vol. 11, No. 2, 1996, pp. 683 - 689.

[101] John Newbury and, William Miller, "Potential Metering Communication Services Using the Public Internet", IEEE Transactions on Power Delivery, Vol. 14, No. 2, 1999, pp. 1202 - 1207.

[102] Sheng-Luen Chung and Wen-Fa Yang, "Data Acquisition and Integration in Heterogeneous Computing Environment", International IEEE/IAS Conference on Industrial Automation and Control: Emerging Technologies, 1995, pp. 598-603.

[103] UCA Specification Version 1.0, EL-7547, "Utility Communications Architecture", Vol. 4, RP 2949-1, Final Report, EPRI, Palo Alto, 1991.

[104] Sandro Gianny Aquiles Perez, "Modeling Relays for Power System Protection Studies", Ph.D. Dissertation, University of Saskatchewan, SK, Canada, 2006.

[105] M. Veeraraghavan and R. Karri, "Architecture and Protocols that Enable New Applications on Optical Network", IEEE Communication Magazine, Vol. 39, No. 3, 2001, pp. 118 – 127.

[106] Wook Hyun Kwon and Beon Jin Chung, “Real-Time Fiber Optic Network for an Integrated Digital Protection and Control System”, IEEE Transactions on Power Delivery, Vol. 7, No. 1, 1992, pp. 160 - 166.

[107] John Gowar, “Optical Communication Systems”, Prentice Hall, 1993.

[108] Xiaoming Mou, Weixing Li and and Zhimin Li, “A Preliminary Study on the Thévenin Equivalent Impedance for Power Systems Monitoring”, 4th International Conference on Electric Utility Deregulation and Restructuring Power Technologies (DRPT), 2011, pp. 730-733.

[109] A. E. Efthymiadis and, Y.H.Guo, “Generator Reactive Power Limits and Voltage Stability”, Power System Control and Management Conference, 1996, pp. 196-199.

APPENDIX A. IEEE 30-BUS TEST SYSTEM

A.1 General description

IEEE 30-Bus test system was used to develop studies presented in Chapter 3, 4 and 5. The IEEE 30-Bus system has seven generation sources and twenty static loads as shown in Figure A.1.

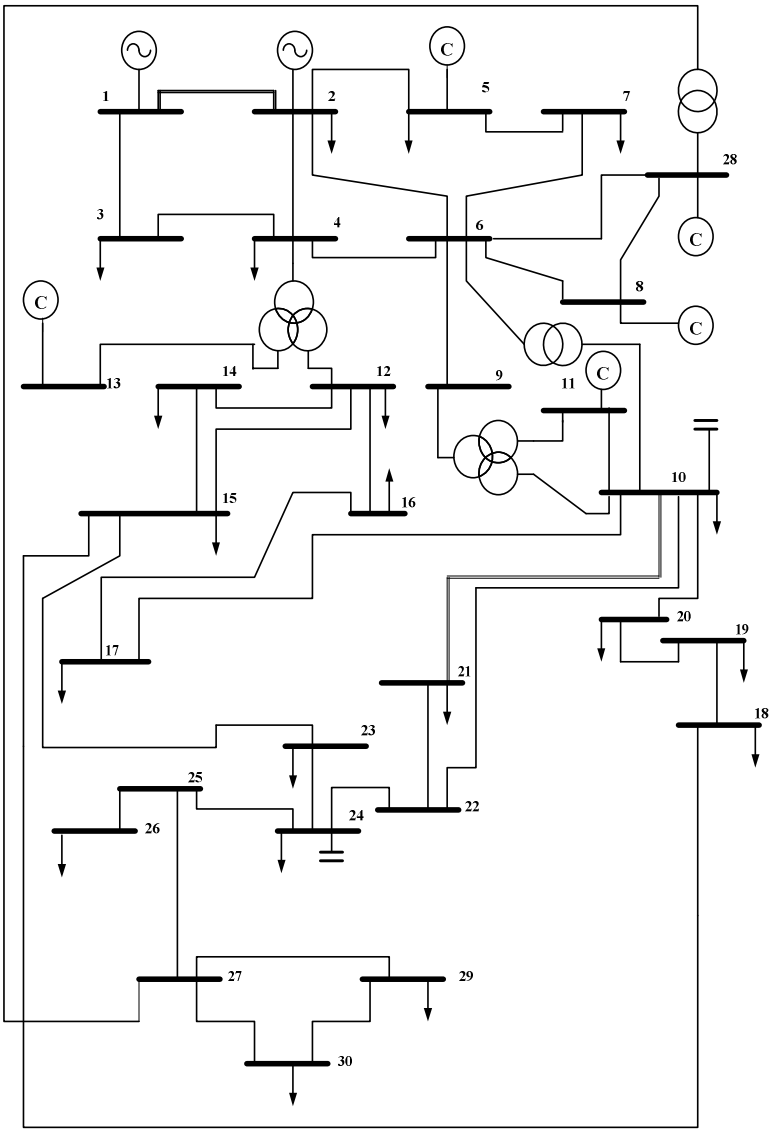

Figure A.1: IEEE 30-Bus test system

A.2 Transmission line data

Parameters used in modelling of transmission line in IEEE 30-Bus test system are listed in Table A.1.

Table A. 1: Transmission line data and parameter

From Bus #	To Bus #	R (pu)	X (pu)	½ B (pu)	Tap setting
1	2	0.0192	0.0575	0.0264	1
1	3	0.0452	0.1852	0.0204	1
2	4	0.057	0.1737	0.0184	1
3	4	0.0132	0.0379	0.0042	1
2	5	0.0472	0.1983	0.0209	1
2	6	0.0581	0.1763	0.0187	1
4	6	0.0119	0.0414	0.0045	1
5	7	0.046	0.116	0.0102	1
6	7	0.0267	0.082	0.0085	1
6	8	0.012	0.042	0.045	1
6	9	0	0.208	0	0.978
6	10	0	0.556	0	0.969
9	11	0	0.2082	0	1
9	10	0	0.11	0	1
4	12	0	0.256	0	0.932
12	13	0	0.14	0	1
12	14	0.1231	0.2559	0	1
12	15	0.0662	0.1304	0	1
12	16	0.0945	0.1987	0	1
14	15	0.221	0.1997	0	1
16	17	0.0824	0.1923	0	1
15	18	0.1073	0.2185	0	1

From Bus #	To Bus #	R (p.u)	X (p.u)	½ B (p.u)	Tap setting
18	19	0.0639	0.1292	0	1
19	20	0.034	0.068	0	1
10	20	0.0936	0.209	0	1
10	17	0.0324	0.0845	0	1
10	21	0.0348	0.0749	0	1
10	22	0.0727	0.1499	0	1
21	22	0.0116	0.0236	0	1
15	23	0.1	0.202	0	1
22	24	0.115	0.179	0	1
23	24	0.132	0.27	0	1
24	25	0.1885	0.3292	0	1
25	26	0.2544	0.38	0	1
25	27	0.1093	0.2087	0	1
28	27	0	0.396	0	1
27	29	0.2198	0.4153	0	0.968
27	30	0.3202	0.6027	0	1
29	30	0.2399	0.4533	0	1
8	28	0.0636	0.2	0.0214	1
6	28	0.0169	0.0599	0	1

A.3 Transformer data

Parameters used in modeling of power transformers are shown in Table A.2.

Table A. 2: Transformer data

Transformer Designation	Tap setting
4-12	0.932
6-9	0.978
6-10	0.969
28-27	0.968

A.4 Machines

Parameters used in modelling of machines are listed in Table A.3. Other important machines data and parameters are shown in Table A.4.

Table A.3 Voltage controlled bus data

Bus #	Voltage Magnitude	Min. MVAR Capacity	Max. MVAR Capacity
2	1.043	-40	50
5	1.01	-40	40
8	1.01	-10	40
11	1.082	-6	24
13	1.071	-6	24

Table A. 4: Injected MVAR data

Bus #	MVAR
10	19
24	4.3

A.5 Loads

Parameters used in modeling of loads in the IEEE 30-Bus test system are listed in Table A.5.

Table A. 5: Load data

Bus #	Bus code	Voltage pu	Angle Degree	MW	MVAR	MW	MVAR	Qmin	Qmax	MVAR
1	1	1.06	0	0	0	0	0	0	0	0
2	2	1.043	0	21.7	12.7	40	0	-40	50	0
3	0	1	0	2.4	1.2	0	0	0	0	0
4	0	1.06	0	7.6	1.6	0	0	0	0	0
5	2	1.01	0	94.2	19	0	0	-40	40	0
6	0	1	0	0	0	0	0	0	0	0
7	0	1	0	22.8	10.9	0	0	0	0	0
8	2	1.01	0	30	30	0	0	-10	40	0
9	0	1	0	0	0	0	0	0	0	0
10	0	1	0	5.8	2	0	0	0	0	19
11	2	1.082	0	0	0	0	0	-6	24	0
12	0	1	0	11.2	7.5	0	0	0	0	0
13	0	1.071	0	0	0	0	0	-6	24	0
14	0	1	0	6.2	1.6	0	0	0	0	0
15	0	1	0	8.2	2.5	0	0	0	0	0
16	0	1	0	3.5	1.8	0	0	0	0	0
17	0	1	0	9	5.8	0	0	0	0	0
18	0	1	0	3.2	0.9	0	0	0	0	0
19	0	1	0	9.5	3.4	0	0	0	0	0
20	0	1	0	2.2	0.7	0	0	0	0	0
21	0	1	0	17.5	11.2	0	0	0	0	0
22	0	1	0	0	0	0	0	0	0	0
23	0	1	0	3.2	1.6	0	0	0	0	0

Bus #	Bus code	Voltage pu	Angle Degree	MW	MVAR	MW	MVAR	Qmin	Qmax	MVAR
24	0	1	0	8.7	6.7	0	0	0	0	4.3
25	0	1	0	0	0	0	0	0	0	0
26	0	1	0	3.5	2.3	0	0	0	0	0
27	0	1	0	0	0	0	0	0	0	0
28	0	1	0	0	0	0	0	0	0	0
29	0	1	0	2.4	0.9	0	0	0	0	0
30	0	1	0	10.6	1.9	0	0	0	0	0

APPENDIX B. MAPLE FUNCTIONS

For each specific case study a symbolic function was created to identify time to voltage collapse polynomial parameters. This cannot be done manually as the equations for the parameters increase considerably with an increasing number of "known" buses. In order to make functions of more than two "know" buses, a Maple program was used. The outputs from Maple functions presented in this appendix is used as input file to a MATLAB function. The algorithm called "time to voltage collapse" can easily be changed to fit other computer programs.

B.1 Loading system

The system is loaded into Maple software using the following script called "system set up. ma" (for the case of three known load buses).

```
With(linalg);
Read "dim.c"
# Description of system
N:=3; # Number of loads
Tot:=8; # Total number of impedances (including loads)
Nbus:=6; # Number of buses (including Thevenin buses)
Nz:=3; # Number of Thevenin equivalents
# Load system
Q:= matrix(readdata("/home/leifwar/maple/case/Q.dat",integer,tot))
Yrem:= readdata("/home/leifwar/maple/case/YYrem.dat",integer,1);
Yrem:= readdata("/home/leifwar/maple/caseyrem.dat",integer,1);
# Make system matrix
Yy:=matrix(tot,tot,(i,j))->
        If i=j and i<= n then
                y[i]
```

```
        elif i=j and i> n and I <= (n+nz) then
                Yz[i-n]
        Elif i=j and i>2*n and I <= tot then
                Ye[i-(n+nz)]
        else 0
fi);
for I from 1 to n do if Yrem[i] = 1 then Yz[i]:=0 fi;od;
Yk:=multiply(Q,yy,transpose(Q));
If nbus = 2*n then
Ekm:= submatrix(-Yk,1..n,n+1..2*n);
Ykm:= submatrix(Yk,1..n,n+1..(n+nz)),
        multiply(submatrix(Yk,1..n,(n+nz) +1..nbus),
                inverse(submatrix(Yk,(n+nz)+1..nbus,(n+nz)+1..nbus)),
                submatrix(Yk,(n+nz)+1..nbus,n+1..(n+nz))));
Ykm:= matadd(submatrix(Yk,1..n,1..n),
        multiply(submatrix(-Yk,1..n,(n+nz)+1..nbus),
                inverse(submatrix(Yk,(n+nz)+1..nbus,(n+nz)+1..nbus)),
                submatrix(Yk,(n+nz)+1..nbus,1..n)));fi;
Ykm_tmp:=matrix(n,n,(I,j)->
        if Ykm[i,j]=0 then
                0
        elif i=j then
                Ym[i,i]
        elif i>j then
                Y[j,i]
        else
                Y[i,j]
        fi );
Ykm_tmp_det:=det(Ykm_tmp);
Ykm_tmp_inv:=inverse(Ykm_tmp/Ykm_tmp_det);
U:=multiply(Ykm_tmp_inv,Ekm,matrix(nz,1,i->E[i]));
for I from 1 to n do Ym[i,i]:=Y[i,i]+y[i]; od;
```

```
T:=coeffs(expand(U[1,1]),indets(sum(y[k],'k'=2..n)),Tt);
N:=coeffs(expand(Ykm_tmp_det),indets(sum(y[k],'k'=1..n)),Nt);
```

The function "dim.c" is used to calculate the dimensions of a vector.

```
dim:=proc (x) local I,j; j:=0; for I in x do j:=j+1; od; j end: # dim
```

B.2 Time to voltage collapse algorithm

In this algorithm the following script was used to create an input file to MATLAB code called "time_to_voltage.ma".

```
assume(t,real);
for I from 1 to 6 do
        Y[i]:=yrm[i]+K*yim[i] + t*(yrd[i]+I*yid[i]);
        assume(yrm[i],real,yim[i],real);od;
S1d := sqrt(coeff(y[1],I,0)^2+coeff(y[1],I,1)^2);
# coefficient a[i] og b [i]
for I from 1 to vectdim([T]) do
        a[i]:= ar[i]+I*aid[i];
        assume(ar[i],real,ai[i],real);od;
for I from 1 to vectdim([N]) do
        b[i]:= br[i]+I*bi[i];
        assume(br[i],real,bi[i],real);od;
# Numerator (atil) og denominator (apri)
atil := coeff(expand(sum(Tt[k]*a[k],k=1..vectdim([T]))),I,0)^2+
        coeff(expand(sum(Tt[k]*a[k],k=1..vectdim([T]))),I,1)^2;
apri := coeff(expand(sum(Nt[k]*b[k],k=1..vectdim([N]))),I,0)^2+
        coeff(expand(sum(Nt[k]*b[k],k=1..vectdim([N]))),I,1)^2;
# Start writing to file "time_to_voltage.m
fd:=fopen("time_to_voltage.m",WRITE)
fprintf(fd,"function [ s ] = vippp_yri(E,Yz,Ye,y,dy)\n");
fprintf(rd,"%c\n",'293);
fprintf(fd,"%c [ s ] = vippp_yri(E,Yz,Ye,y,dy)\n",\293;
```

```
fprintf(fd,"%c\n",\293);
fprintf(fd,"yrm=real(y);\nyim=imag(y);\nyrd=real9dy);\nyid=imag9dy);\n");
for I from 1 to rowdim(Ykm) do
        for j from 1 to rowdim(Ykm) do
                if Ykm[i,j] <> 0 and i<=j and i<>j then
                fprintf(fd,"Y%a%a=%a;\n",i,j,Ykm[i,j]);
                elif Ykm[i,j] <> 0 and i<=j then
                fprintf(fd,"Y%a%a=%a;\n",i,i,Ykm[I,i]-y[i]; fi;od;od;# a og b
for I from 1 to vectdim([T]) do
        fprintf(fd,"a%a%=a%;\nar%a=real(ar%a);ai%a=imag(ai%a);\n",I,collect(T[i],
        indets(T[i])),i,i,i,i)od;
for I from 1 to vectdim([N]) do
        fprintf(fd,"b%a=%a;\nbr%a=real(br%a);bi%a=imag(bi%a);\n",I,collect(N[i],
        indets(N[i])),i,i,i,i)
# c,d og e.
for i from 0 to degree(atil,t ) do
        fprintf(fd,"c%a=%a:\n",i,coeff(atil,t,i));od;
for i from 0 to degree(S1d^2,t) do
        fprintf(fd,"e%a=%a;\n",i,coeff(S1d^2,t,i));od;
for i from 0 to degree 9apri,t ) do
        fprintf(fd,"e%a=%a;\n",i,coeff(apri,I,i));od;
S1 :=sum('c[k]*t^k','k'=0..degree(atil,t))*
        sqrt(sum('d[k]*t^k','k'=0..degree(S1d^2,t)))/
        sum('e[k]*t^k','k'=0..degree(apri,t));
eq:numer(diff(S1,t));
for i from 0 to degree(eq,t) do
        fprintf(fd,"s%a=%a;\n",I,coeff(eq,t,i));od;
fprintf(fd,"s = [ ");
for i from 0 to degree(expand(eq),t) do fprintf(fd," s%a",I,coeff(eq,t,i)); od;
fprintf(fd," };\n");
fclose(fd);
```

APPENDIX C. PHAOR MEASUREMENT UNIT (PMU)

C.1 Introduction

Phasor Measurement Unit is a power system device capable of measuring the synchronized voltage and current phasors in power system. Synchronicity among PMUs is achieved by same-time sampling of voltage and current waveforms using a common synchronizing signal from the Global Positioning Satellite (GPS). The ability of calculating synchronized phasors makes the PMU one of the most important measuring devices in the future of power system monitoring and control [93,94,69,95].

The technology behind PMUs traced back to the field of computer relaying. In this equally revolutionary field in power system protection, microprocessors technology made the direct calculation of the sequence components of phase quantities possible [96,57,97]. Phasor is defined as a complex form which represents the steady-state waveform with a nominal power frequency (see Figure C.1).

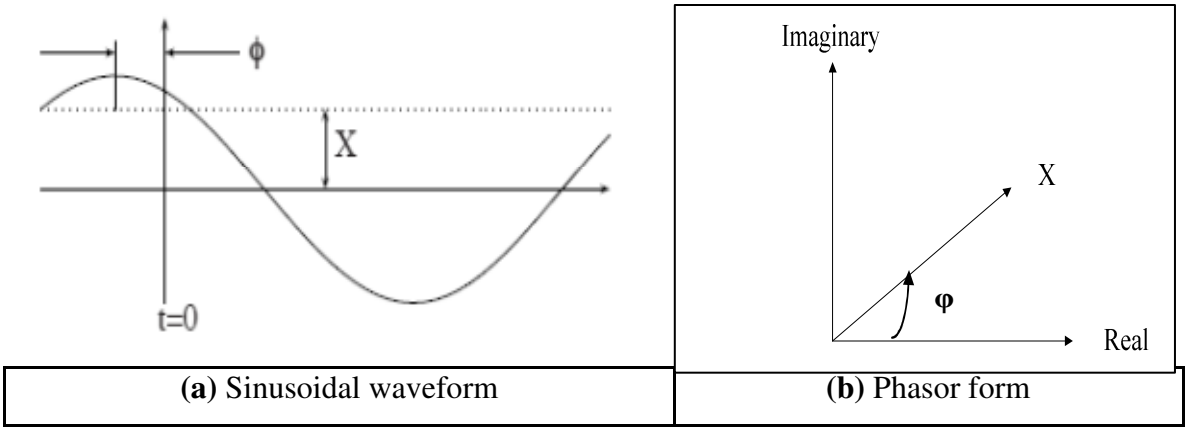

(a) Sinusoidal waveform | **(b)** Phasor form

Figure C.1: Phasor representation of a sinusoidal waveform

A sinusoidal quantity shown in Figure C.1 (a) has a phasor representation as shown in Equation C.1.

$$X \equiv \frac{X_k}{\sqrt{2}} e^{j\varphi} \qquad (C.1)$$

where,

X_k represents the maximum value,

Although the concept of a phasor is defined for a pure sinusoid, it can be also used in the presence of transient components by stipulating that the phasors represent the fundamental frequency component of a waveform observed over a finite duration (observation window).

Synchronization of sampling is achieved using a common timing signal available locally at the substation. Timing signal accuracy in the order of milliseconds suffices for the relaying application. It is clear that the same approach could be extended to the field of power system monitoring.

Figure C.2 shows a hardware block diagram of a phasor measurement unit. The anti-aliasing filter is used to filter out from the input waveform frequencies above the Nyquist rate. The phase locked oscillator converts the GPS a pulse per second into a sequence of high-speed timing pulses used in the waveform sampling. The microprocessor executes the DFT phasor calculations. Finally, the phasor is time stamped and uploaded to a collection device known as a data concentrator. An IEEE standard format now exists for real time phasor data transmission [98,80,99]. The benefits of synchronized phasor measurements to power system monitoring, operation and control have been well recognized [105, 106, 107].

PMUs improve the monitoring and control of power systems through accurate, synchronized and direct measurement of the system state. For example, the positive sequence components of the fundamental frequency bus voltages are used directly by such advanced control center applications as contingency analysis and on-line load flow. With PMUs the security indicators produced by these advance applications are representative of the true real time status of the power system. It must be recognized that the current thrust of utilities is to install fiber optic links among substations.

The phasor measurement unit uploads its time stamped phasor data using such medium as dedicated telephone line or through the wide area network (WAN) [100,76].

A system of PMUs must be supported by communication infrastructure of sufficient speed to match the fast streaming PMU measurements. Oftentimes power systems are not totally equipped with matching communication. As such, any potential move to deploy PMUs must recognize this limitation. It is a possibility that the benefits brought forth by PMUs could justify the installation of their matching communication infrastructure. However, it must be recognized that deployment of PMUs in every bus is a major economic undertaking and alternative placement techniques must consider partial PMU deployment [101,102,103].

The foremost concern among potential users is the application that will justify initial installation of PMUs. As expected from an emerging technology, initial installation of PMUs was made for purposes of gaining experience with the device and its applications. For this purpose, PMUs were deployed mainly on a localized basis. However the greatest positive impact of the PMU would be for system applications such as state estimation and wide area protection and control.

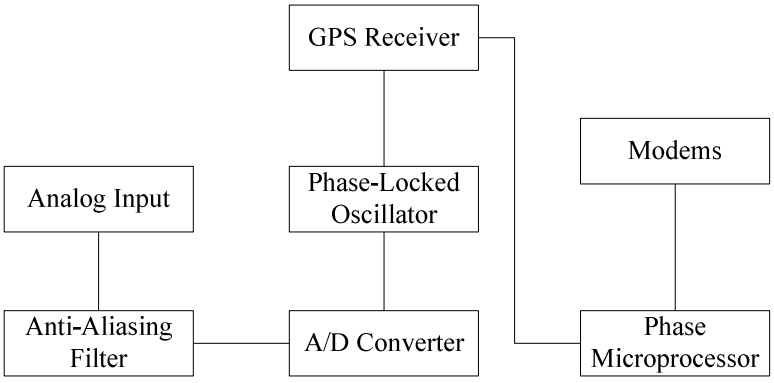

Figure C.2: Phasor measurement unit hardware block diagram

APPENDIX D. ESTIMATION OF SYSTEM PARAMETER USING DELTA TECHNIQUE IN POLAR COORDINATES

The voltage at the load bus of the system shown in Figure 3.1 at time t can be described in polar coordinate form as shown in Equation D.1.

$$\begin{aligned} |E_{th}| \cos \delta_{Eth} &= V_L \cos(\delta_{VL}) + IZ_{th} \cos(\delta_I + \delta_{Zth}) \\ |E_{th}| \sin \delta_{Eth} &= V_L \sin(\delta_{VL}) + IZ_{th} \sin(\delta_I + \delta_{Zth}) \end{aligned} \tag{D.1}$$

where,

δ_{Eth} is the angle of Thévenin voltage,

δ_{Zth} is the angle of Thévenin impedance,

δ_{VL} is the angle of load voltage, and

δ_I is the angle of load current.

Time derivation of Equation D.1 is shown in Equation D.2.

$$\begin{aligned} 0 &= -V_L \sin(\delta_{VL}) \frac{d\delta_{VL}}{dt} + \cos(\delta_{VL}) \frac{dV_L}{dt} - IZ_{th} \sin(\delta_I + \delta_{Z_{th}}) \frac{d\delta_I}{dt} + Z_{th} \cos(\delta_I + \delta_{Zth}) \frac{dI}{dt} \\ 0 &= V_L \cos(\delta_{VL}) \frac{d\delta_{VL}}{dt} + \sin(\delta_{VL}) \frac{dV_L}{dt} - IZ_{th} \cos(\delta_I + \delta_{Z_{th}}) \frac{d\delta_I}{dt} + Z_{th} \sin(\delta_I + \delta_{Zth}) \frac{dI}{dt} \end{aligned} \tag{D.2}$$

Solving for Thévenin impedance, the following equations are obtained:

$$Z_{th} = \sqrt{\frac{(V_L \frac{d\delta_{VL}}{dt})^2 + (\frac{dV_L}{dt})^2}{(I \frac{d\delta_I}{dt})^2 + (\frac{dI}{dt})^2}} \tag{D.3}$$

$$\delta_{Zth} = -\delta_I + \tan\left(\frac{(IV_L\frac{d\delta_I}{dt}\frac{d\delta_{VL}}{dt}+\frac{dI}{dt}\frac{dV_L}{dt})\sin\delta_{VL} - (I\frac{dV_L}{dt}\frac{d\delta_I}{dt} - V\frac{dI}{dt}\frac{d\delta_{VL}}{dt})\cos\delta_{VL}}{(IV_L\frac{d\delta_I}{dt}\frac{d\delta_{VL}}{dt}+\frac{dI}{dt}\frac{dV_L}{dt})\cos\delta_{VL} - (I\frac{dV_L}{dt}\frac{d\delta_I}{dt} - V_L\frac{dI}{dt}\frac{d\delta_{VL}}{dt})\sin\delta_{VL}}\right) \quad \text{(D.4)}$$

Using the approximation that $\frac{df}{dt} \approx \frac{\Delta f}{\Delta t}$, Equations D.3 and D.4 in duration of Δ_t can be written as:

$$Z_{th} = \sqrt{\frac{(V_L\Delta\delta_V)^2+(\Delta V_L)^2}{(I\Delta\delta_I)^2+(\Delta I)^2}} \quad \text{(D.5)}$$

$$\delta_{Zth} = -\delta_I + \tan\left(\frac{(IV_L\Delta\delta_I\Delta\delta_{VL}+\Delta I\Delta V_L)\sin\delta_{VL} - (I\Delta V_L\Delta\delta_I - V_L\Delta I\Delta\delta_{VL})\cos\delta_{VL}}{(IV_L\Delta\delta_I\Delta\delta_{VL}+\Delta I\Delta V_L)\cos\delta_{VL} - (I\Delta V_L\Delta\delta_I - V_L\Delta I\Delta\delta_{VL})\sin\delta_{VL}}\right) \quad \text{(D.6)}$$

Equations D.5 and D.6 can be used to track Thévenin impedance of the system, using local voltage and current measurements.

APPENDIX E. VARIABLE LOAD MODEL DESIGN METHODOLOGY IN PSCAD/EMTDC

E.1 Developed variable load model design methodology

The existing static load model in PSCAD/EMTDC library is unable to successfully follow gradual load increases. During the course of research a new load component was created and added to the PSCAD/EMTDC library. The load model called Variable Load Model.

The developed methodology uses a program to design a variable load model and embeds the designed load model inside a power system model. The developed algorithm makes use of the variable load model and enables a more easy and efficient study of voltage collapse scenarios.

The developed methodology requires that a power system first be modelled in PSCAD/EMTDC. For that, PSCAD/EMTDC provides a complete library of the typical elements presented in typical power systems.

The modelling of a variable load is initiated by employing a PSCAD/EMTDC feature called "Component". A PSCAD/EMTDC component is a computational resource for creation of user-custom models. PSCAD/EMTDC components share the same computational structures as the models belonging to the PSCAD/EMTDC libraries. This structure is constituted by an icon that activates the element in the graphical interface PSCAD, an editor that adds code to process the inputs and address the outputs of the element, and associated dialog boxes that provide parameters and/or gain access to the internal variables of the demand.

For the developed variable load model, a PSCAD/EMTDC component must be initialized. The initialized component must be provided with both the necessary number of inputs and outputs and the load type of the load (R, RL, RC, or RLC). The internal variables to be monitored and the

graphs to illustrate them must then be created. Finally, control the input signals to the component, a control panel must be designed using the multi-run model within the PSCAD/EMDC main library.

E.1.1 Initialization a of new PSCAD/EMTDC component

The simplest manner for initializing of a new component in a PSCAD/EMTDC case is by employing the PSCAD/EMTDC "Component Wizard". The Component wizard is a dialog box in PSCAD/EMTDC that creates the template for a new component based on the parameters entered by the user. To initialize a new component with component wizard, the following procedure must be undertaken [104]:

1. Open the PSCAD/EMTDC case by double-clicking on the case name in the "Project Tree".

2. Right-click on the background of the main window of PSCAD. In the menu that appears, select the option "Special is selected".

3. In the next menu that appears, use the option "Create New Component" (see Figure E.1) to activate the component wizard definition window shown in Figure E.2.

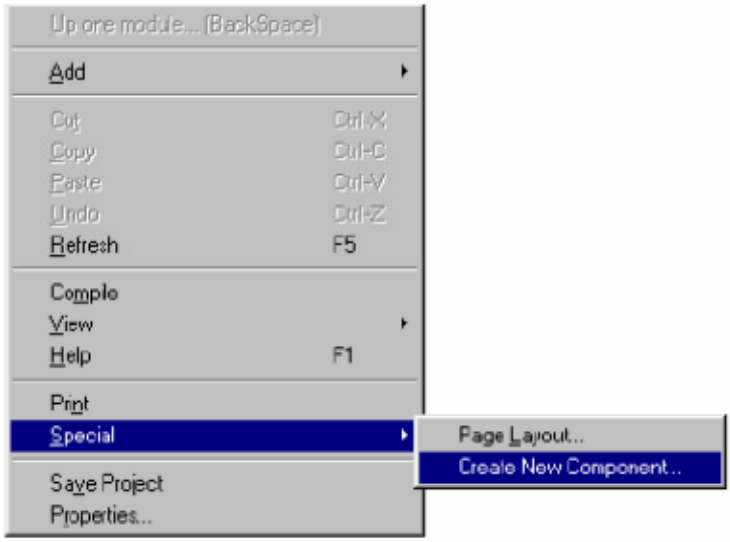

Figure E.1: Activated component wizard window

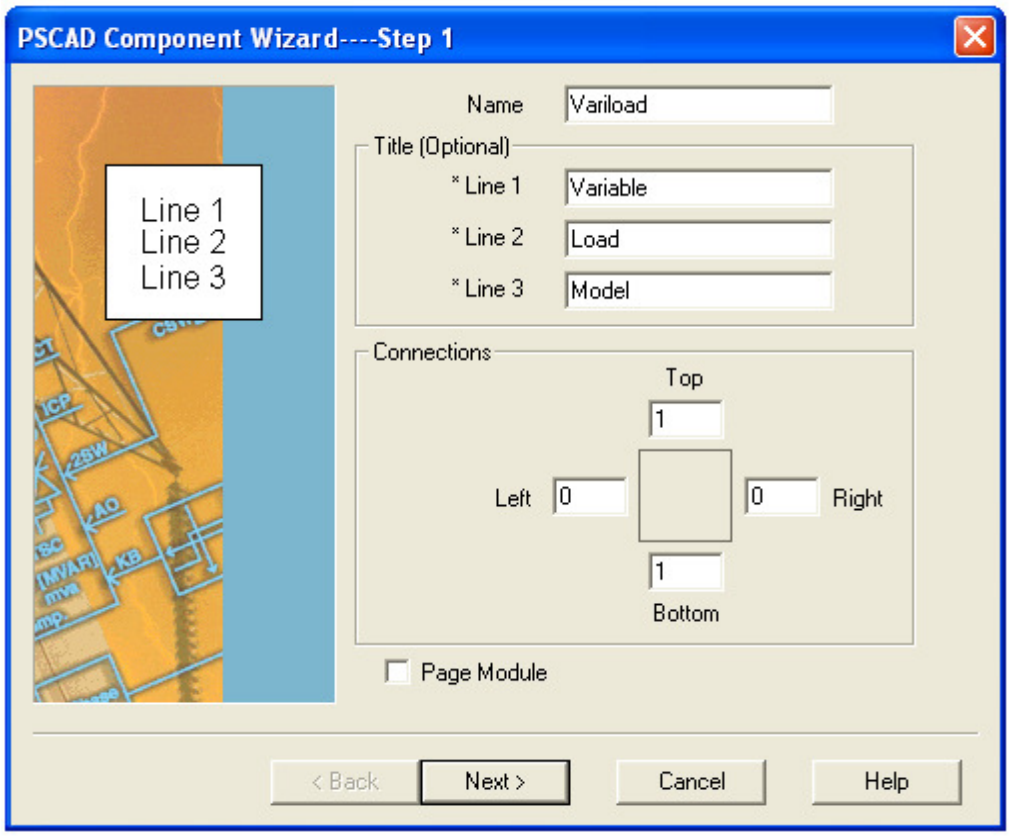

Figure E.2: Component wizard definition window

4. Provide an alphanumeric name (beginning with a letter and containing no spaces) is provided to set the "Definition Name" of the component. In the example, the Definition Name was set as "Variload", as shown in Figure E.2.

5. Fill in the front textbox shown by the icon of the component in the graphical interface PSCAD. In this example, the front text was set as "Variable Load Model". What results is a rectangular icon shown in Figure E.4.

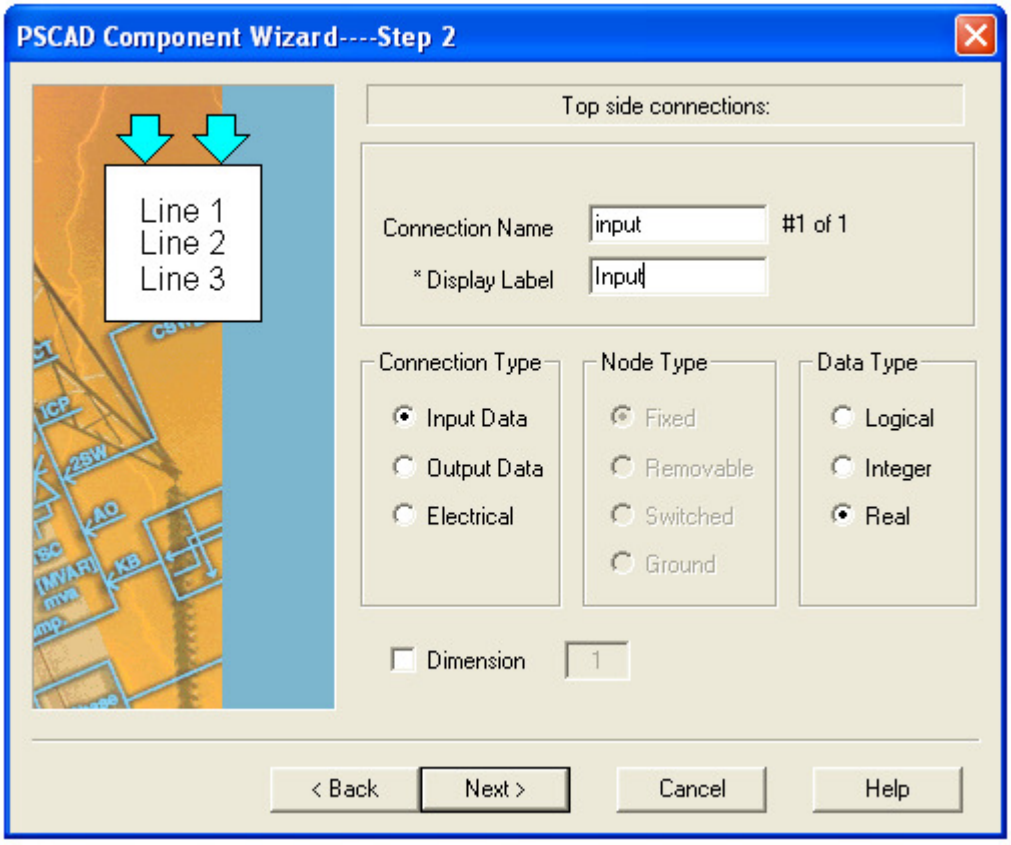

Figure E.3: Component wizard connection

6. Provide a short alphanumeric name (beginning with a letter and containing no spaces) to set the "Definition Name" of the component. In the example, the *Definition Name* was set as "Variload", as shown in Figure E.4.

7. Provide Component wizard with the number of input and output component. These inputs and outputs are reflected in the rectangular icon of the component. It is recommended that the inputs be set in one side of the rectangular component and the outputs in the opposite side. In the example, for the file "Variload.txt", one input was created in the top side of the icon and one output was created in the bottom side of the icon, and they were set as shown in Figure E.3.

8. The *Component Wizard* presents a connection window as shown in Figure E.3 per each input and output specified in the *Component Wizard* definition window. The following procedure is carried out for each of the inputs or outputs specified. Type the "Connection Name" in the order provided by the text file. Select input in the "Connection Type" for every output as pointed in the text file. Choose "Real "in the data type for all inputs and outputs and the rest of the parameters as they are. Figure E.3 shows the Component Wizard connection window for the first connection, and the data entered according to the informative file.

9. To review or modify the entered parameters, click "Prev" or "Next". Click the "Cancel" key to exit the Component Wizard without initializing the component at any time. Click the "Finish" key to accept the entered parameters and to close the Component Wizard window. The Prev, Next, Cancel, and Finish buttons are shown in Figure E.3.

10. The component icon shows the graphical interface PSCAD once the Component Wizard window is closed, and the c*omponent* appears as an element on the PSCAD/EMTDC page.

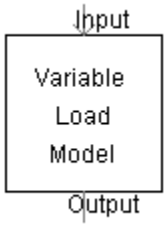

Figure E.4: Graphic design for the created variable load model component

E.1.2 Structure of the PSCAD/EMTDC component

The component recently created is employed as the computational base of the variable load model in a PSCAD/EMTDC case. Components are constituted by an icon in the graphical interface PSCAD, an internal code in FORTRAN, and dialog boxes to establish user parameters.

The graphical icon permits the component to interact with other elements in the PSCAD/EMTDC case. The internal code processes the inputs and retrieves the outputs. Through the dialog boxes

the user sets values to parameters of the internal code of the component on the PSCAD/EMTDC case.

The "Component Workshop" is opened by placing the pointer in the icon of the component in PSCAD and right-clicking on it; from the menu that appears the option "Special" is selected and, from the next drop-down menu that appears, "Edit Definition" is chosen, as shown in Figure E.5.

The Component Workshop window is shown in Figure E.5. The main page of the Component Workshop shows the three main sections of the component, which are the "Graphics", "Parameters", and "script" sections. The Graphics section corresponds to the icon as shown in Figure E.4, the Parameters section corresponds to the dialog boxes and Script correspond to the internal code of the component. The right side view of the Component Workshop is the "edit view". The "Graphics" and "Parameters" sections have graphical editors, and "script" has a text editor. The workspace with the main sections of the *Component* is shown in Figure E.6.

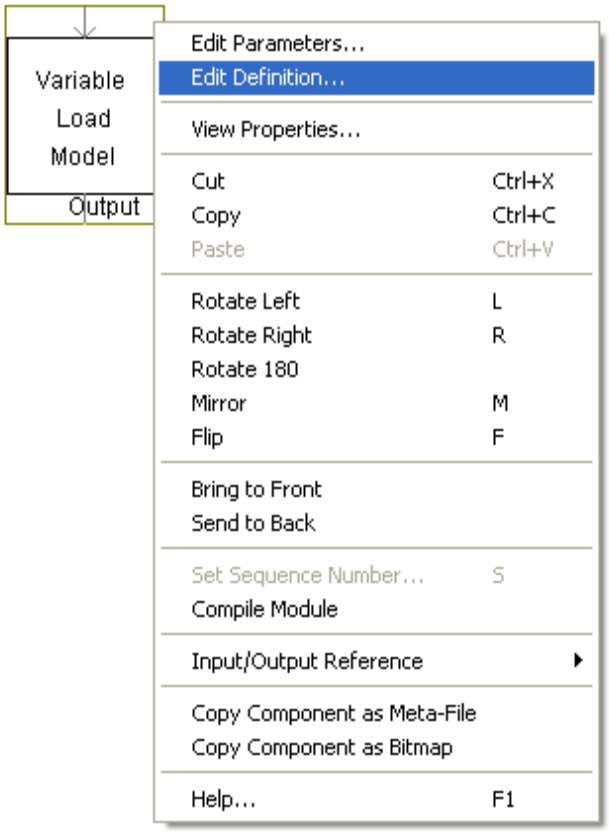

Figure E.5: Editing the new component

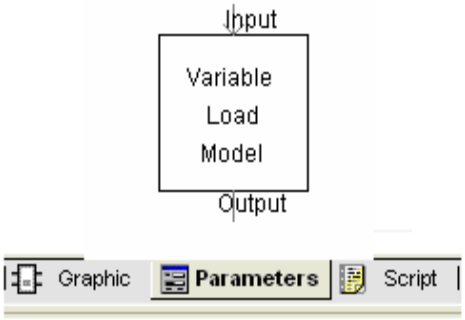

Figure E.6: Component workspace window

E.1.3 Creating a dialog box to access variable load model internal parameters

The parameters section permits designing the dialog boxes to assign values to the parameters of the component. In this thesis, the Parameters dialog boxes are employed to gain access to the internal variables of the variable load model from the graphical interface. The internal variables are possible to plot once access to them has been established. Just one parameters dialog box is needed for establishing access to the internal variables of the component, as follows.

1. Create new category in the Parameters section by right-clicking with the pointer positioned on the Parameters section in the workspace of the Component Workshop. From the menu that pops up, select the "New" option and, from the next menu that appears, select "Category", (as depicted in Figure E.7). A new Category named "Variable Load Parameters" emerges as a subsection under the section Parameters, as shown in Figure E.8.

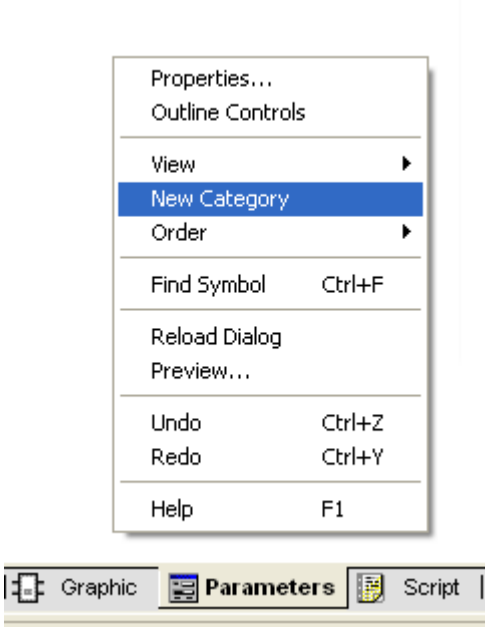

Figure E.7: Creating a new category of parameters

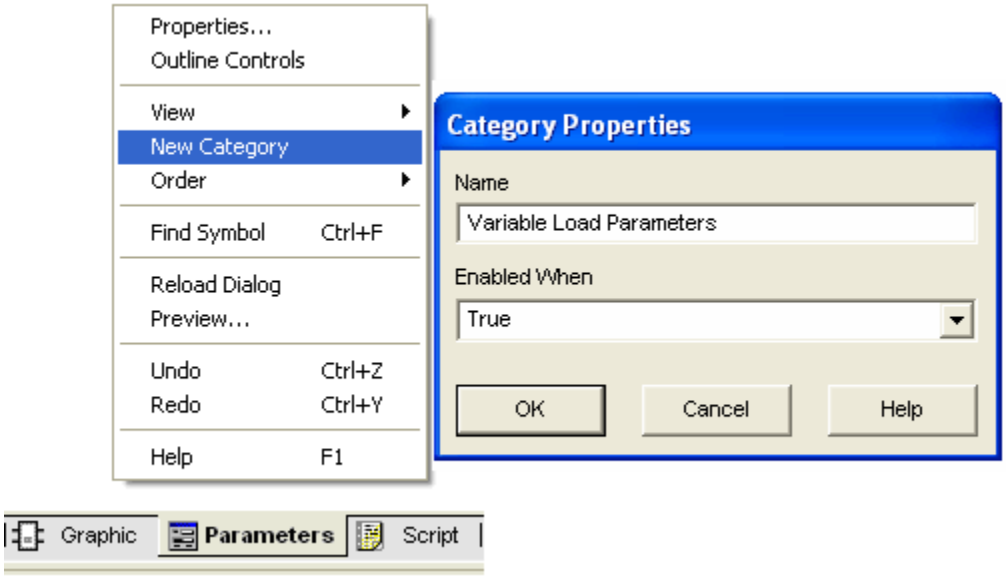

Figure E.8: Naming the new category of parameters

2. The category just created must be named. Right-click with the pointer positioned on the "Variable Load Model" category under the Parameters section in the workspace of the

Component Workshop. From the menu that emerges, select "New Control". The New Control window will then appear as depicted in Figure E.9.

3. Entries now must be added to the new category. The number of these entries depends on the number of internal variables that the user wishes to access. For the purpose of describing the procedure, just one entry will be added. Click on the Variable Load Model category under the Parameters section to reveal the initial dialog box of the N*ew* category in the "edit view", then click on the gray of this initial dialog box. From the menu that pops up select New, then from the next menu that appears, select "Text Field "(as shown in Figure E.10). The "Textbox Properties" window then pops up as (see Figure E.9), a resource that customizes the entries of the categories.

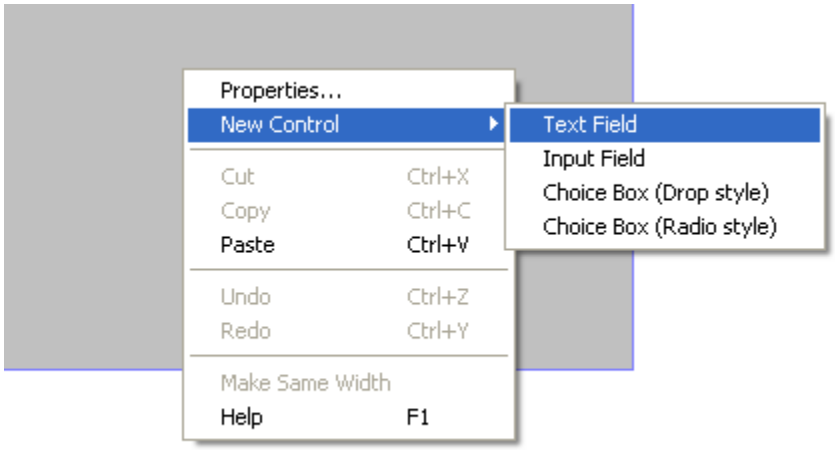

Figure E.9: Adding an entry to the dialog box in the parameters section

4. The entries then must be customized. A variable name to handle the internal variable load parameter to be accessed "Symbol" must be written in the field of the Textbox Properties window. The parameters name typed in Symbol must be different from that of any other variable name used in the same PSCAD/EMTDC case. In this example, the selected variable name in Symbol is Nominal Voltage (KV), as shown in Figure E.10. The legend appearing beside the entry in the dialog box is typed under "Caption". In the example, (Figure E.10), the Caption field has been set arbitrarily as Input 1. The rest of the fields in the "Text Properties" window are left unchanged.

5. Steps 3 and 4 are repeated for each l variable of the load model to be created.

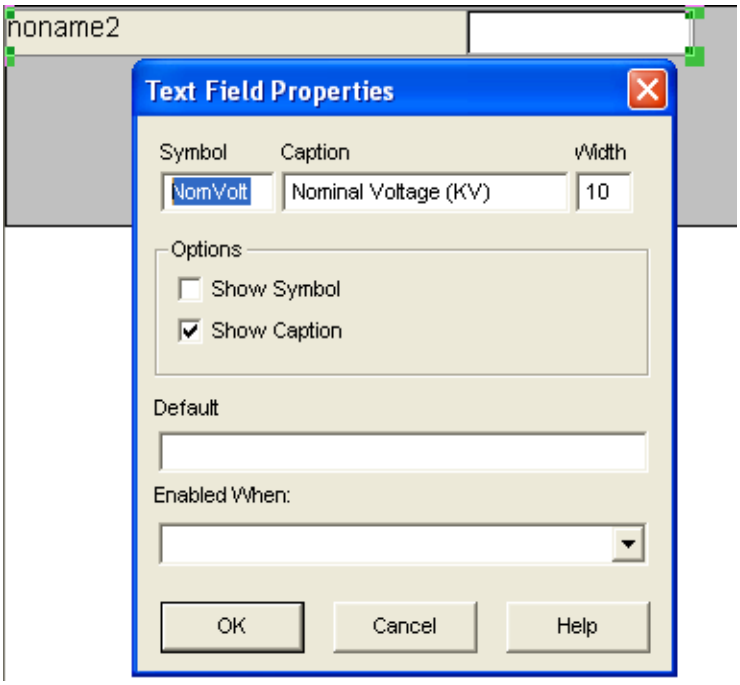

Figure E.10: The textbox properties window appearance

E.1.4 Inserting the variable load model code in the component

The PSCAD/EMTDC *Component* is defined as a variable load model mainly by the code stored in the Script section. Clicking on Script in the workspace expands the default applications *Branch* and *DSDYN* under the subsection EMTDC as shown in Figure E.11 and Figure E.12.

The "Branch" section is where the user can define what type of elements should be placed between the electrical connections defined in the Graphics section of the component definition. Branch statements can be used to place resistors, capacitors, and inductors (in series and parallel), as well as to define switching branches and those that contain an ideal voltage source.

The variable load model component is a Branch based component. The most noticeable difference between the Branch-based and node-based components is that all elements of the branch-based

component are indexed through branch numbers, not through node numbers. Also, these elements are not reset each time step, and therefore do not need to be redefined. The Branch section directly defines the branches composed of a combination of variable load component variables (R, L, and C).

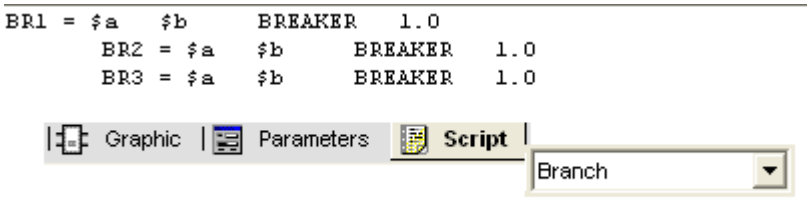

Figure E.11: Branch section

The DSDYN section is where the FORTRAN code, which defines what the component is to model, is placed. Code entered in this section should be in the form of either standard formatted FORTRAN 77 or PSCAD script (or a combination of these two). In section all code will be forced into the DSDYN subroutine in the EMTDC system dynamics.

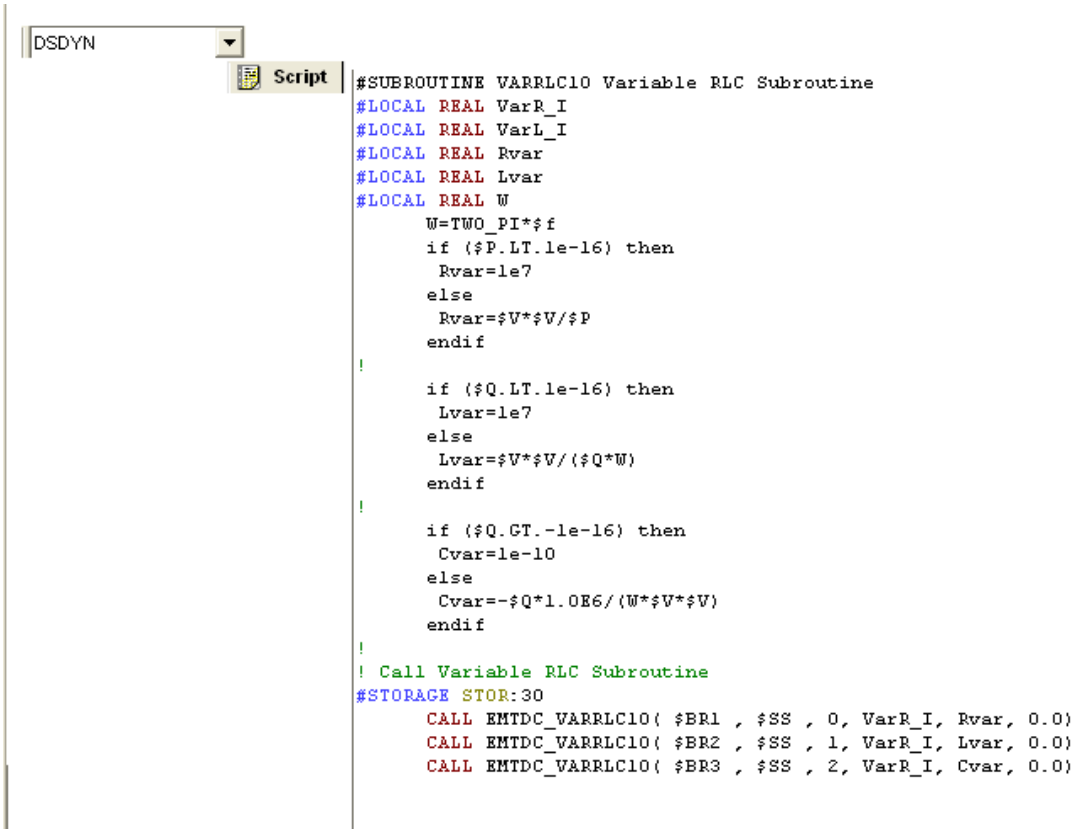

Figure E.12: DSDYN section

The power system modelled in PSCAD/EMTDC is solved in discrete time steps. In order to solve the power system, EMTDC first searches for changes that have occurred within the network and then solves the power system equations and obtains the currents and voltages in the branches and nodes of the power system. The FORTRAN code stored in DSDYN processes the variables. The variable load model is controlled by a control panel which controls the active power of the variable load component branch as shown in Figure E.13.

Figure E.13 shows a control panel with a multi-run component which controls two signals (P and P1) and records two variables (voltage and current) on the output file for each run. The start range value, increment change, and end range value for both controllable signals can be easily set up within the configuration page of the multi-run control panel (see
Figure E.14). The controllable input of the variable load component (real power) is updated in the network before EMTDC solves the power system equations in the next time step.

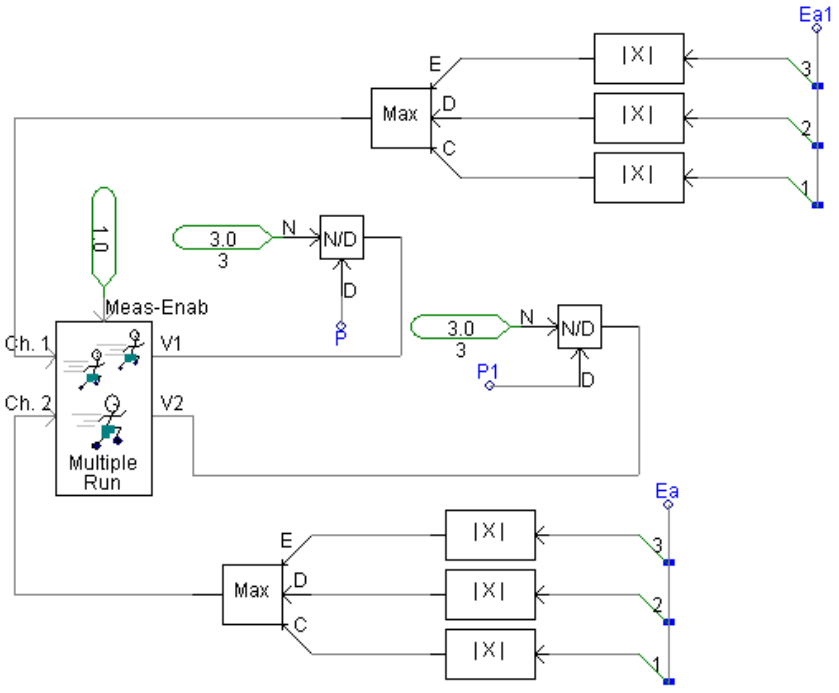

Figure E.13: Control panel with variable inputs and outputs

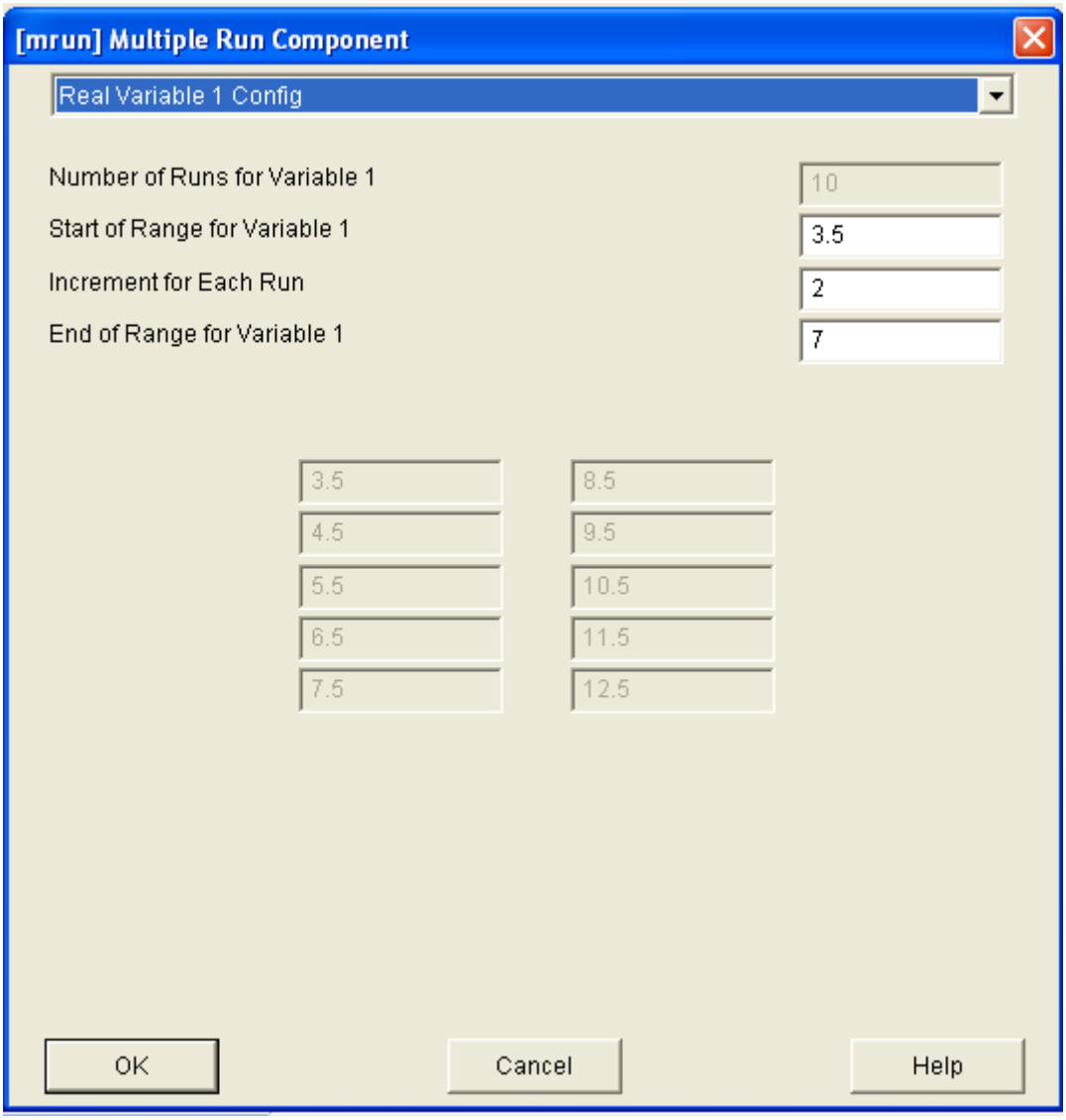

Figure E.14: Configuration page of multi-run component